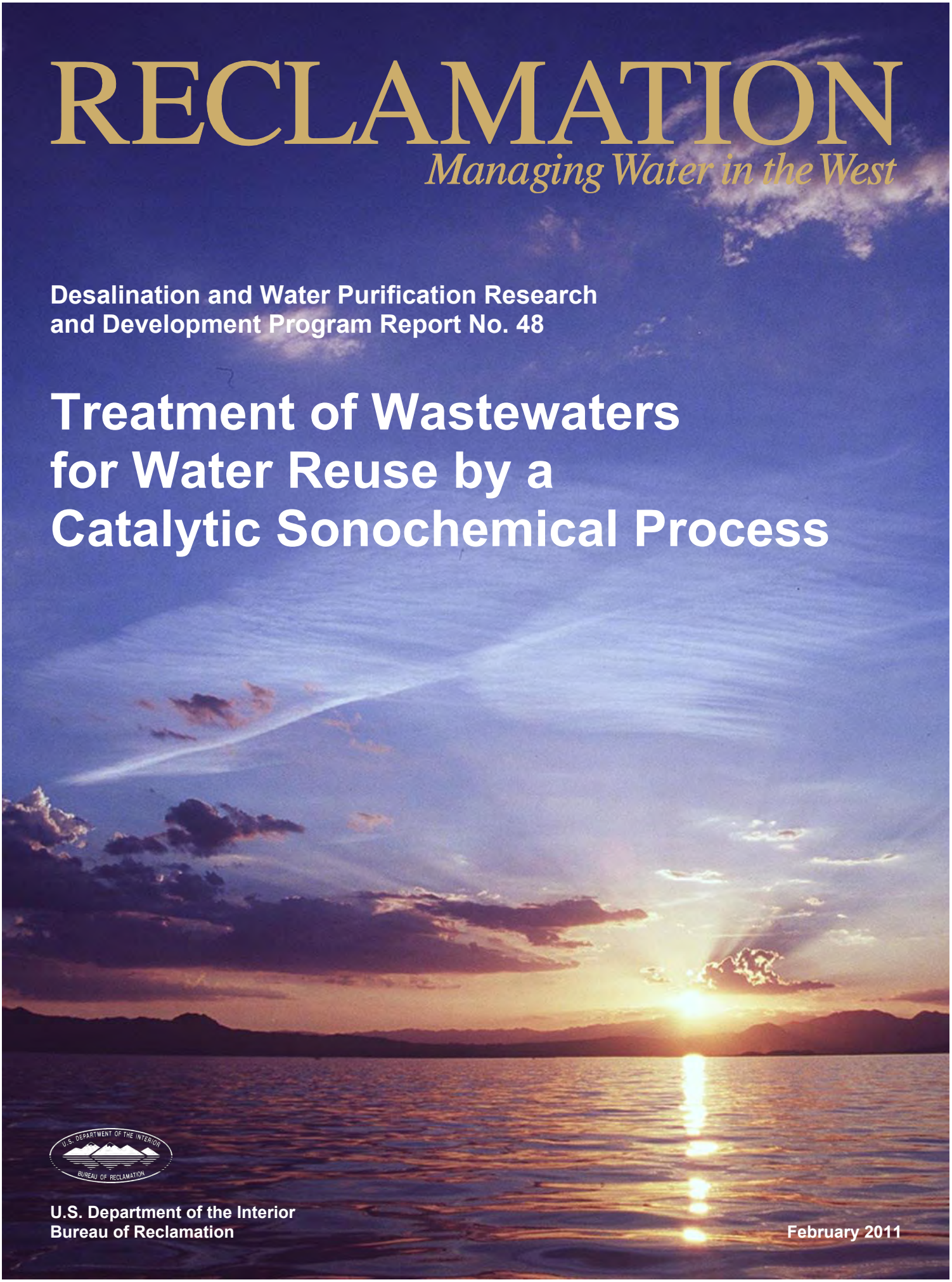

RECLAMATION

Managing Water in the West

Desalination and Water Purification Research and Development Program Report No. 48

Treatment of Wastewaters for Water Reuse by a Catalytic Sonochemical Process

U.S. Department of the Interior
Bureau of Reclamation

February 2011

REPORT DOCUMENTATION PAGE

Form Approved
OMB No. 0704-0188

T1. REPORT DATE *(DD-MM-YYYY)*	T2. REPORT TYPE	T3. DATES COVERED *(From - To)*
February 2011	Final	

T4. TITLE AND SUBTITLE
Treatment of Wastewaters for Water Reuse by a Catalytic Sonochemical Process

5a. CONTRACT NUMBER
Agreement No. 98-FC-81-0052

5b. GRANT NUMBER

5c. PROGRAM ELEMENT NUMBER

6. AUTHOR(S)
C.P. Huang; Pei Chiu; Samuel P. Myoda; Il-Kyu Kim and Michael Sung (Graduate Research Assistant)

5d. PROJECT NUMBER

5e. TASK NUMBER

5f. WORK UNIT NUMBER

7. PERFORMING ORGANIZATION NAME(S) AND ADDRESS(ES)
Department of Civil end Environmental Engineering
University of Delaware

8. PERFORMING ORGANIZATION REPORT NUMBER

9. SPONSORING / MONITORING AGENCY NAME(S) AND ADDRESS(ES)
U.S. Department of the Interior
Bureau of Reclamation,
Denver Federal Center
PO Box 25007, Denver CO 80225-0007

10. SPONSOR/MONITOR'S ACRONYM(S)

11. SPONSOR/MONITOR'S REPORT NUMBER(S)
DWPR Report No. 48

12. DISTRIBUTION / AVAILABILITY STATEMENT
Available from the National Technical Information Service
Operations Division, 5285 Port Royal Road, Springfield VA 22161

13. SUPPLEMENTARY NOTES
Report can be downloaded from Reclamation Web site:
www.usbr.gov/pmts/water/publications/reports.html

14. ABSTRACT *(Maximum 200 words)*
The research project was to develop a catalytic ultrasonic (enhanced sonochemical) technology to treat secondary effluents for reuse as potable water resources. To this end, two groups of common contaminants were studied: pathogens and trace organics, including polycyclic hydrocarbons, humic substance, and trihalomethane (THM). Batch experiments were conducted. Results showed that sonochemical process was promising for the inactivation of *Cryptosporidium* and the removal of trace organic compounds. Results indicated that, among a number of variables studied, energy intensity appeared to be the most important factor governing the inactivation of *Cryptosporidium*. The sonochemical process can readily decompose humic substance and polycyclic aromatic compounds (PACs) such as dibenzothiophene (DBT), benzothiophene (BT), naphthalene, and phenanthrene. The sonochemical decomposition rates of THMs followed the order: chloroform > dichlorobromomethane > dibromochloromethane > bromoform. Based on the preliminary results obtained with the Nearfield™ Acoustical Processor, the estimated cost, including energy and capital, is $0.74 per 1,000 gallons to achieve one log *Cryptosporidium* removal. This clearly demonstrated that the sonochemical process could be competitive with other technologies.

15. SUBJECT TERMS
Water reuse, wastewater treatment, ultrasound, disinfection, sonochemical process

16. SECURITY CLASSIFICATION OF:			17. LIMITATION OF ABSTRACT	18. NUMBER OF PAGES	19a. NAME OF RESPONSIBLE PERSON
a. REPORT	b. ABSTRACT	c. THIS PAGE			Katie Guerra
UL	UL	UL	UL	130	19b. TELEPHONE NUMBER *(include area code)* 303-445-2013

Standard Form 298 (Rev. 8/98)
Prescribed by ANSI Std. 239-18

Desalination and Water Purification Research and Development Program Report No. 48

Treatment of Wastewaters for Water Reuse by a Catalytic Sonochemical Process

by

C.P. Huang
Pei Chiu
Samuel P. Myoda
Il-Kyu Kim
Michael Sung (Graduate Research Assistant)

Department of Civil and Environmental Engineering
University of Delaware

U.S. Department of the Interior
Bureau of Reclamation
Technical Service Center
Water and Environmental Resources Division
Water Treatment Engineering Research Group
Denver, Colorado

February 2011

MISSION STATEMENTS

The U.S. Department of the Interior protects America's natural resources and heritage, honors our cultures and tribal communities, and supplies the energy to power our future.

The mission of the Bureau of Reclamation is to manage, develop, and protect water and related resources in an environmentally and economically sound manner in the interest of the American public.

Disclaimer

The views, analysis, recommendations, and conclusions in this report are those of the authors and do not represent official or unofficial policies or opinions of the United States Government, and the United States takes no position with regard to any findings, conclusions, or recommendations made. As such, mention of trade names or commercial products does not constitute their endorsement by the United States Government.

Acronyms and Abbreviations

Al	aluminum
BOD	biochemical oxygen command
Br^-	bromine
BT	benzothiophene
Ca	calcium
Cl_2	chloride
ClO_3^-	chlorate anion
cm	centimeter
CO_2	carbon dioxide
DABCO	4-diazabicyclo-[2.2.2]octane
DAPI	4', 6-diamidino-2-phenylindole
DBP	disinfection byproducts
DBT	dibenzothiophene
ECD	electron capture detector
EI	electron impact
EPA	U.S. Environmental Protection Agency
Fe	iron
FITC	fluorescein isothiocyanate
gal/day	gallon per day
gal/min	gallon per minute
HAA	haloacetic acids
H_2	hydrogen
HCl	hydrochloric acid
H_2O	water
H_2O_2	hydrogen peroxide
hp	horsepower
HS	humic substances
Hz	hertz
i.d.	inside diameter
K	kelvin
kJ/mole	kilojoules per mole
kHz	kilohertz
L	liter

Acronyms and Abbreviations (continued)

M	meter
M	molar
Mg	magnesium
Mg-$CaCO_3$/L	milligrams of carbonate per liter
mg/L	milligrams per liter
mg/mL	milligrams per milliliter
MHz	megahertz
mHz	millihertz
mL	milliliter
mL/min	milliliter per minute
mM	millimolar
mm	millimeter
Mn	manganese
NaCl	sodium chloride
NaOH	sodium hydroxide
$NaClO_4$	sodium perchlorate
NaH_2PO_4	sodium phosphate, dibasic
nm	nanometer
NOM	natural organic matter
NTU	nephometric turbidity unit
O_3	ozone
OH	hydroxyl
PAC	polycyclic aromatic compound
PBS	phosphate buffer solution
psi	pounds per square inch
RO	reverse osmosis
THM	thrihalomethane
THMFP	thrihalomethane formation potential
TOC	total organic carbon
V	volt
W	watt
W/cm^2	watts per square centimeter
WWTP	wastewater treatment plant

Acronyms and Abbreviations (continued)

~	approximately
°C	degree Celsius
>	greater then
<	less then
%	percent
µg/L	micrograms per liter
µL	microliter
µm	micrometer

Table of Contents

Table of Contents (continued)

List of Tables

List of Figures

List of Figures (continued)

List of Figures (continued)

List of Figures (continued)

List of Figures (continued)

1. Executive Summary

Stringent water quality regulations, increasing demands in industrial and domestic water supplies, and public awareness of water conservation are increasing the need for water reuse and reclamation. In the United States, wastewater reuse is limited mostly to secondary effluents from municipal wastewater treatment facilities. The main purpose of water reuse is for agricultural irrigation and, to a lesser extent, industrial cooling tower application. Very little effort is made to reuse municipal secondary effluents for potable water, mainly due to poor public acceptance and high cost. Other issues, such as technology availability, can play a key role in the future development of wastewater reclamation.

The major goal of this research project is to develop a catalytic ultrasonic (enhanced sonochemical) technology to remove residual organic matter, both refractory and hazardous, from wastewater effluents and to inactivate protozoan pathogens in wastewater. The technology developed involves using ultrasound in the presence of hydrogen peroxide (H_2O_2). Ultrasound can be a powerful means of treating mixed contaminants such as effluents from wastewater plants. The hydroxyl radical can react with a wide spectrum of soluble organic chemicals, such as halogenated hydrocarbons, among other recalcitrant and refractory compounds. It also can render the protozoan pathogens inactive.

Batch experiments were conducted to remove *Cryptosporidium* from wastewater effluents. Results indicate that the destruction of *Cryptosporidium* is directly proportional to the ultrasonic energy intensity and the initial oocyst concentration. Temperature, pH, and hydrogen peroxide concentration have a smaller effect on *Cryptosporidium* destruction than the energy intensity. We believe that the primary mechanism in oocyst destruction is physical—that is, the oocysts are shattered when the cavitation bubbles formed by the ultrasonic waves collapse. Within 9 minutes at an energy intensity level of 413 watts per square centimeter (W/cm^2), we can achieve a 3-log removal, which satisfies current regulations.

For the ultrasonic process to be a viable water reclamation treatment technology, the cost must be considered. To gain information on the economic feasibility, a Nearfield™ Acoustical Processor, capable of treating up to 15 gallons per minute in a continuous flow mode was used. Preliminary results show an increase in overall treatment efficiency. The time required to significantly reduce the thrihalomethane formation potential also was decreased from hours to minutes. The time required to effectively inactivate *Cryptosporidium* was reduced from minutes to seconds. Based on the preliminary results obtained with the Nearfield™ Acoustical Processor, the estimated cost, including energy and capital, is $0.74 per 1,000 gallons to achieve 1-log *Cryptosporidium* removal. This clearly demonstrates that the sonochemical process can be competitive

with other technologies. The Nearfield™ Acoustical Processor is a competitive technology for the removal of refractory organics and the inactivation of pathogenic protozoans.

2. Introduction

2.1 Water Reuse

Only about 5 percent (%) of the earth's surface water is classified as freshwater, of which only 0.62% is available for human consumption. Furthermore, over 70% of delivered drinking water ends up in municipal sewer lines. It is estimated that freshwater withdrawals in the United States will decrease in the future due to an increase in water demand and shortage of water resource (Council of Environmental Quality, 1987–88; Water Resource Council, 1978). Therefore water reclamation, reuse, and recycling will continue to increase.

Wastewater reuse is limited mostly to secondary effluent from municipal wastewater treatment facilities. Reuse purposes are mostly for agricultural irrigation and, to a lesser extent, industrial cooling tower application. Very little effort is made to reuse municipal secondary effluent as a direct reuse potable water supply. Public acceptance and cost appear to be the two major issues in the direct reuse of wastewater for a potable purpose. However, other issues, such as technology availability, can play a key role in future development of wastewater reclamation. The current practice of wastewater reclamation is indirect, namely through ground water recharge and irrigation. Direct recycling of wastewater is done by extended lagooning followed by sedimentation, filtration, carbon adsorption, a membrane process such as reverse osmosis, and chlorination. This type of treatment is expensive, making it harder to gain public acceptance.

2.2 Organics in Secondary Effluent

Fractionation of organic matter in secondary effluent indicates that 40–50% of the organics can be classified as humic substances (humic, fulvic, and hymathomelanic acids), with the majority being fulvic acid. The remainder of the organic matter consists of ether extractables, anionic detergents, carbohydrates, proteins, and tannins (Rebhun et al., 1971). Results from gel permeation chromatography revealed that the majority of the humic compounds isolated from the secondary effluents were within the molecular weight range of 1,000–5,000 Daltons. The molecular weight distribution of humic substances isolated from secondary effluents is presented in table 1.Many treatment methods have been used to remove organic compounds. The most common processes include activated-carbon adsorption, activated-sludge, powdered activated carbon, chemical oxidation.

Table 1. Molecular Weight Distribution of Humic Substances from Secondary Effluents (Manka et al., 1974)

Molecular Weight (Dalton)	Humic Compounds Present (%)		
	Fulvic acid	Humic acid	Hymathomeianic acid
< 500	27.5	17.9	4.5
500–1,000	7.8	6.2	12.2
1,000–5,000	35.7	29.4	48.0
5,000–10,000	15.3	7.8	28.0
10,000–50,000	9.4	36.7	7.5
> 50,000	4.3	2.0	0

2.3 Disinfection Byproducts (DBPs)

The excellent ability of the chlorine disinfection process to inactivate harmful microorganisms is clouded by the potentially toxic disinfection byproducts formation. In 1975, the U.S. Environmental Agency (EPA) began preliminary investigations into the health threat posed by DBPs. These investigations led to the regulation of trihalomethanes (THMs) in drinking water in 1979. Table 2, shown later in this report, lists some of the DBPs generated by chlorine disinfection. Singer (1993) suggested the following general equation for the formation of THMs and other halogenated DBPs:

$HOCl + Br^- + \text{natural organic matter (NOM)} \Rightarrow \text{THMs} + \text{other halogenated DBPs}$

The initial efforts to control DBPs fell into two categories: disinfectant substitution and precursor elimination. The first effort dealt with the use of alternate disinfectants, such as ozone. However, it was soon realized that each new disinfectant produced alternative DBPs. The main focus then was shifted to eliminating the DBP precursors. Initially, natural organic matter (NOM) was shown to be a major precursor for THMs. However, NOM can be only loosely defined with exact composition varying from source to source (Minear and Amy, 1994). Furthermore, it is known that bromine (Br^-) can be an important precursor of DBPs.

2.4 Biological Contaminants in Secondary Wastewater Effluent

Organisms such as *Cryptosporidium* and *Giardia* can survive the wastewater treatment processes and pose a potential treat to public health in reclaimed water. *Cryptosporidium* parvum (figure 1) is a coccidian parasite that can cause adverse

health effects in immunocompromised persons (Deng et al., 1997). Eliminating the biological contaminants with large doses of chlorine creates the DBP problem, while minimizing the DBP formation requires reduced rates of chlorine, leading to a larger population of microorganisms. A balance must be reached so that the contaminants can be minimized.

C. parvum oocyst & sporozoites

(from Fayer, R. *et al.* in *Cryptosporidiosis of Man and Animals,* 1990)

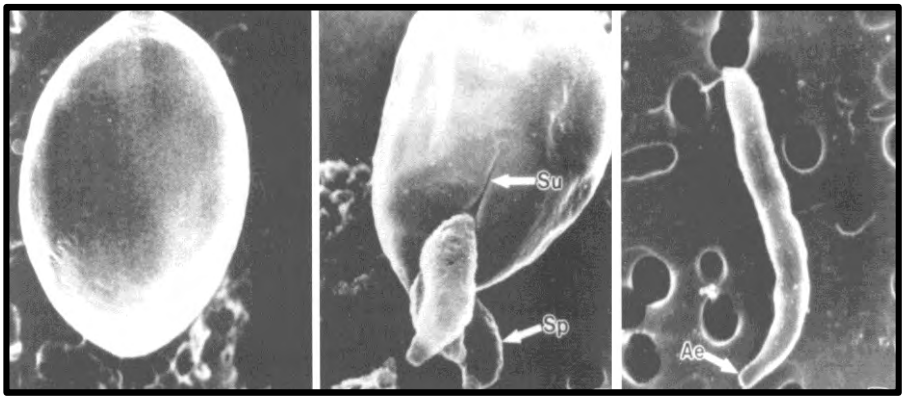

oocyst sporozoites exiting an oocyst sporozoite

Figure 1. *Cryptosporidium* oocysts and sporozoites (R. Fayer et al., 1990).

2.5 Project Objectives

The major goal of this research project is to develop a catalytic ultrasonic (enhanced sonochemical) technology to remove organic matter and inactivate protozoan pathogens such as *Giardia* and *Cryptosporidium* from wastewater for potable uses. Laboratory experiments were conducted to decompose the THM precursors, humic substances (HS) from Wilmington wastewater effluent using sonochemical processes. We also selected refractory organic compounds such as benzothiophene (BT) and dibenzothiophene (DBT) as precursor surrogates. Factors such as total carbonate concentration, ultrasonic energy intensity, dose of hydrogen peroxide, solution pH, solution temperature, turbidity, and concentration of metals were examined.

The following are the specific objectives of this study:

1. Study the effect of pH, oocyst concentration, temperature, and energy intensity on the disinfection of pathogenic protozoa (i.e., *Cryptosporidium,* using sonochemical process).

2. Study the degradation of residual biochemical oxygen demand (BOD) and selected refractory organic compounds.

3. Conclusions

Results clearly indicate that the primary variable in oocyst destruction is the ultrasonic energy intensity. Within 9 minutes at an energy intensity level of 413 watts per square centimetre (W/cm^2), we achieved a 3-log removal, which satisfies current regulations; and we were able to achieve 4-log removals in 15 minutes at the same intensity. In all cases, the ultrasonic destruction of *Cryptosporidium* followed a first order reaction. The initial oocyst concentration also seems to affect the disinfection process. We believe that the primary mechanism in the oocyst destruction is physical—that is, the oocysts are shattered when the cavitation bubbles formed by the ultrasonic wave collapse. The optimum pH seemed to be around 7.0, and the optimum temperature was around 33 degrees Celsius (°C). Although the efficiency was lower at pH 9.3 and at temperatures above and below 33 °C, the decrease was relatively minor. This indicates that no pretreatment or temperature controls would be required to utilize this process in real world applications.

The extent of total organic carbon (TOC) removal was proportional to factors such as ultrasonic energy intensity and hydrogen peroxide concentration, while increasing total carbonate, pH, temperature, and turbidity decreased the extent of TOC removal of humic substances. The metal ions such as iron (Fe)(II) and manganese (Mn) (II) showed catalytic effect ,while aluminium (Al)(III), calcium (Ca)(II), and magnesium (Mg)(II) had an inhibition effect on the TOC removal of humic substances in sonochemical reaction with hydrogen peroxide. The Langmuir-Hinshelwood model provided a good fit of the experimental data. Experimental results also showed that the dose of hydrogen peroxide (H_2O_2) affected the formation of disinfection byproducts. Chloroform and dichlorobromomethane were formed as major THMs during chlorination.

The sonochemical process can readily decompose DBT, benzothiophene, naphthalene, and phenanthrene. Decomposition of benzothiophene showed an apparent toxicity reduction and a complete mineralization to carbon dioxide and inorganic sulfur compound. The sonochemical reaction can be described by a mechanism involving hydroxyl radicals. The main intermediate, found in the initial step, is 3-hydroxybenzo-thiophene. Further decomposition of 3-hydroxybenzothiophene leads to the production of 2,3-dihydroxybenzothio-phene and benzothiophene-2,3-dione, which can be further decomposed and mineralized to carbon dioxide and sulfite. The possible pathway for the decomposition of benzothiophene can be described by hydroxyl (OH) radical addition, hydrogen abstraction, ring cleavage, and mineralization. The kinetic model based on the pseudo first-order reaction provided a good fit of the experimental data.

The representative refractory organic compound, DBT, was decomposed rapidly by a sonochemical process in an aqueous solution. The sonochemical decomposition of DBT followed the first-order reaction kinetics. The

sonochemical reaction in aqueous solution was affected by the steady-state temperature, and the activation energy calculated from the Arrhenius expression is 12.6 kilojoules per mole (kJ/mole) for DBT in controlled reaction conditions. The sonochemical decomposition of dibenzothiophene produces monohydroxydibenzothiophene as an identified intermediate product. It was proposed that further decomposition of monohydroxydibenzothiophene yields 2,3-dihydroxydibenzothiophene and dibenzothiophene-2,3-dione, which can be mineralized to carbon dioxide and inorganic sulfur species.

THMs were decomposed rapidly by sonochemical irradiation in the aqueous phase. The sonochemical decomposition rates occur in the following order: chloroform > dichlorobromomethane > dibromochloromethane > bromoform. This means that the decomposition rate increases as the vapor pressure (Henry's law constant) increases for THMs in aqueous solution. It is supported by measuring the concentrations of chloride and bromide released from decomposition of THMs. Chlorine atoms are evolved faster than bromine atoms. It also is observed that the sonochemical decomposition rate of THMs is affected by the ultrasonic energy intensity, the steady-state temperature of solution, the initial concentration of THMs, and the ionic strength. The activation energy values calculated from the Arrhenius expression are 12.7 kJ/mole for chloroform, 7.3 kJ/mole for dichlorobromomethane, 12.6 kJ/mole for dibromochloromethane, and 14.6 kJ/mole for bromoform in the controlled sonochemical reaction condition.

The sonochemical process can readily decompose dibenzothiophene, benzothiophene, naphthalene, and phenanthrene. Decomposition of benzothiophene showed an apparent toxicity reduction and a complete mineralization to carbon dioxide and inorganic sulfur compound. The sonochemical reaction can be described by a mechanism involving hydroxyl radicals.

In order to consider the ultrasonic process, a viable water reclamation treatment technology, the cost of the process must be considered. Our experiments primarily have been done using a probe reactor with small volumes (20 millilters [mL]) in the batch mode. This is not considered a realistic mode of operation. To gain information on the economic feasibility, a Nearfield™ Acoustical Processor, capable of treating up to 15 gallons per minute (gal/min) in a continuous flow mode, was used. Our preliminary results show an incredible increase in overall treatment efficiency. The estimated cost, including energy and capital, for the ultrasonic process is $0.74 per 1,000 gallons to achieve 1-log *Cryptosporidium* removal. This clearly has demonstrated that the sonochemical process can be competitive with other technologies. Moreover, the time required to significantly reduce the thrihalomethane formation potential (THMFP) also has been decreased from hours to minutes. The Nearfield™ Acoustical Processor is a competitive technology for the removal of refractory organics and the inactivation of pathogenic protozoa.

4. Material and Methods

4.1. Wastewater Characterization

The initial step in the laboratory work was to characterize the wastewater samples. Grab samples (before and after chlorination) periodically were taken from the Wilmington Wastewater Treatment Plant (WWTP). Also obtained were 24-hour composite samples (after chlorination). The Ca (II), Mn (II), Fe (II), and Mg (II) contents were evaluated using the direct air-acetylene flame method (method 3111 B) described in *Standard Methods for the Examination of Water and Wastewater*, 18th edition, 1992. Typical results of this analysis are shown in table 2. Also reflected in this table are the pH and alkalinity values. The alkalinity value was calculated using the titration method (method 2320 B), and the pH value was calculated using the electrometric method (method 4500-H^+ B); these procedures also are outlined in *Standard Methods for the Examination of Water and Wastewater*, 18th edition, 1992.

Table 2. Typical Characteristics of WWTP Samples[1]

Characteristics	Before chlorination	After chlorination
pH	7.71 ± 0.09	7.88 ± 0.04
Mn(II) (µg/L)	183.9 ± 48.2	180.2 ± 26.7
Fe(II) (µg/L)	[2]127	[2]157
Mg(II) (mg/L)	9.60 ± 0.57	9.58 ± 0.41
Ca(II) (mg/L)	[3] 30.57	30.35 ± 0.35
Alkalinity (mg-$CaCO_3$/L)[4]	182.5 ± 3.6	185.0 ± 8.7

[1] µg/L = micrograms per liter; mg/L = milligrams per liter.

[2] Results from the November 20,1998, sample only.

[3] Results from the January 7, 1999, composite sample only.

[4] mg-$CaCO_3$/L = milligrams of calcium carbonate per liter.

4.2 Spiked Sample Preparation

The wastewater effluent (prechlorination) was filtered with 0.22 micrometer (µm) filter paper and spiked with *Cryptosporidium* parvum oocysts (Waterborne, P102 – 10^8 live in water) to obtain a concentration of 10^5 oocysts per liter. All method development and experimental procedures were executed using these spiked wastewater samples.

4.3 Humic Acid Preparation

A potable reverse osmosis (RO) system was used to collect and concentrate humic substances from Wilmington Wastewater Plant effluent. Effluent was first pumped through in-line filters (1 and 0.45 μm) to remove particulate matter and was then collected in a 40-liter (L) sample reservoir. In the sample reservoir, a 1/16-horsepower (hp) submersible pump (Simer Pump, Model 2310, Kansas City, Missouri) pumped the filtered samples through a cation exchanger (Dowex-50 cation exchange resin in the sodium form, Dow Chemical, Midland, Michigan). The filtered and cation-exchanged sample then was delivered to the RO membrane by a high-pressure pump (Hypro, Model 2230B, New Brighton, Minnesota), which boosted the pressure to 150–200 pounds per square inch (psi). The RO membrane (Filmtec FT30, Dow Chemical) consisted of a 0.2-μm thick, highly crosslinked aromatic polyamide skin on a 35-μm polysulphone support and was designed for tap water desalination. The percent rejection of 0.2% sodium chloride (NaCl) solution by the Filmtec RO membrane ranged from 99.0–99.7%, depending on the operating pressure (E.M. Perdue, personal communication). The retentate solution from the RO system was collected into the sample reservoir and mixed with filtered sample. The recycling of the retentate solution to the sample reservoir was continued until the desired enrichment of HS was achieved.

4.4 Wastewater Sample Chlorination

The chlorine demand of the wastewater sample, appropriate dilution factor to prepare the chlorine dosing solution, volume of chlorine dosing solution per sample volume, and the residual chlorine concentrations after THMFP tests were determined via titration using a Hach CN-65 test kit. The titration was done by adjusting/diluting the sample volume to 40 mL with the addition of distilled, deionized water (if the original sample was less than (<) 40 mL or if the initial chlorine concentration was greater than (>) 20 milligrams per milliliter [mg/mL]) and a sulfite 1-reagent powder pillow (Hach 2203-99) was added. A sulfamic acid powder pillow (Hach 1055-99) was then added, and the sample was placed on a VWR Magnestir and mixed; a blue color developed indicating the presence of chlorine. The prepared sample was reduced in volume to 30 mL (6 mL for high chloride [Cl_2] samples) and titrated with 2.46×10^{-3} nitrogen (N) sodium thiosulfate standard solution (Hach 24085-37) until the sample became colorless. Each drop of titrant used to bring about the color change represented 0.2 mg/L (2.0 mg/L for high Cl_2 samples) of chlorine (after correcting for appropriate dilution factors).

The chlorine dosing solution was prepared in the following manner: 1 mL of 5% aqueous sodium hypochlorite solution (stock hypochlorite) was added to 25 mL of distilled, deionized water and titrated to a starch-iodide endpoint using a sodium thiosulfate titrant. Chlorine concentration was determined as outlined above (stock hypochlorite solutions with less than 20 milligrams [mg] Cl_2/mL

were discarded). A chlorine dosing solution (5 mg CL_2/mL) was prepared using the following formula:

$$mL\ required = \frac{1{,}250}{stock\ hypochlorite\ conc.\ mg\ Cl_2 / mL} \quad (4.1)$$

This calculated volume (22.2 mL) was added to the appropriated volume of distilled, deionized water to generate a 250-mL dosing solution. This solution was stored in an amber bottle at 4 °C and was discarded if the chlorine concentration dropped below 4.7 mg Cl_2/mL.

The chlorine demand of the wastewater was determined to be 60 mg/L using the following procedure: 2.5 mL of chlorine dosing solution was pipetted into a 125-mL amber bottle and completely filled with distilled, deionized water, capped with a TFE-lined screw cap and shaken. The initial chlorine concentration of the sample was determined to be 95 mg/L (C_I). A second sample was prepared in the same fashion with the exception that 2.5 mL of phosphate buffering solution was also added, and the sample was stored in the dark for over 4 hours prior to titration. This titration indicated that the residual chlorine concentration of the wastewater sample was 35 mg/L (C_R). The volume of chlorine dosing solution (0.45 mL) needed to chlorinate each sample for the THMPF test was determined using the following formula:

$$V_d = \frac{D_{Cl} + 3}{5} x \frac{V_s}{1000} \quad (4.2)$$

Where, V_d = volume of dosing solution, V_s = volume of sample (35 mL) and $D_{Cl} = C_I - C_R$ (60 mg/L).

4.5 Chemicals

Cryptosporidium parvum oocysts (#P102, live in water) and Crypt-a-Glo™ (#A400, fluorescent labeled IgM antibodies) were obtained from Waterborne Inc. (New Orleans, Louisiana). Dynabeads anti-*Cryptosporidium* (#730.01) antibody coated magnetic beads were obtained from Dynal (New Hyde Park, New York). Glycerol (#G-6279), 1,4-diazabicyclo-[2.2.2]octane (DABCO, #D-2522), 4', 6-diamidino-2-phenylindole (DAPI, #D-9542) hydrogen chloride (HCl), and Sodium phosphate, dibasic (NaH_2PO_4) $2H_2O$ were purchased from Sigma (St. Louis, Missouri). Vectabond™ reagent slide treatment (#SP-1800) was purchased from Vector Laboratories (Burlingame, California). Na_2HPO_4 (#33,198-8) and NaCl (#22,351-4) were purchased from the Aldrich Chemical Company (Milwaukee, Wisconsin). Sodium hydroxide (NaOH) (#S318-500) was purchased from Fisher Chemical (Fair Lawn, New Jersey). Absolute methanol (#9070-1) was purchased from the J.T. Baker Chemical Co. (Phillipsburg, New Jersey). All chemicals were American Chemical Society (ACS) reagent grade or better. Distilled, deionized water (reagent water) was prepared using a Corning

Mega-pure 1-L water distillation system and a Zenon (Burlington, Ontario) ZenoPure Mega 90 water deionization system.

Chloroform, dichlorobromomethane, dibromochloromethane, and bromoform were obtained from the Aldrich Chemical Company (Milwaukee, Wisconsin). Stock solution of THMs was prepared in Optima grade methanol. Each sample was prepared with spiking the pre-selected volume of THM stock solution into the deionized water.

Hydrogen peroxide with a purity of 31.5% was obtained from the Fisher Scientific Company. Perchlorate salts of metals were obtained from the Aldrich Chemical Company (Milwaukee, Wisconsin).

Benzothiophene was obtained from the Aldrich Chemical Company (Milwaukee, Wisconsin). The purity of the organic compound is 99%. Benzothiophene-sulfoxide and benzothiophene-sulfur dioxide were obtained from Lancaster Chemical Company (Lancaster, Pennsylvania). Stocks of the selected organic compounds were prepared in a stirred glass flask, which was sealed by a Teflon-covered rubber stopper to prevent organic vapor from escaping, by dissolving a given amount of these organic chemicals in deionized water. It took several days to complete the dissolution.

4.6 Quantification and Qualification of *Cryptosporidium*

Quantification of viable *Cryptosporidium* oocysts has presented a problem for researchers because sporozoites may or may not be present inside an oocyst. A qualification and quantification method has been developed based on EPA Method 1623: *Cryptosporidium* and *Giardia* in Water by Filtration/IMS/FA that provides accurate and reproducible counts. Utilizing fluorescent labeled IgM antibodies to identify the oocysts and 4',6-diamidino-2-phenylindole (DAPI) staining to detect sporozoites inside the oocysts, we microscopically examined well slides to determine viable oocyst counts.

The primary deviation in this methodology from the EPA Method 1623 is the way in which we microscopically observed the oocysts and sporozoites. Instead of viewing the slide through the eyepiece, we have equipped our Olympus AX 70 microscope with an Optronics CCD camera and Sony monitor, figure 2. This allows us to view the image in a larger format, making evaluation much easier. The monitor screen represents one grid on the well slide, eliminating the overlap associated with multiple grid viewing within a circular field. This advancement has been taken a step further by installing a Prior motorized stage and X-keys

Figure 2. Olympus AX 70 microscope, Optronics CCD camera, Prior motorized stage, Sony monitor , computer control.

(Tiger Direct, #P55-2000) 16-key programmable keyboard. This keyboard has been programmed so that single key strokes precisely control the stage movement up, down, left, and right, eliminating the error associated with manually moving the stage. These improvements allow us to examine the well slides in a quick and efficient manner while ensuring 100% coverage without any over or under-lapping that would result in too high or low oocyst counts.

Although significant, the previously mentioned improvements are only minor relative to the improvements made in image evaluation. Currently, EPA Method 1623 calls for the separate evaluation of oocysts and sporozoites using both fluorescein isothiocyanate (FITC) and DAPI filter cubes. The image first must be evaluated using the FITC filter to identify the oocysts; next, the filter must be changed over to the DAPI filter to evaluate the sporozoites. One problem with this method is that no sporozoites will be detected in oocysts that have not been labeled with FITC antibodies; and although the oocysts and sporozoite position generally is known, there is uncertainty in their exact positions; the sporozoites could be within the oocyst or outside the oocysts. To eliminate this problem, dual dichroic cubes that allow the simultaneously viewing of the FITC and DAPI labeled samples were tested. Commercially available dual dichroic cubes were found to be ineffective. Upon closer inspection of their characteristic curves (transmission ratio [%] versus wavelength [nm]), it was determined that they were designed for the high DAPI and low FITC concentrations typical of most biological samples. *Cryptosporidium* has exactly the opposite characteristics—high FITC and low DAPI concentrations. The FITC signal was overwhelming the DAPI signal, and the sporozoites could not be detected. A filter cube that would block some of the FITC signal without limiting the DAPI signal was designed.

A filter cube consists of three components: the barrier filter, dichroic mirror, and excitation filter. After identifying the general shapes of the characteristic curves of the filters needed, a variety of cube configurations were tested. The final combination arrived at was the barrier filter and an excitation filter from an U MWU ultraviolet (UV) wide band (Hitech Instruments, #U-M536) coupled with a dichroic mirror from a M51000 DAPI/FITC cube. The wide band UV components let enough FITC and DAPI signal through, and the dichroic mirror gave us better differentiation between blue and green. This custom cube allowed the simultaneous viewing of oocysts and sporozoites, figure 3. Until commercially available cubes designed for this application become available, this is a feasible and relatively low-cost alternative anyone can utilize to cut analysis time in half and greatly improve accuracy.

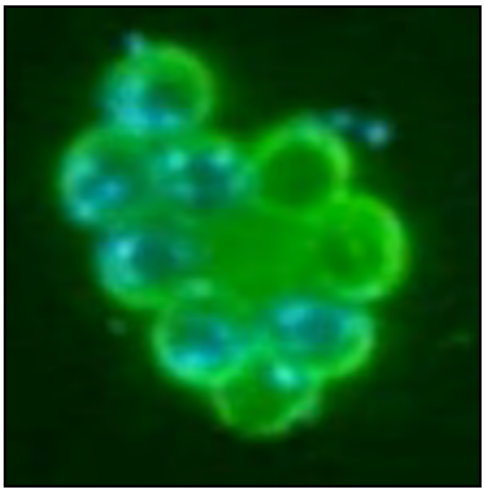

Figure 3. Oocysts and sporozoites viewed simultaneously with the custom cube.

A method to concentrate and stain viable *Cryptosporidium* oocysts was developed based on EPA Method 1623: *Cryptosporidium* and *Giardia* in Water by Filtration/IMS/FA. For samples with an estimated oocyst concentration between 10^4–10^5 oocysts/mL, a 1-mL aliquot of the sample to be analyzed was diluted with 9 mL of distilled, deionized (reagent) water. After vortexing for at least 2 minutes, 50 microliters (µL) of this dilution was overlaid on a Dynal 9-millimeter (mm) well slide and dried in an incubator for approximately (~)1 hour at 42 °C. After drying, 40 µL of absolute methanol was applied to the slide and allowed to air dry for ~10 minutes. After that time, 50 µL of 1X Waterborne A400FL Crypto-a-Glo (Mab) was applied to the slide. The slides were placed on a rack over wet paper towels in a sealed Tupperware container (humid chamber) and incubated at 37 °C for 30 minutes. The excess Mab was aspirated with disposable transfer pipettes and washed three times with a 150-millimolar (mM) phosphate buffer solution (PBS). Next, 50 µL of DAPI staining solution was applied and allowed to stand for ~10 minutes. The slide

then was washed three more times with PBS and once with reagent water. After drying at 37 °C in an incubator on a rack over desiccant in a sealed Tupperware container (dry box), 6 µL of 2% 1,4-diazabicyclo-[2.2.2]octane (DABCO) mounting media (78% glycerol, 22% water) was applied. After drying, a cover slip was installed and sealed with clear nail polish. Slides were stored in a dry box in the dark prior to microscopic examination.

Samples that had an estimated oocyst concentration between 10^3–10^4 oocysts/mL were prepared following the above procedure with the following exception: the initial 1-mL sample was not diluted with 9 mL of reagent water.

Samples that had an estimated oocyst concentration $<10^3$ oocysts/mL were concentrated via immunomagnetic separation prior to slide preparation. A 0.5-mL sample was added to 9.5 mL of reagent water in a Dynal L10 tube containing 1 mL 10X SL buffer A and 1 mL 10X SL buffer B; 100 µL of vortexed Dynabeads anti-*Cryptosporidium* beads were added; and the tube was rotated on a Dynal sample mixer for 1 hour. The L10 tubes then were removed from the mixer and placed in Dynal MPC-1 magnetic concentrators and gently rocked for 1 minute. The supernatant then was decanted, the magnet removed, and the oocyst/bead complexes were resuspended in 1 mL of 1X SL buffer A. This suspension was then transferred into a 1.5-mL Eppendorf tube. The tube was placed in a Dynal MPC-M magnet and was gently rocked for 1 minute. The

Slide Preparation

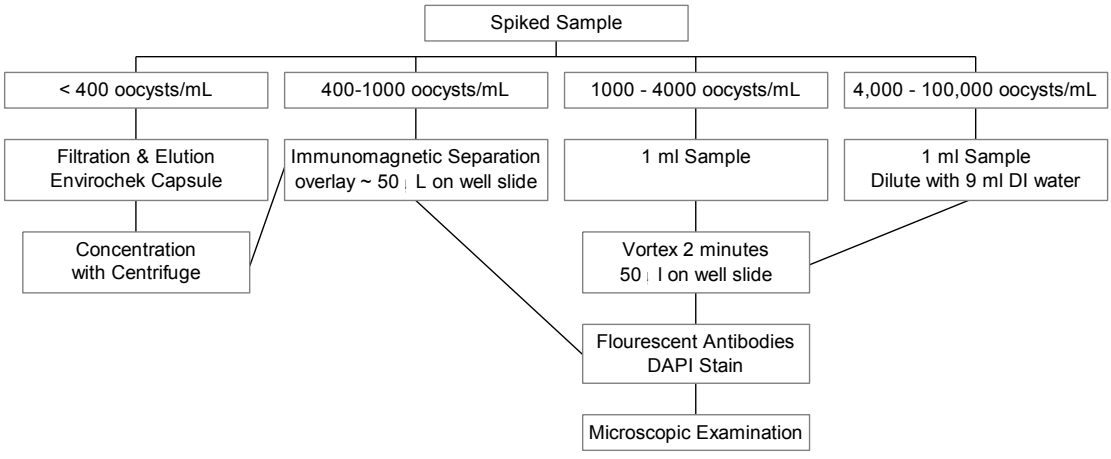

Positive and negative controls were analyzed with each sample series. Positive controls were prepared by pipetting 10 μL of positive antigen onto ~ 500 oocysts on a well slide; negative controls were prepared by adding 75 μL of PBS on a well slide. The slides then were stained following the methodology described previously.

Slides were examined using an Olympus AX70 microscope. Each well slide was scanned following the pattern represented in figure 5.

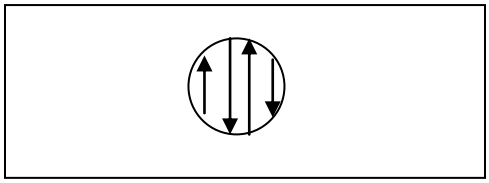

Figure 5. Well slide scanning pattern.

4.7 Procedure for Ultrasonic *Cryptosporidium* Destruction

Figure 6 shows the experimental setup used to sonicate the sample solutions. Ultrasonic processes are conducted with an ultrasonic generator (Cole Palmer 600-watt (W), 20-kilohertz (kHz), ultrasonic homogenizer 4710) equipped with a titanium probe transducer (Cole Palmer, Model CV 17) and 40-mL glass reactor which is sealed with the Teflon-covered rubber stoppers in the batch mode. The power output of generator could be varied from 0–600 W. The diameter of titanium probe was 13 mm. Titanium tips with a flat radiating surface were used for all reactions. The surface of the tip was always checked for wear before the experiment, and tips were discarded based on the condition of the surface (too much erosion) and percentage output power for tuning. A Frigomix 1495 water circulation and temperature control system were used to maintain the bulk solution temperature at 25 °C inside the reactor. A pH controller (New Brunswick Scientific Inc.) with a pH probe (Cole Palmer, Model 7543) was used to measure the pHs of the solutions.

Ultrasonic degradation experiments were carried out utilizing this equipment. Under a variety of conditions, 20 mL of the spiked wastewater samples (10^5 oocysts/mL) were subjected to ultrasonic irradiation. Every 3 minutes, 1-mL samples were drawn and analyzed following the procedure previously outlined. Prior to each experimental run, a wastewater sample without oocysts was ultrasounded under the same conditions as the run to generate wastewater that was used to replace the 1 mL drawn out of the reactor at each time interval. This was done to maintain the sample volume and ultrasonic energy intensity during the run.

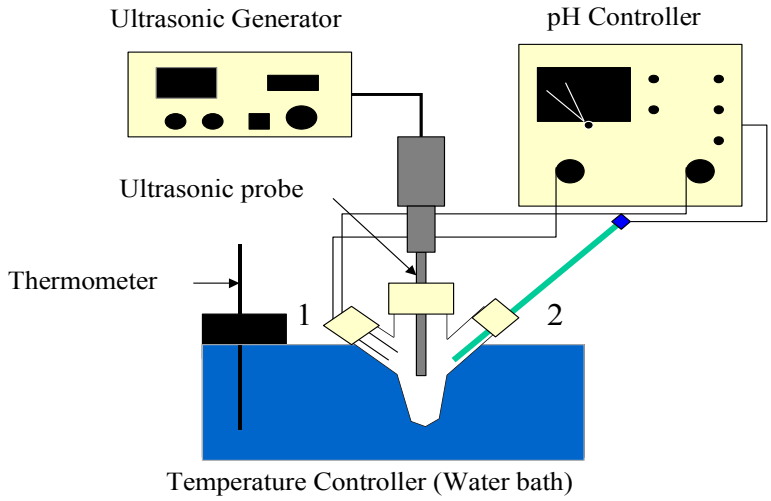

1. Sample Port, Acid/Base lines, or Thermometer
2. pH probe

4.8 Procedure for Ultrasonic Humic Acid Degradation

In order to obtain a carbonate-free sample, bicarbonate was removed by acidifying the sample to pH 4 with perchlorate acid and bubbling with pure nitrogen gas. Sonochemical treatments were conducted with an ultrasonic generator (Cole-Parmer 600-W, 20-kHz, ultrasonic homogenizer 4710) equipped with a titanium probe transducer (Cole Parmer, Model CV 17). Experiments with HS were conducted in an open glass reactor (Sonics & Materials, 20 mL) in the batch mode. Experiments with BT, DBT, and THMs were conducted in a closed, zero-head space, glass reactor (Sonics & Materials, 40 mL) sealed Taflon-covered rubber stoppers and operated in the batch mode. The reactor was filled with a sample and immersed in a water bath (Frigomix 1495 Water Circulation and Temperature Control System). The temperature was kept at a preselected value. Hydrogen peroxide was manually added at the starting point. The solution pH was adjusted to a preselected value at the last step before starting the sonochemical irradiation. The treated HS samples immediately were injected to TOC analyzer and adjusted pH 7 with pH buffer solution. Sodium hypochloride solution was added to samples, which were kept in sealed, zero-headspace, and amber bottles, then stored in darkness at 25 °C.

4.9 Analytical Methods

THMs in a 0.5-mL sample from the reactor were extracted using the liquid-liquid extraction method and analyzed with gas chromatography (Hewlett-Packard model 5890) equipped with a Supelco-608 column (L = 30 meters [m], internal

diameter = 0.5 micrometers), a Hewlett-Packard model 7376 autosampler injector, and an electron capture detector (ECD). The injector was in splitless mode. Nitrogen was the carrier gas set at a flow rate of 30 milliliters per minute (mL/min). The temperatures of the injection port and detector were 250 °C and 300 °C, respectively. The temperature program began at 50 °C and was held for 3 minutes, followed by a 15-°C-per-minute ramp until a final temperature of 200 °C was reached and held for 2 minutes.

Total organic carbon was determined using a Tekmar-Dohrmann DC-190 TOC analyzer (Rosemont Analytical Inc., Dohrmann Division, Cincinnati, Ohio).

Carbon dioxide (CO_2) concentration was measured by the flow injection analysis method.

Organic compounds (BT or DBT) in aqueous solutions were extracted using the liquid-liquid extraction method and analyzed by ultraviolet spectrophotometry (Hewlett Packard, HP 8452A Diode-array UV-Visible Spectrophotometer) and gas chromatography equipped with a flame ionization detector.

Concentration of sulfite and sulfate ions were measured by ion chromatography using a Dionex ion chromatography equipped with a Dionex pulsed electrochemical detector and a Dionex PAC-100 metal-free anion column (25 centimeters [cm] long, 4.6 mm inside diameter[i.d.]). The eluent was a mixture of 87% deionized water, 10% of 0.2N NaOH, and 3% of acetonitrile; the flowrate was 1 mL/min, and the injection loop was 50 µL in volume.

Concentration of sulfide ion was measured by adding sulfide reagents (Hach Co., Loveland, Colorado) into a 2-mL aliquot of sample, diluting to 25 mL with distilled water and detecting by a visible spectrophotometer (Hach DR/2000, Loveland, Colorado) at a wavelength of 665 nanometer (nm).

For the analysis of intermediates using GC/MS, the samples were either extracted by solvent for direct injection or derivatized in pyridine. For the derivatization, the samples were first evaporated to dryness, and then 1 mL of pyridine and 100 µL of derivatization reagent (MTBSTFA + 1% TBDMCS, Pierce Company) were added to the dry residue. The samples then were heated at 65 °C, for ~1–2 hours to assure complete derivatization, and then gently evaporated to dryness in a nitrogen steam. Finally, the residue was re-dissolved in 0.2 mL of hexane. GC/MS analysis was performed with a gas chromatograph (Hewlett-Packard Model 5890 Series II) equipped with a HP 5971 mass selective detector and a HP-5MS capillary column (30 meters [m] x 0.25 mm i.d. x 0.2-µm film thickness). The injection port temperature was 300 °C, and the column temperature, initially 50 °C, was held constant for 2 minutes, then increased to 250 °C at a ramp rate of 8 °C per minute over a 30-minute run time. The GC/MS interface line was maintained at 300 °C. The mass selective detector was scanned at a rate of 1.2 seconds per decade from mass 50 to 550. The mass spectra were produced using the standard electron ionization (70 eV) in electron

impact (EI) mode. The concentrations of the reaction intermediates were determined from the areas of isomers, benzothiophene-surfoxide, and benzothiophene-sulfur dioxide with GC/FID.

The acute toxicity was evaluated with a short-term toxicity test using *Escherichia coli* (Jardim et al., 1990). *E. coli* population was exposed for 2 days in a static system to a series of samples from the treated and untreated solutions of BT. The acute toxicity test used in this experiment is based on the degree of inhibition in the microbial activities of *E. coli*. This inhibition is quantified by measuring the amount of CO_2 produced by organisms, stressed by a given sample, and compared to that obtained by a nonstressed control. The CO_2 determination is carried out by using Warburg respirometer with paired samples. It is possible to determine the carbon dioxide produced during oxygen uptake by using two identical samples—one with NaOH and one without NaOH. The sample with NaOH in the center well measures only the oxygen uptake, while the sample without the NaOH measures the pressure change due to oxygen uptake and carbon dioxide release. The culture that received no addition acts as a control.

5. Results and Discussion

5.1 Ultrasonic Destruction of *Cryptosporidium*

5.1.1 Visualization of *Cryptosporidium* Destruction

The method we developed for quantification and qualification of viable oocyst concentrations proved to be very reproducible and reliable. It is faster than the EPA Method 1632 and is much more accurate. Using the custom cube with a fluorescent light source, oocysts appeared as brilliant apple-green spherical objects 4–6 μm in diameter with bright-lighted edges. Up to four sporozoites appeared within the oocysts as the DAPI stained their nuclei sky blue. Oocysts exhibiting both these characteristics were counted as viable oocysts. Virtually all (88–100%) of the oocysts that exhibited the characteristic brilliant apple-green spherical shape with highlighted edges contained sporozoites in samples that had undergone at least a 1-log removal by ultrasound.

Figures 7 through 10 illustrate typical images as seen on the Sony monitor during oocyst quantification.

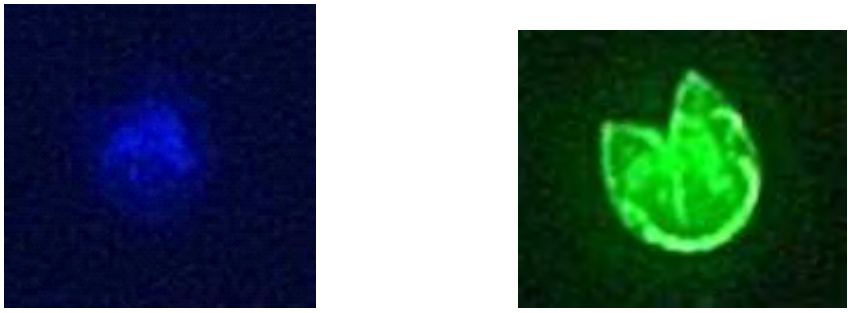

(a) (b)

Figure 7. DAPI (a) and FITC (b) images (20 times) of an open oocyst with two sporozoites.

(a)

Figure 8. DAPI (a) and FITC (b) Images (100 times) of an open oocyst with two sporozoites.

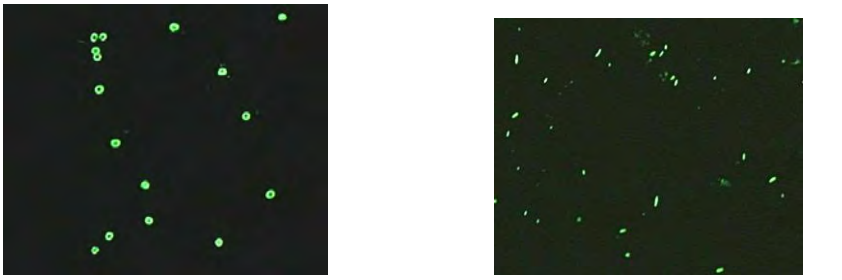

(a) (b)

Figure 9. Oocysts (20 times) prior to (a) and debris left after (b) ultrasound at 248 W/cm^2, pH 7.8, 25 °C.

(a) (b)

Figure 10. DAPI (a) and FITC (b) images (100 times) of an oocyst with four sporozoites.

We hypothesize that oocyst destruction is primarily due to physical destruction. Oocysts that are entrapped within the cavitation bubble during collapse are literally smashed to tiny pieces. Debris fields as shown in figure 9b support this conclusion. Additionally, experiments were conducted in which the ultrasonic generator probe was placed inside the well slide so that a movie capturing the ultrasonic destruction of the oocysts could be generated. The movie showed oocyst being shaterred by the ultrasonic process.

5.1.2 Effect Ultrasonic Energy Intensity

Figures 11a and b illustrate the effect of ultrasonic energy intensity on the destruction of *Cryptosporidium*. The energy intensity had a significant effect on destruction rates. At low energy intensities (83 W/cm^2), there was virtually no inactivation. As the energy intensity was increased, the destruction rate also increased. This also helps support our hypothesis. From the ultrasonic principles (appendix A), we can see that increasing the energy intensity should allow more cavitation bubbles to form. We ran experiments using up to 496 W/cm^2 and did not see significant diminishing returns as energy intensities were increased. However, at some point, we will expect to see diminishing returns as we increase energy intensity. We currently are running experiments with a new reactor capable of generating much higher energy intensities to determine what the most efficient intensity is.

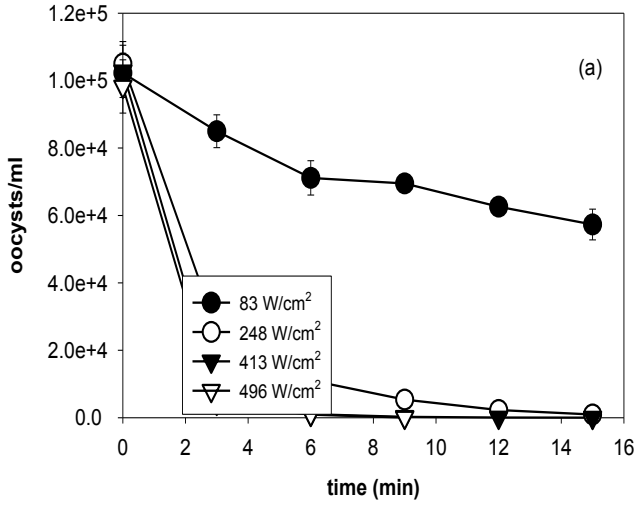

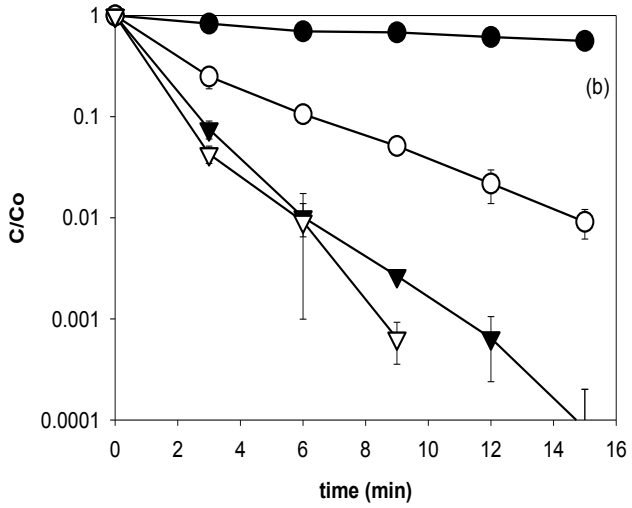

Figure 11a and b. The effect of ultrasonic energy intensity on *Cryptosporidium* destruction. (Experimental conditions: pH = 7.8, T = 25 °C.)

5.1.3 Effect of Hydrogen Peroxide

Oocysts were exposed to 10^{-1} M H_2O_2, pH 7.8, and T=25 °C without ultrasound to determine the extent of the destruction brought by $OH^{\bullet}$ radical reactions. After the prescribed time period, the $OH^{\bullet}$ radical reaction was quenched with sodium thiosulfate, and the oocyst concentration was determined. Results indicate that H_2O_2 was not effective in inactivating *Cryptosporidium*. Figure 12 shows the effect of 10^{-1}M H_2O_2 (no ultrasound) on the destruction of *Cryptosporidium*.

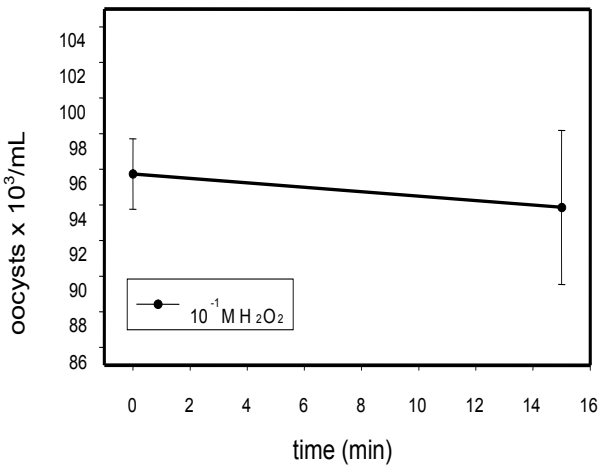

Figure 12. The effect of H_2O_2 on *Cryptosporidium* destruction (at pH = 7.8, T = 25 °C).

5.1.4 Effect of Temperature

Figures 13a and b illustrate the effect of temperature on the destruction of *Cryptosporidium*. As expected, increasing the temperature to 33 °C increased the destruction rate. Above this point, the destruction efficiency went down. The optimum temperature for this reaction lies somewhere between 33 and 50 °C. The difference between temperatures between 23 and 33 °C was negligible. This is significant because it indicates that no temperature controls would be required at treatment plants located in most climates.

5.1.5 Effect of Initial Concentration

Figure 14 illustrates the effect of the initial oocyst concentration on the reaction rate. Results indicate that the higher the initial oocyst concentration, the greater the inactivation efficiency. These results support our hypothesis that oocysts are trapped inside cavitation bubbles and are being shattered as the bubbles collapse, which is a correct assumption. When the oocyst concentration is high, the probability of oocysts being captured within cavitation bubbles increase, refecting a greater inactivation rate.

5.1.6 Effect of pH

Changes in pH did not have a significant effect on inactivation efficiency. This also supports our hypothesis. The change in pH affects the $OH^{\bullet}$ concentration but has little effect on cavitation bubble formation. We expect to see pH having a significant effect on ultrasonic processes driven by the $OH^{\bullet}$ radical reaction. Figures 15a and b illustrate the effect of pH on the destruction of *Cryptosporidium*.

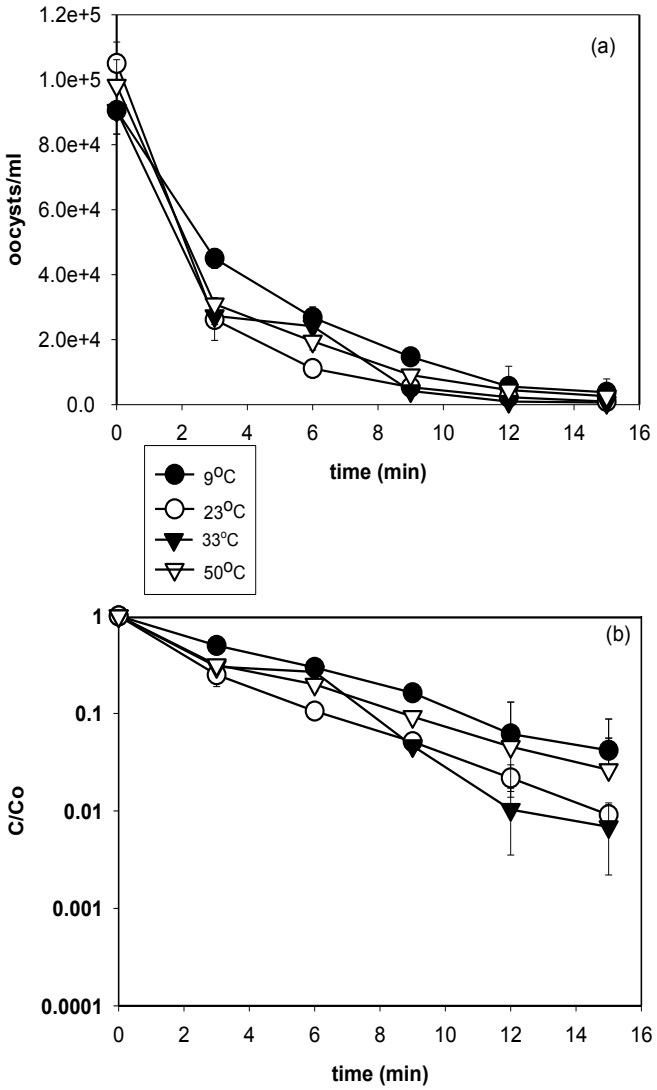

Figure 13a and b. The effect of temperature on ultrasonic *Cryptosporidium* destruction. (Experimental conditions: pH = 7.8, ultrasonic energy intensity 248 W/cm^2.)

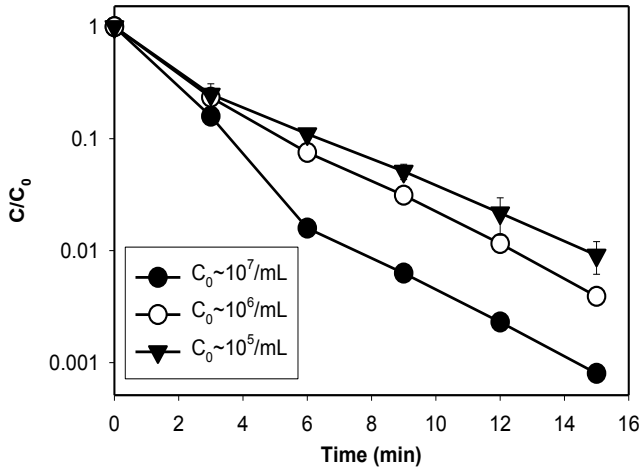

***Cryptosporidium* destruction (at pH = 7.8, T = 25 °C, energy intensity = 248 W/cm^2).**

Results clearly indicate that the primary variable in oocyst destruction is the ultrasonic energy intensity. We were able to achieve 4-log removals in 15 minutes at 413 W/cm^2. In all cases, the ultrasonic destruction of *Cryptosporidium* followed a first order reaction. The optimum pH seemed to be around 7.0, and the optimum temperature was around 33 °C. Although the efficiency was lower at pH 9.3 and at temperatures above and below 33 °C, the decrease was relatively minor. This indicates that no pretreatment or temperature controls would be required to utilize this process in real world applications.

5.2. Total Organic Carbon Degradation

5.2.1 Effect of Ultrasonic Energy Intensity

Figure 16 shows the effect of ultrasonic energy intensity on TOC decomposition of humic substances in wastewater effluent. The effect of energy intensity was tested at four different energy intensity levels (0, 142, 283, and 340 W/cm^2).

Figure 17 displays three different reaction levels. In the first level, at ultrasonic energy intensities less than 120 W/cm^2 (Level I), the rate constant does not increase significantly with increasing intensity. The ultrasonic energy intensity seems to be not high enough to break the backbone of humic substances. Between 120 and 283 W/cm^2, increasing the ultrasonic energy intensity resulted in an increase in the reaction rate constant (Level II). There is no further increase in the reaction rate above 283 W/cm^2 of energy intensity (Level III).

Since the energy intensity determines the number of cavitation bubbles and their size in unit volume of liquid (Mason, 1990), the number of bubbles and their size appear to reach their maximum values (Stage III).

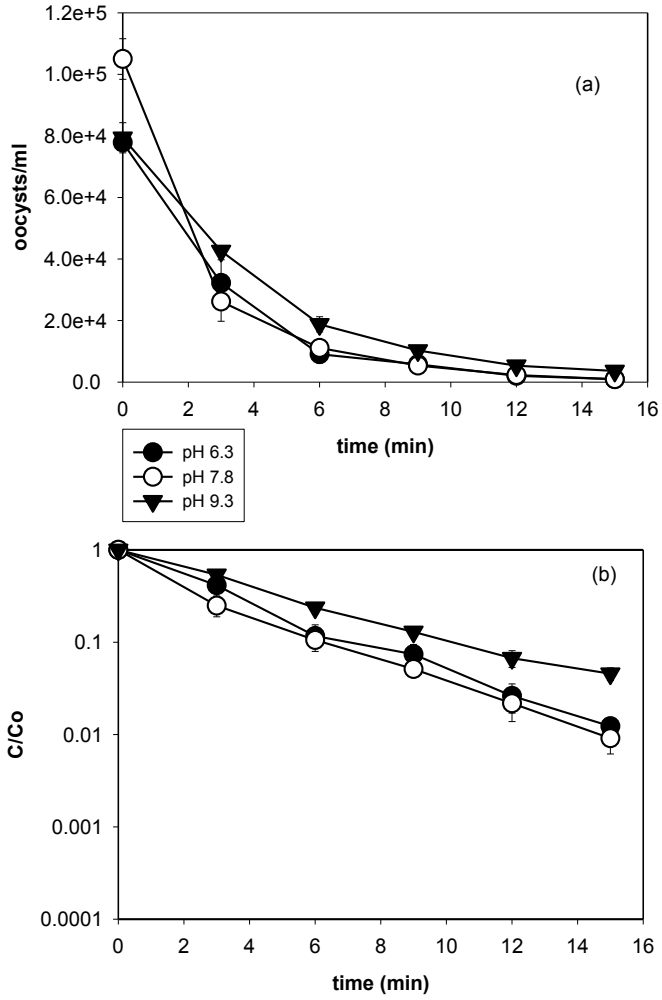

Figures 15a and b. The pH effect on ultrasonic destruction of *Cryptosporidium*. (Experimental conditions: T = 25 °C, ultrasonic energy intensity 248 W/cm^2.)

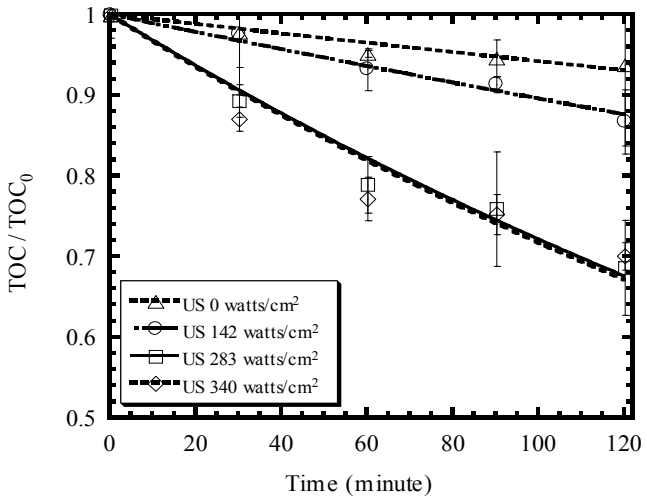

Figure 16. Effect of ultrasonic energy intensity on decomposition of HS in wastewater effluent. Experimental conditions: H_2O_2 10 mM, C_0 = TOC 10 mg/L, pH_0 = 7, temperature = 25 °C, ionic strength = 0.05 M sodium perchlorate ($NaClO_4$).

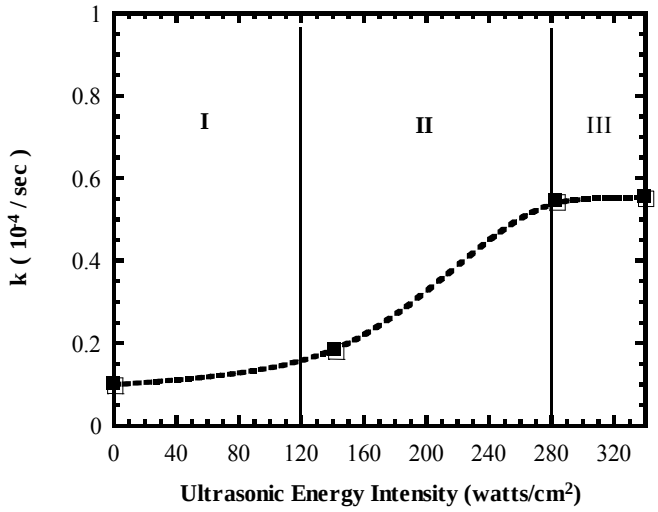

Figure 17. Effect of ultrasonic energy intensity on decomposition rate of HS in wastewater effluent. Experimental conditions: H_2O_2 10 mM, C_0 = TOC 10 mg/L, pH_0 = 7, temperature = 25 °C, ionic strength = 0.05 M $NaClO_4$.

5.2.2 Effect of Hydrogen Peroxide

The effect of hydrogen peroxide was tested at four different concentration levels of hydrogen peroxide (0, 2.5 x 10^{-3}, 5.0 x 10^{-3}, 10 x 10^{-3} Molar). Hydrogen peroxide has long been recognized as a free radical producer. Although hydrogen peroxide can be produced by sonochemical irradiation alone in aqueous solution, the amount may be not enough to be significant to decompose the humic substances in wastewater effluent. The addition of hydrogen peroxide is considered to initiate and promote the free radical reaction.

Figure 18 shows the effect of hydrogen peroxide on the TOC removal of humic substances in wastewater effluent. The extent of TOC removal increases with the increasing dose of hydrogen peroxide. While little extent of removal is observed with the ultrasound alone, over 30% of TOC removal is achieved with 10^{-2} M of hydrogen peroxide concentration after 120 minutes of reaction time.

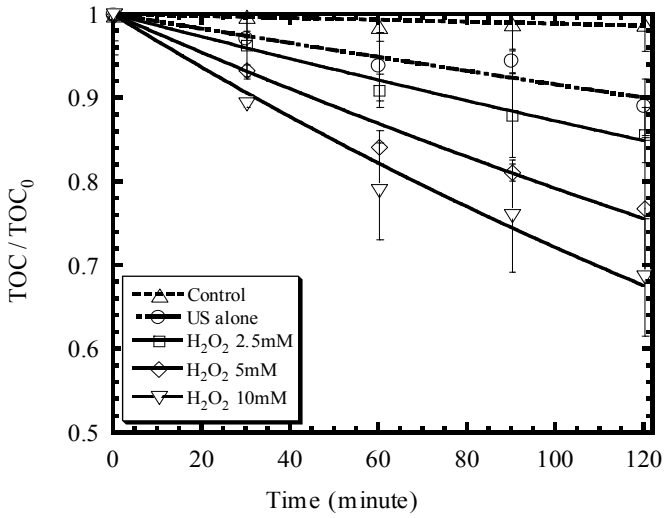

Figure 18. Effect of hydrogen peroxide on decomposition of HS in wastewater effluent. Experimental conditions: ultrasonic energy intensity = 283 W/cm^2, total volume = 10 mL, C_0 = TOC 10 mg/L, pH_0 = 7, temperature = 25 °C, ionic strength = 0.05 M $NaClO_4$.

Figure 19 shows the semi-log plot of rate constant for the reaction rate constant and the dose of hydrogen peroxide. In the experiments without sonochemical irradiation, the rate constant of TOC decomposition remains at low levels.

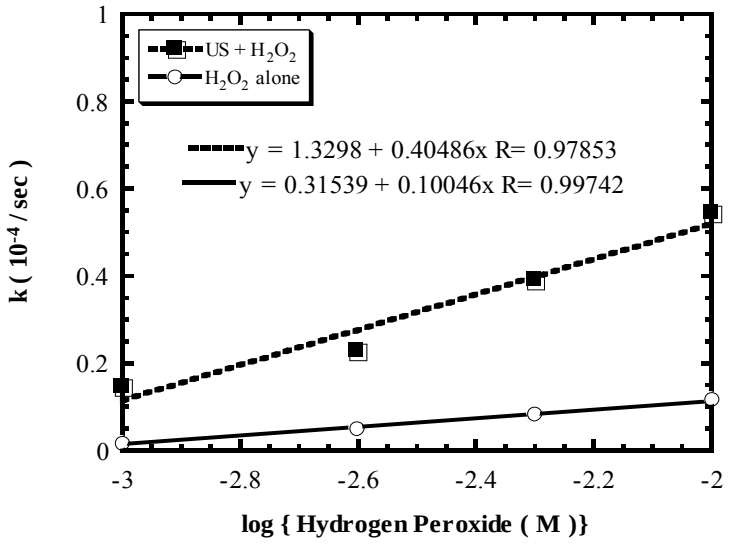

Figure 19. Effect of hydrogen peroxide on decomposition rate of HS in wastewater effluent (semi-log plot). Experimental conditions: ultrasonic energy intensity = 283 W/cm^2, total volume = 10 mL, C_0 = TOC 10 mg/L, pH_0 = 7, temperature = 25 °C, ionic strength = 0.05 M $NaClO_4$.

5.2.3 Effect of Temperature

Figure 20 shows the effect of steady-state solution temperature on TOC decomposition of humic substances in wastewater effluent. The effect of temperature was tested at four different levels (25, 35, 40, and 45 °C). The extent of TOC removal decreases as the temperature increases. The extent of TOC removal was largest at 25 °C in the temperature range of 25–45 °C. It was observed that the decomposition rate of hydrogen peroxide increased with as temperature increased.

Figure 21 shows the relationship between the temperature and the decomposition rate constant for two sonochemical systems. In the system of sonochemical reaction without hydrogen peroxide, the rate constant remains at low levels and slightly increases as temperature increases.

5.2.4 Effect of Initial TOC Concentration of Humic Substances

Figure 22 shows the effect of initial TOC concentration of humic substances on TOC decomposition in wastewater effluent. The effect of initial TOC concentration was tested at five different levels (2.5, 10, 20, 30, and 50 mg/L).

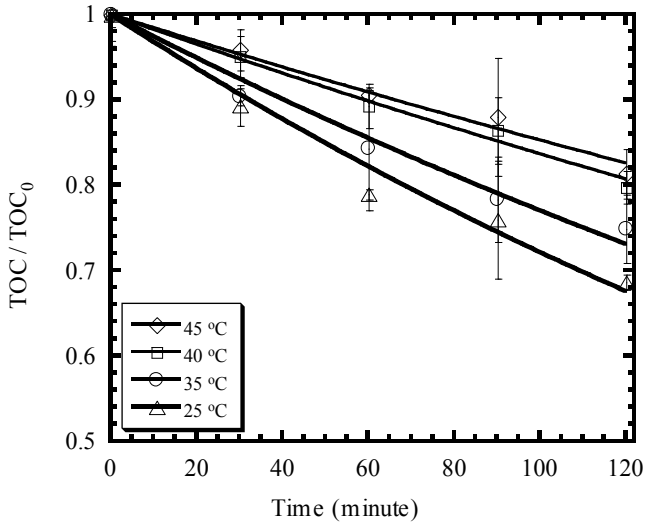

Figure 20. Effect of temperature on decomposition of HS in wastewater effluent. Experimental conditions: ultrasonic energy intensity = 283 W/cm^2, total volume = 10 mL, H_2O_2 10 mM, C_0 = TOC 10 mg/L, pH_0 = 7, ionic strength = 0.05 M $NaClO_4$.

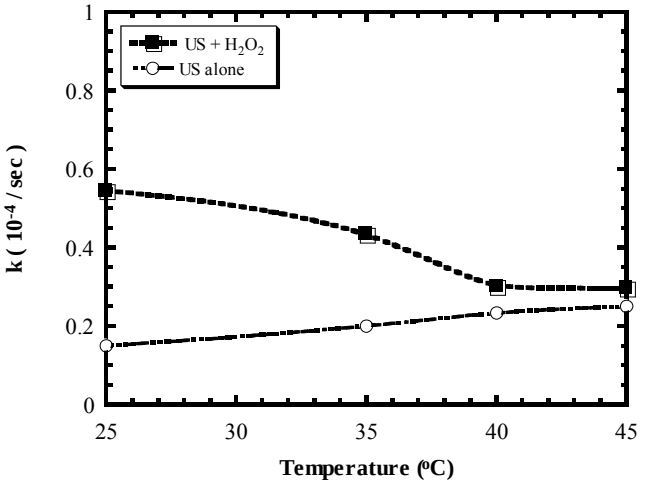

Figure 21. Effect of temperature on decomposition rate of HS in wastewater effluent. Experimental conditions: ultrasonic energy intensity = 283 W/cm^2, H_2O_2 10 mM, C_0 = TOC 10 mg/L, pH_0 = 7, ionic strength = 0.05 M $NaClO_4$.

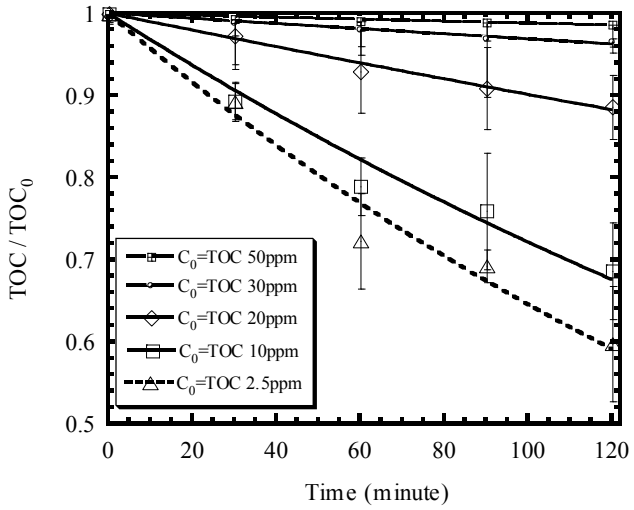

Figure 22. Effect of initial TOC concentration on decomposition of HS in wastewater effluent. Experimental conditions: ultrasonic energy intensity = 283 W/cm^2, total volume = 10 mL, H_2O_2 10 mM, pH_0 = 7, temperature = 25 °C, ionic strength = 0.05 M $NaClO_4$.

The decomposition rate decreases as the initial TOC concentration increases (figure 23). The decomposition rate was found to be dependent on the initial TOC concentration of humic substances.

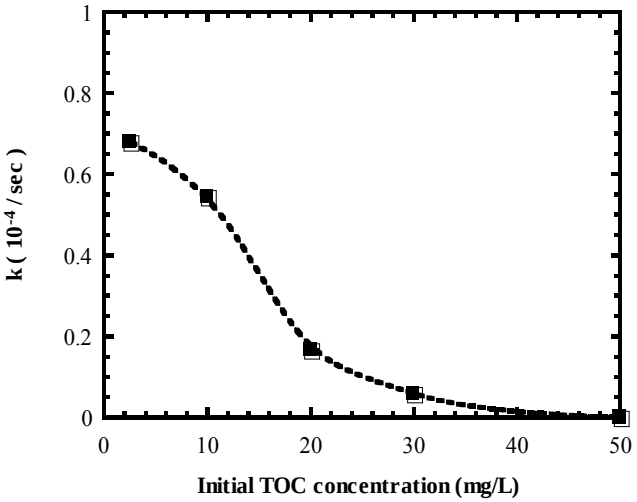

Figure 23. Effect of initial TOC concentration on decomposition rate of HS in wastewater effluent. Experimental conditions: ultrasonic energy intensity = 283 W/cm^2, H_2O_2 10 mM, pH_0 = 7, temperature = 25 °C, ionic strength = 0.05 M $NaClO_4$.

To explain the effect of initial TOC concentration on the sonochemical reaction rate, the Langmuir-Hinshelwood model was introduced and modified with the following assumptions.

1. The bubble-liquid interfacial area is regarded as a surface.

2. The main decomposition reaction of humic substances takes place in the interfacial surface; that is, the decomposition of humic substances inside cavitation bubbles and in the bulk solution is ignoble.

$$A\ (humic\ substances) \Rightarrow products\ (CO_2, H_2O) \tag{5.1}$$

The decompostion rate is taken to be proportional to the quantity of A in the interfacial surface. Then:

$$-\frac{dC_A}{dt} = k\theta_A \tag{5.2}$$

The value of θ_A is given by Langmuir isotherm:

$$\theta_A = \frac{KC_A}{(1+KC_A)} \tag{5.3}$$

Combining these two equations,

$$-\frac{dC_A}{dt} = \frac{kKC_A}{(1+KC_A)} \tag{5.4}$$

where, θ_A: the occupied fraction of the interfacial surface, A: Humic substances, C_A: TOC concentration of humic substances, k: Overall decomposition reaction rate constant, and K: ratio of k_1 and k_2 (= k_1 / k_2).

The constant k_1 and k_2 are obtained as follows.

The rate of association on interfacial surface dN_A/dt is proportional to the fraction of unoccupied sites and the TOC concentration of humic substances in solution,

$$\left(-\frac{dN_A}{dt}\right)_{association} = k_1(1-\theta_A)C_A \tag{5.5}$$

The rate of dissociation on interfacial surface is proportional to the number of molecules on the interfacial surface,

$$\left(-\frac{dN_A}{dt}\right)_{dissociation} = k_2\theta_A \tag{5.6}$$

At equilibrium, the rate of association equals the rate of dissociation, so that

$$\theta_A = \frac{k_1 C_A}{(k_2 + k_1 C_A)} = \frac{K C_A}{(1 + K C_A)} \quad (7)$$

Combining with equation 4, then we can get the equation 5.6.

If the system follows the Langmuir-Hinshelwood model, the reaction rate should be first order at sufficiently low values of C_A. As C_A increases, the order of reaction should gradually drop and become zero order.

Results of the kinetic studies for TOC removal of humic substanes were fitted with the kinetic model described above (equation 5.4), and fitted values along with correlation coefficients are show in table 3. Figure 24 shows the fitted kinetic curves for TOC removal with different initial TOC concentration of humic substances. The calculated concentration versus time profiles are obtained by numerical integration with a fourth-order Runge-Kutta routine. These fitted results indicated that the Langmuir-Hinshelwood model provided a good fit of the experimental data.

Table 3. Fitted Parameters K, k, and Coefficient of the Langmuir-Hinshelwood Model for Decomposition of Humic Substances. Conditions for Experimental Data: Ultrasonic Energy Intensity = 283 W/cm^2, Total Volume = 10 mL, H_2O_2 10 mM, pH_0 7, C_0 = TOC 10 mg/L, Temperature = 25 °C, Ionic Strength = 0.05 M $NaClO_4$

Run	TOC_0 (mg/L)	K (mg^{-1} L)	K (mg L^{-1}min^{-1})	R
1	2.5	10	0.004	0.9487
2	10	10	0.0032	0.9698
3	20	10	0.0011	0.9589
4	30	10	0.00035	0.9778
5	50	10	0.00015	0.9682

5.2.5 Effect of Solution pH

Figure 25 shows the effect of solution pH on TOC decomposition of humic substances in wastewater effluent. The effect of solution pH was tested at five different levels (4, 6, 7, 8, and 10). The extent of TOC removal increases as the solution pH decreases.

The decomposition rate of hydrogen peroxide also increases with increasing pH (Schumb, 1955). It was reported that more hydrogen peroxide was decomposed without improving oxidation of organic materials above pH 4. That is, hydrogen peroxide was decomposed without producing hydroxyl radicals (Huang et al., 1993).

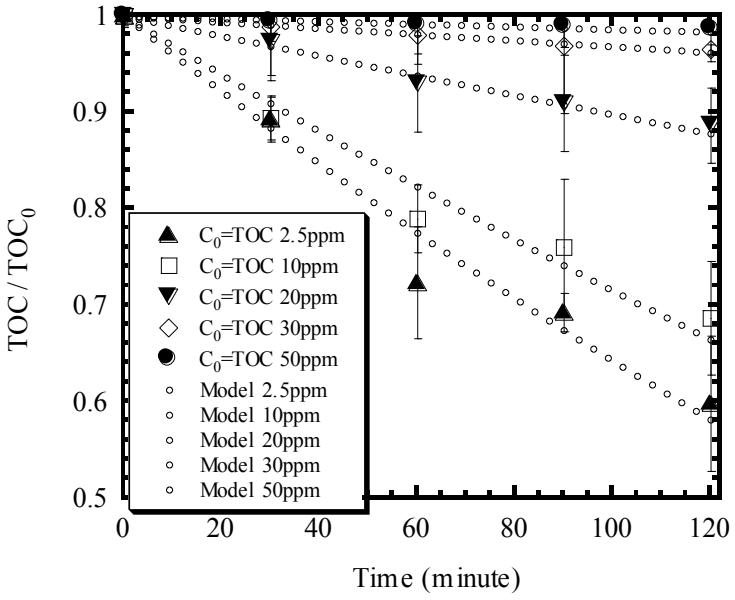

Figure 24. Kinetics of HS decomposition for different initial TOC concentrations. Experimental conditions: ultrasonic energy intensity = 283 W/cm^2, total volume = 10 mL, H_2O_2 10 mM, pH_0 7, temperature = 25 °C, ionic strength = 0.05 M $NaClO_4$.

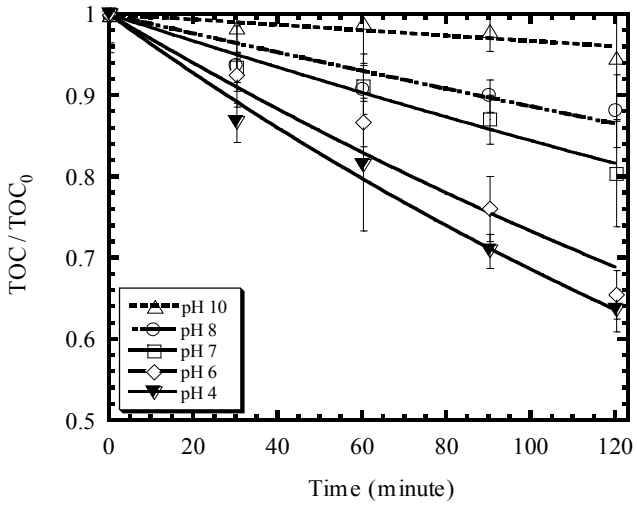

Figure 25. Effect of pH on decomposition of HS in wastewater effluent. Experimental conditions: ultrasonic energy intensity = 283 W/cm^2, total volume = 10 mL, H_2O_2 10mM, C_0 = TOC 10 mg/L, temperature = 25 °C, ionic strength = 0.05 M $NaClO_4$.

Figure 26 shows the relationship between the solution pH and the decomposition rate constant. The decomposition rate slightly decreases in the pH range of 4 to 6 and rapidly decreases as pH becomes greater than 6.

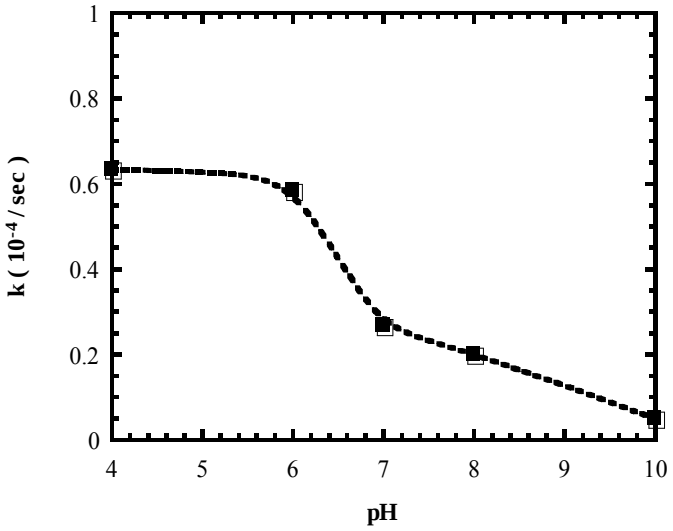

Figure 26. Effect of pH on decomposition rate of HS in wastewater effluent. Experimental conditions: ultrasonic energy intensity = 283 W/cm^2, total volume = 10 mL, H_2O_2 10 mM, C_0 = TOC 10 mg/L, temperature = 25 °C, ionic strength = 0.05 M $NaClO_4$.

A number of researchers have attempted to quantify the functional groups of humic substances, particularly the acidic groups. The main acidic groups are carboxyl (R-C = O-OH) and acidic phenolic OH groups in table 4. Similar results for humic substances from the Wilmington wastewater plant were observed (Ma, 1999).

Table 4. Functional Groups (mole per kilogram [mol/kg]) in Humic Substances (Zelazny and Carlisle, 1974)

	Total acidity	Carboxyls	Phenolic OH	Alcoholic OH	Carbonyls
Humic acids	7.20	2.00	3.10	3.60	2.60
Fulvic acids	8.60	4.00	4.60	0.80	4.30

Humic substances have variable charge components. Since their points of zero charge (pzc) are low (about 3), humic substances are negatively charged at pH values greater than 3 (Sparks, 1995). As pH increases, the degree of negative charge increases due to the deprotonation or dissociation of H^+ from functional groups. Many researchers found that the sonochemical decomposition rate decreased with increasing solution pH values (Kotronarou at al., 1991; Okouchi et al., 1992; Currell et al., 1963). It also was observed that the sonochemical

decomposition rates of polar organic compounds were smaller than those of nonpolar compounds when the similar organic compounds were tested (Seymour et al., 1997). Since it is well known that the majority of decomposition reaction takes place in bubble-liquid interface (Henglein, 1990), the enhanced accessibility and, subsequently, increased amount of less polar compound in the interface can increase the sonochemical reaction rate. Consequently, decreasing solution pH decreased the negative charge of humic substances and, hence, enhanced the sonochemical decomposition in the interface.

5.2.6 Effect of Turbidity

Figure 27 shows the effect of turbidity on TOC decomposition of humic substances in wastewater effluent. The effect of turbidity was tested at four different concentration levels of Kaolinite (1, 10, 30, and 50 mg/L).

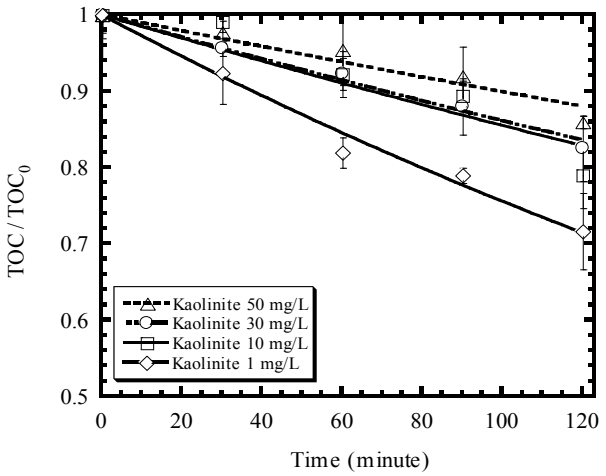

Figure 27. Effect of turbidity on decomposition of HS in wastewater effluent. Experimental conditions: ultrasonic energy intensity = 283 W/cm^2, total volume = 10 mL, H_2O_2 10 mM, pH_0 7, C_0 = TOC 10 mg/L, temperature = 25 °C, ionic strength = 0.05 M $NaClO_4$.

The decomposition rate decreases as the turbidity increases in the range of 1–10 mg/L of Kaolinite, then slightly decreases upon further increase in the turbidity above 10 mg/L (figure 28).

5.2.7 Effect of Total Carbonate

Figure 29 shows the effect of total carbonate on decomposition of humic substances measured by TOC in wastewater effluent. The effect of total carbonate was tested at four different concentration levels of sodium carbonate (0, 50, 150, and 300 mM of sodium carbonate).

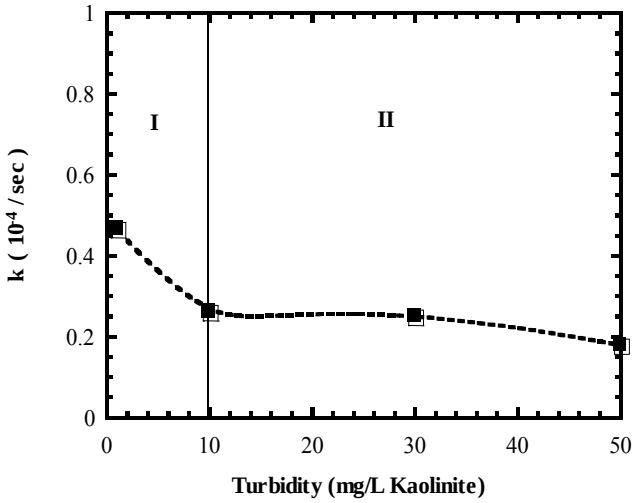

Figure 28. Effect of turbidity on decomposition rate of HS in wastewater effluent. Experimental conditions: ultrasonic energy intensity = 283 W/cm^2, total volume = 10 mL, H_2O_2 10 mM, pH_0 7, C_0 = TOC 10 mg/L, temperature = 25 °C, ionic strength = 0.05 M $NaClO_4$.

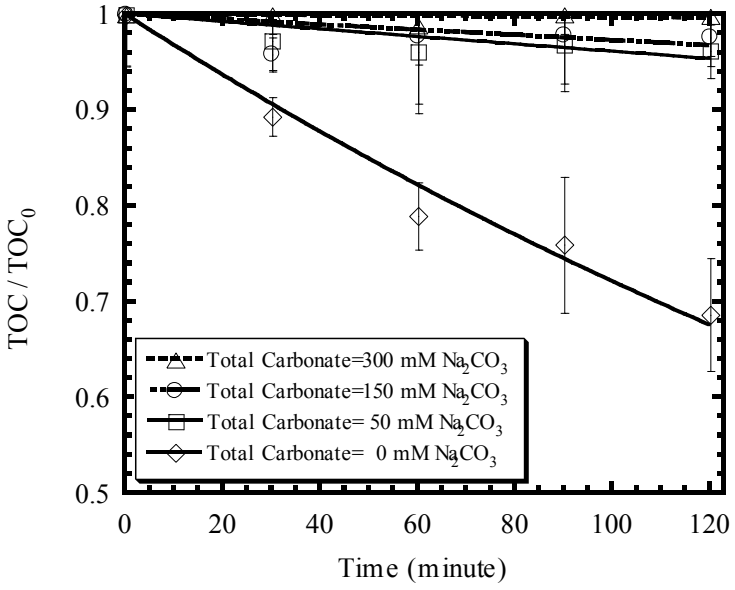

Figure 29. Effect of total carbonate on decomposition of HS in wastewater effluent at ultrasonic energy intensity = 283 W/cm^2, total volume = 10 mL, H_2O_2 10 mM, C_0 = TOC 10 mg/L, pH_0 = 7, temperature = 25 °C, ionic strength = 0.05 M $NaClO_4$.

The extent of TOC removal decreases as the concentration of total carbonate increases. After 120 minutes of reaction time, the extent of TOC removal without addition of sodium carbonate reaches 31%, while the removal extents with sodium carbonate concentrations of 50, 150, and 300 mM are below 10% in the given experimental condition.

Figure 30 shows the semi-log plot of TOC removal of humic substances over reaction time. The decomposition trend of humic substances without carbonate appears to follow the first-order kinetics in the initial stage of the reaction.

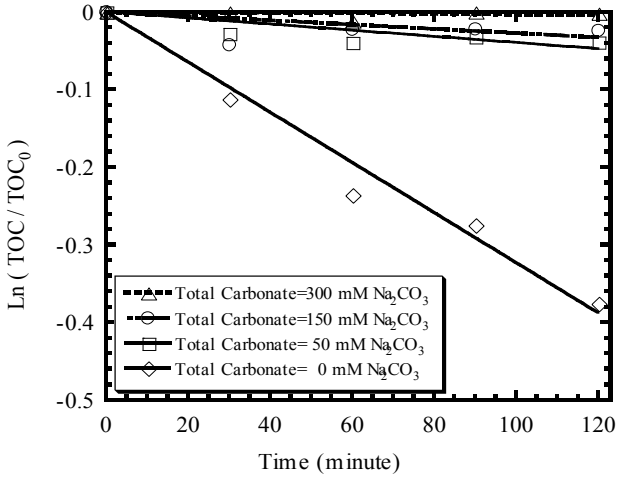

Figure 30. Effect of total carbonate on decomposition of HS in wastewater effluent (semi-log plot). Experimental conditions: ultrasonic energy intensity = 283 W/cm^2, total volume = 10 mL, H_2O_2 10 mM, C_0 = TOC 10 mg/L, pH_0 = 7, temperature = 25 °C, ionic strength = 0.05 M $NaClO_4$.

The carbonate and bicarbonate are well-known radical scavengers and compete with hydroxyl radical scavengers to inhibit the reaction between the humic substances and hydroxyl radicals. Therefore, carbonate and bicarbonate decrease the sonochemical decomposition rate of humic substances (figure 31).

Figure 32 shows the semi-log plot of the total carbonate concentration and the reaction rate constant.

5.2.8 Effect of Metal Ions

5.2.8.1 Aluminum (Al)

Figure 33 shows the effect of Al(III) on TOC decomposition of humic substances in wastewater effluent. The effect of Al(III) was tested at four different concentration levels of Al(II) (0, 1, 5, and 10 mg/L). The extent of TOC removal decreases with increasing the Al(II) concentration.

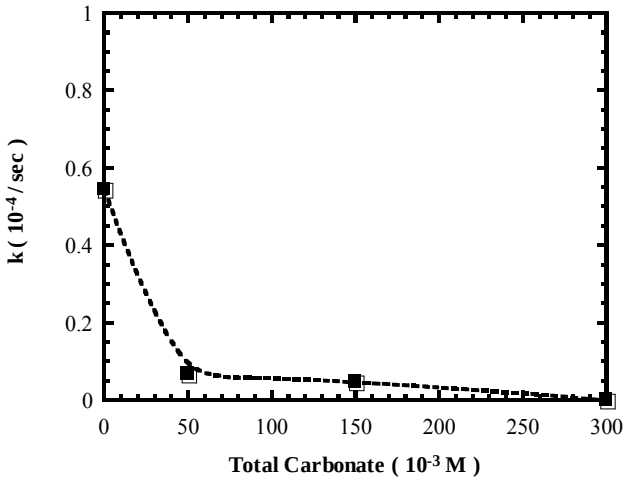

Figure 31. Effect of total carbonate on decomposition rate of HS in wastewater effluent. Experimental conditions: ultrasonic energy intensity = 283 W/cm^2, total volume = 10 mL, H_2O_2 10 mM, C_0 = TOC 10 mg/L, pH_0 = 7, temperature = 25 °C, ionic strength = 0.05 M $NaClO_4$.

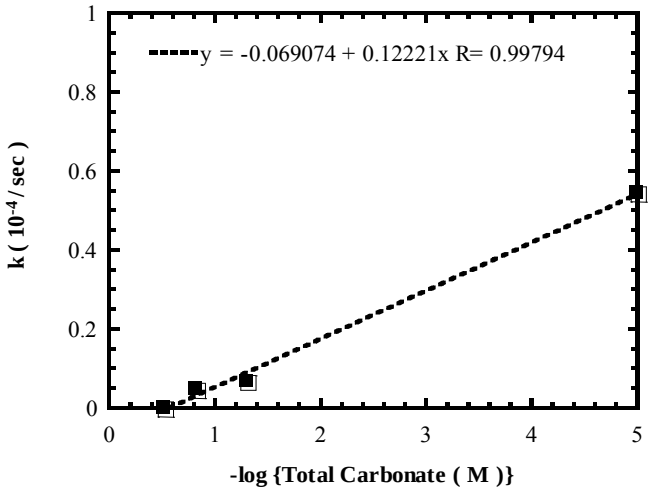

Figure 32. Effect of total carbonate on decomposition rate of HS in wastewater effluent (semi-log plot). Experimental conditions: ultrasonic energy intensity = 283 W/cm^2, total volume = 10 mL, H_2O_2 10 mM, C_0 = TOC 10 mg/L, pH_0 = 7, temperature = 25 °C, ionic strength = 0.05 M $NaClO_4$.

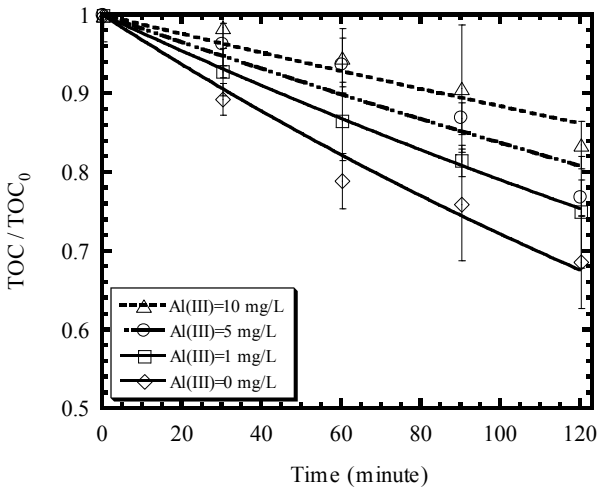

Figure 33. Effect of Al(III) on decomposition of HS in wastewater effluent. Experimental conditions: ultrasonic energy intensity = 283 W/cm^2, total volume = 10 mL, H_2O_2 10 mM, pH_0 7, C_0 = TOC 10 mg/L, temperature = 25 °C, ionic strength = 0.05 M $NaClO_4$.

The decomposition rate decreases rapidly as the dose of Al(III) increases from 0 to 1 mg/L, then decreases slightly above 1 mg/L of Al(III) concentration (figure 34).

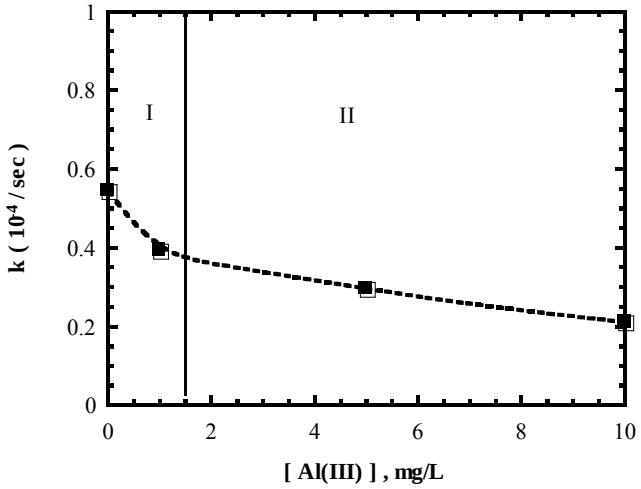

Figure 34. Effect of Al(III) on decomposition rate of HS in wastewater effluent. Experimental conditions: ultrasonic energy intensity = 283 W/cm^2, total volume = 10 mL, H_2O_2 10 mM, pH_0 7, C_0 = TOC 10 mg/L, temperature = 25 °C, ionic strength = 0.05 M $NaClO_4$.

5.2.8.2 Calcium

Figure 35 shows the effect of Ca(II) on TOC decomposition of humic substances in wastewater effluent. The effect of Ca(II) was tested at four different concentration levels of Ca(II) (0, 50, 100, and 200 mg/L).

The decomposition rate decreases as the Ca(II) concentration increases from 0 to 100 mg/L, then remains constant above 100 mg/L of Ca(II) concentration (figure 36).

5.2.8.3 Magnesium

Figure 37 shows the effect of Mg(II) on TOC decomposition of humic substances in wastewater effluent. The effect of Mg(II) was tested at four different concentration levels of Mg(II) (0, 5, 20, and 50 mg/L).

The decomposition rate decreases as the Mg(II) concentration increases from 0 to 5 mg/L, then decreases slightly above 5 mg/L of Mg(II) concentration (figure 38).

5.2.8.4 Iron

Figure 39 shows the effect of Fe(II) on TOC decomposition of humic substances in wastewater effluent. The effect of Fe(II) was tested at four different concentration levels of Mg(II) (0, 0.5, 1, and 5 mg/L).

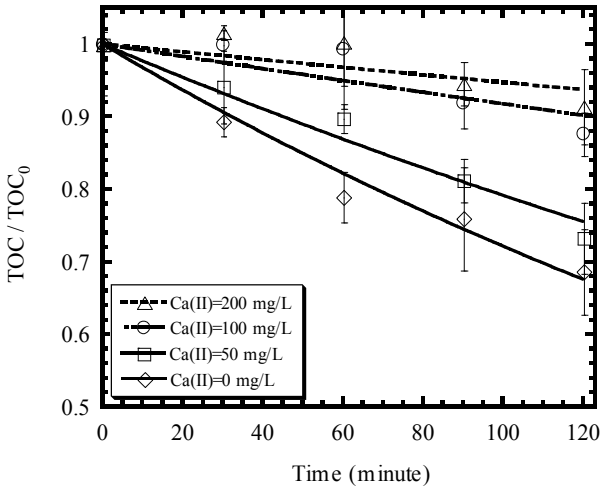

Figure 35. Effect of Ca(II) on decomposition of HS in wastewater effluent. Experimental conditions: ultrasonic energy intensity = 283 W/cm^2, total volume = 10 mL, H_2O_2 10 mM, pH_0 7, C_0 = TOC 10 mg/L, temperature = 25 °C, ionic strength = 0.05 M $NaClO_4$.

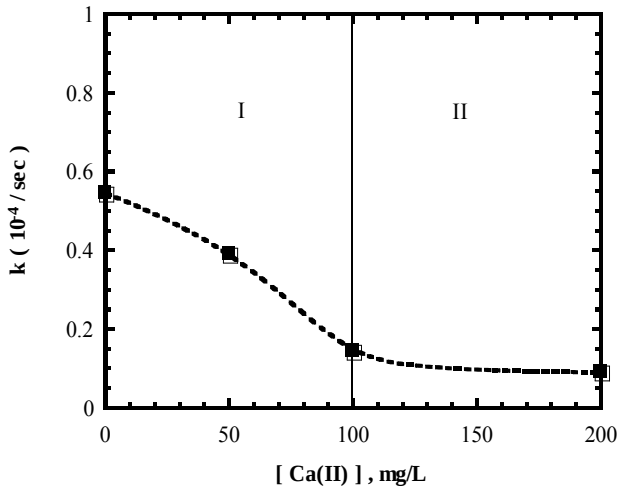

Figure 36. Effect of Ca(II) on decomposition rate of HS in wastewater effluent. Experimental conditions: ultrasonic energy intensity = 283 W/cm^2, total volume = 10 mL, H_2O_2 10 mM, pH_0 7, C_0 = TOC 10 mg/L, temperature = 25 °C, ionic strength = 0.05 M $NaClO_4$.

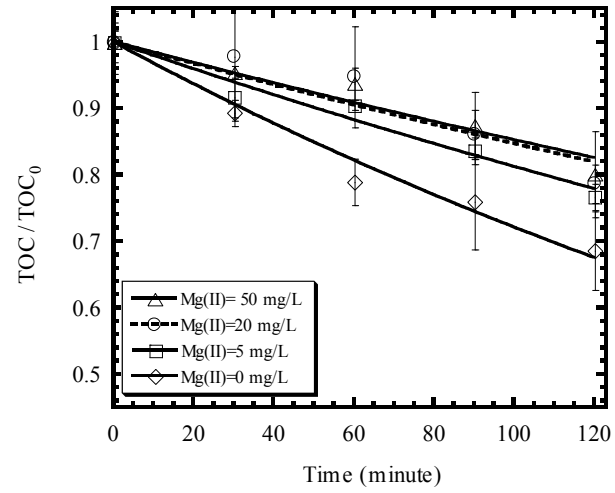

Figure 37. Effect of Mg(II) on decomposition of HS in wastewater effluent. Experimental conditions: ultrasonic energy intensity = 283 W/cm^2, total volume = 10 mL, H_2O_2 10 mM, pH_0 7, C_0 = TOC 10 mg/L, temperature = 25 °C, ionic strength = 0.05 M $NaClO_4$.

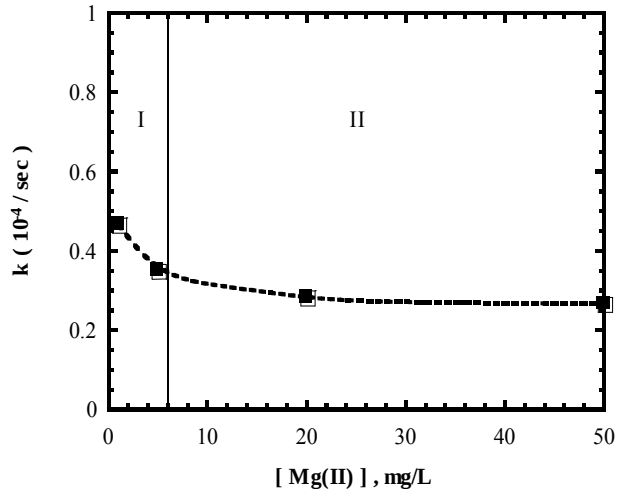

Figure 38. Effect of Mg(II) on decomposition rate of HS in wastewater effluent. Experimental conditions: ultrasonic energy intensity = 283 W/cm^2, total volume = 10 mL, H_2O_2 10mM, pH_0 7, C_0 = TOC 10 mg/L, temperature = 25 °C, ionic strength = 0.05 M $NaClO_4$.

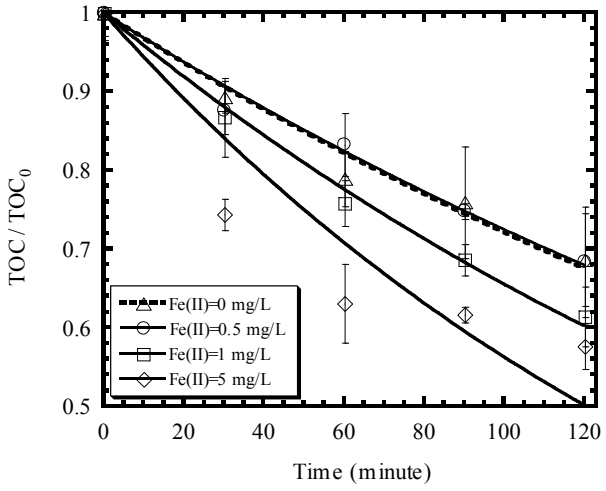

Figure 39. Effect of Fe(II) on decomposition of HS in wastewater effluent. Experimental conditions: ultrasonic energy intensity = 283 W/cm^2, total volume = 10 mL, H_2O_2 10 mM, pH_0 7, C_0 = TOC 10 mg/L, temperature = 25 °C, ionic strength = 0.05 M $NaClO_4$.

The extent of TOC removal increases with increasing the Fe(II) concentration. The change of the decomposition rate shows a similar trend to that with Fe(II). The decomposition rate has small change with a small dose (0.5 mg/L), but it increases rapidly from 0.5 to 2 mg/L, then increases slightly from 2 to 5 mg/L of Fe(II) concentration (figure 40).

5.2.8.5 Manganese

Figure 41 shows the effect of Mn(II) on TOC decomposition of humic substances in wastewater effluent. The effect of Mn(II) was tested at four different concentration levels of Mg(II) (0, 0.5, 1, and 5 mg/L).

The weak acid character of humic substances is ascribed to complexation with free metals, such as Al(III), Mg(II), and Ca(II), and hydroxy-metals (Martin and Reeve, 1958). Two significant modes of binding are as following: (1) the formation complexes or chelates between the functional groups of the humic substances and metal, and (2) an association between the humic substances and colloidal particles of metal hydroxide (possibly through sorption on the surface of the particle), whereby the colloidal particles are stabilized in suspension. If two or more organic functional groups coordinate the metal ion, forming an internal ring structure, chelation, a form of complexation, occurs (figure 4.30). It also was reported that adsorption of humic substances onto kaolinite took place to a large extent (Jayasundera et al., 1997).

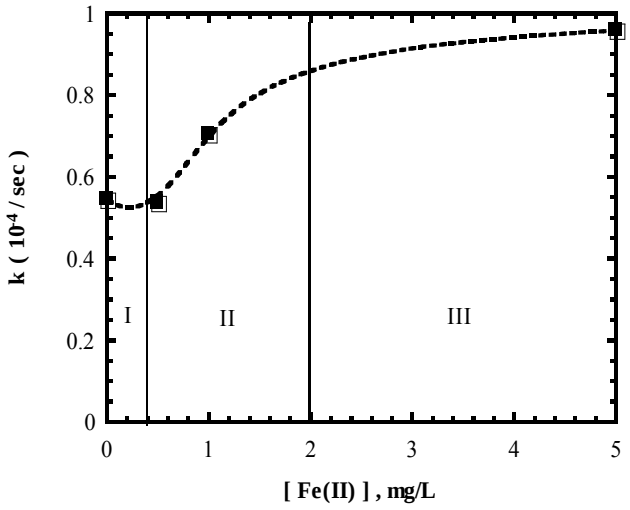

Figure 40. Effect of Fe(II) on decomposition rate of HS in wastewater effluent. Experimental conditions: ultrasonic energy intensity = 283 W/cm^2, total volume = 10 mL, H_2O_2 10 mM, pH_0 7, C_0 = TOC 10 mg/L, temperature = 25 °C, ionic strength = 0.05 M $NaClO_4$.

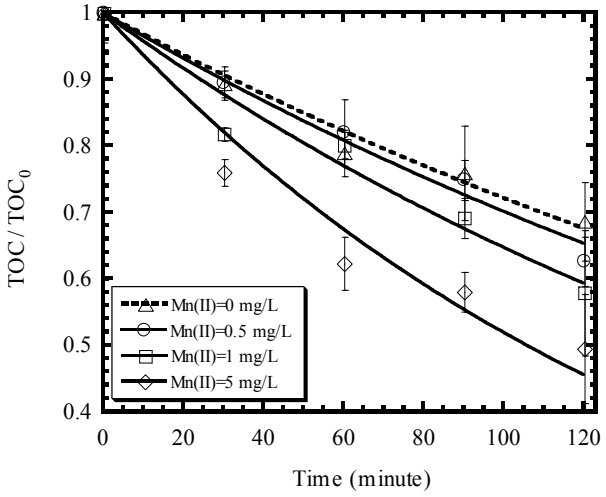

Figure 41. Effect of Mn(II) on decomposition of HS in wastewater effluent. Experimental conditions: ultrasonic energy intensity = 283 W/cm^2, total volume = 10 mL, H_2O_2 10 mM, pH_0 7, C_0 = TOC 10 mg/L, temperature = 25 °C, ionic strength = 0.05 M $NaClO_4$.

The above two mechanisms, complexation and sorption, appear to increase the degree of aggregation of humic substances and, consequently, inhibit the transport of humic substances which and their monomers produced through the depolymerization of HS polymers; then they decreases the overall decomposition rate of humic substances. This trend is observed at the Stage I in figures 34, 38, 40, and 42. Beyond the complexation and sorption capacity of humic substances, the surplus dose of metal ions and Kaolinite seems to have no more inhibitory effect on the reaction rate (Stage II).

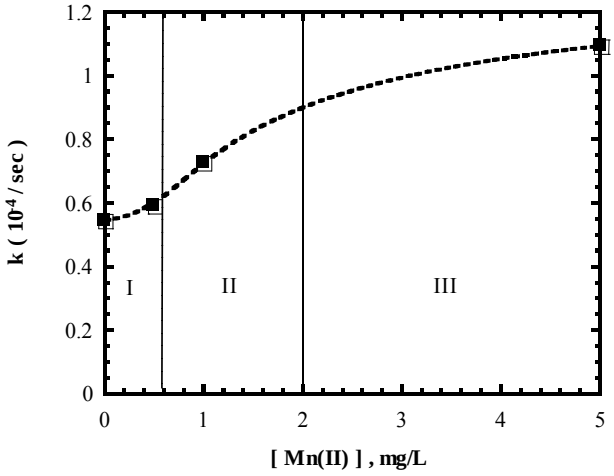

Figure 42. Effect of Mn(II) on decomposition rate of HS in wastewater effluent. Experimental conditions : ultrasonic energy intensity = 283 watts/cm^2, total volume = 10 mL, H_2O_2 10 mM, pH_0 7, C_0 = TOC 10 mg/L, temperature = 25 °C, ionic strength = 0.05 M $NaClO_4$.

The determination of stability constants for HS-metal complexes provides information on the affinity of the metal for the organic ligand (figure 43). Schmitzer and Hansen (1970) reported the stability constants for metal-HS complexes and found that the order of stability was:

Fe(III) > Al(III) > Cu(II) > Ni(II) > Co(II) > Pb(II) > Ca(II) > Zn(II) > Mn(II) > Mg(II)

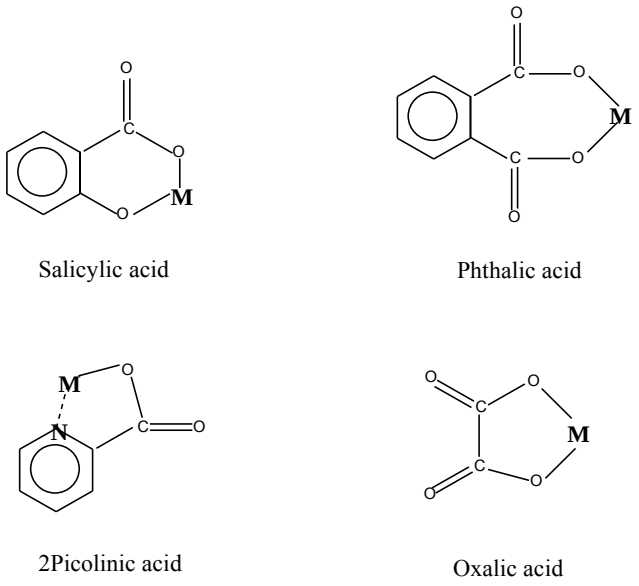

Figure 43. Chelation of metal ions by organic compounds (Thurman, 1985).

Figure 44 shows the variation of decomposition rate of humic substances versus the dose of five different metal ions. The decomposition rates increase significantly with an increasing dose of Fe(II) and Mn(II), while the rates decrease with an increasing dose of Al(III), Ca(II), and Mg(II). Fe(II) and Mn(II) show an important catalytic effect promoting the decomposition of humic substances in wastewater effluent. It was observed that Fe(II) and Mn(II) showed the catalytic effect combining with hydrogen peroxide (Schumb, 1955). The catalytic effect of transition metals (manganese and iron) also was found in ozonation processes for decomposition of humic substances (Gracia et al., 1995). The Mn(II) had a larger extent of TOC removal of humic substances than that of Fe(II) in ozonation.

The mechanism of the reaction of hydrogen peroxide with transition metals as catalysts consists of initiating the hydrogen peroxide decomposition chain producing $^{\cdot}OH$ radicals. For the start of radical chain reaction, transition metals as an initiator transfer an electron to hydrogen peroxide. It is known that sonochemical irradiation can initiate and promote the hydrogen peroxide decomposition producing $^{\cdot}OH$ radicals. The larger extent of TOC removal of humic substances previously was obtained with a dose of hydrogen peroxide in the experiments investigating the concentration effect of hydrogen peroxide.

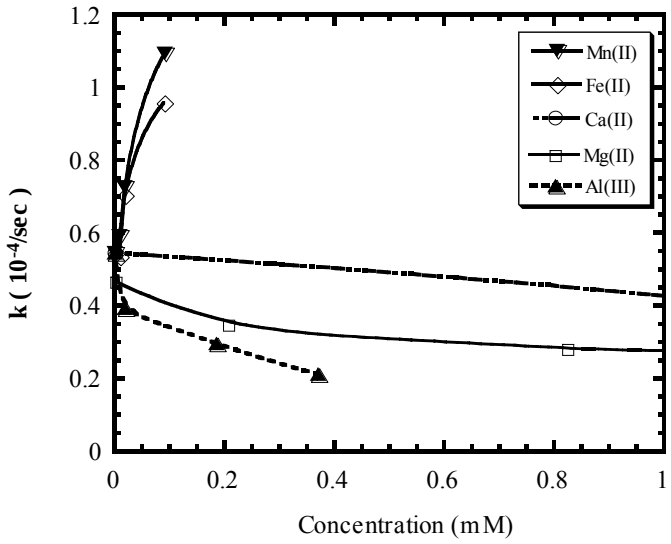

Figure 44. Effect of different metal ions on decomposition rate of humic substances in wastewater effluent. Experimental conditions: ultrasonic energy intensity = 283 W/cm^2, total volume = 10 mL, H_2O_2 10 mM, pH_0 7, C_0 = TOC 10 mg/L, temperature = 25 °C, ionic strength = 0.05 M $NaClO_4$.

Consequently, the sonochemical irradiation and the catalytic effect of transition metals initiates and promotes the radical reaction with hydrogen peroxide, which increases the extent and the decomposition rate of humic substances.

It is observed that the sonochemical reaction in the presence of transition metal has three different reaction stages (figures 40 and 42). At the first stage, the small dose of Fe(II) and Mn(II) has no significant catalytic effect. The abundant carboxylic and phenolic groups of humic substances appear to scavenge the OH radicals generated at this leg phase. The large amount of OH radicals produced by the increasing dose of transient metals decomposes the humic substances, then mineralizes to carbon dioxide (Stage II). But the carbonate ions produced at Stage II start to work as the competitive radical scavengers (Stage III).

Figure 45 illustrates the decrease in THMFP as a function of sonochemical reaction time with different dose levels of hydrogen peroxide.

5.3 Decomposition of Benzothiophene

Target polycyclic aromatic compound (PAC) solutions (40 mL) were exposed to ultrasonic irradiation at an energy output of 400 watts (226 W/cm^2). The amount of organic compound remaining in solution decreases exponentially over time (figure 46).

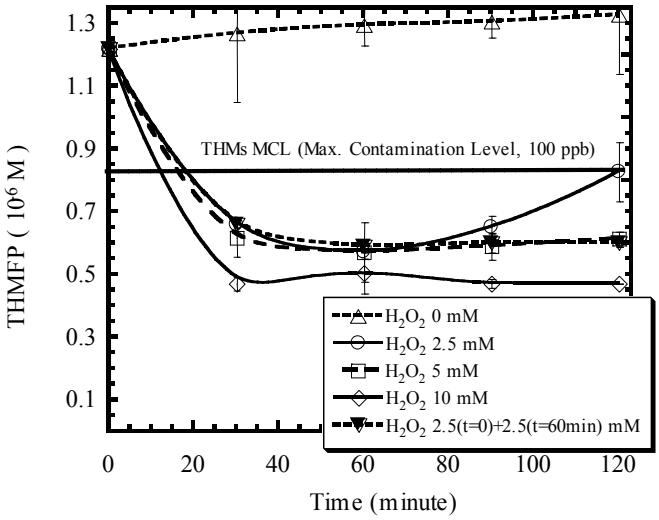

Figure 45. Effect of ultrasonis irradiation and hydrogen peroxide on THMFP of HS in wastewater effluent (Wilmington Wastewater Plant). Experimental conditions : ultrasonic energy intensity = 283 W/cm^2, total volume = 10 mL, pH$_0$ 7, C$_0$ = TOC 10 mg/L, temperature = 25 °C, ionic strength = 0.05 M NaClO$_4$.

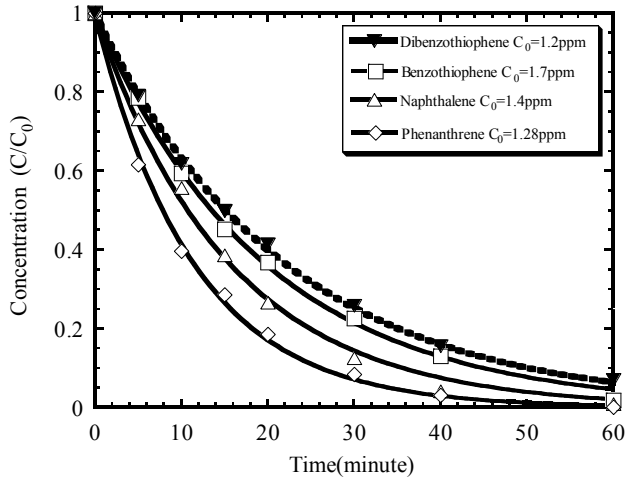

Figure 46. Sonochemical decomposition of PACs in aqueous solutions. Experimental conditions: ultrasonic energy intensity = 226 W/cm^2, total volume = 40 mL, pH = 5, temperature = 25 °C, ionic strength = 0.05 M NaClO$_4$.

The decomposition of all benzothiophene proceeds rapidly. The other PACs, such as dibenzothiophene, naphthalene, and phnanthrene, were tested with the same experimental methods. Little decomposition was observed in the controls. The degradation rate can be expressed by the following equation:

$$-\frac{d[C]}{dt} = k[C] \quad \text{or} \quad C = C_0 \exp(-kt) \tag{4.10}$$

where, C = the concentration of target compounds at time t, C_o = initial concentration, k = rate constant, and t = sonication time.

The calculated rate constants are 7.63 x 10^{-4} sec^{-1} for DBT, 8.53 x 10^{-4} sec^{-1} for BT, 10.77 x 10^{-4} sec^{-1} for naphthalene, and 14.67 x 10^{-4} sec^{-1} for phenanthrene.

5.3.1 Effect of Ultrasonic Energy Intensity

Increasing energy density will accelerate the decomposition rate of organic compounds. Huang (1994) reported that enhancing energy density increases the reactivity. Target organic compound in aqueous solution was exposed to ultrasonic irradiation at different energy outputs from 80 to 400 watts. This is equivalent to an energy intensity of 45 to 226 W/cm^2. As described above, the amount of BT present in solution decreases exponentially over sonochemical reaction time. The rate of decomposition increases with increasing of energy density. Figure 47 shows the first-order plot of BT verses the reaction time.

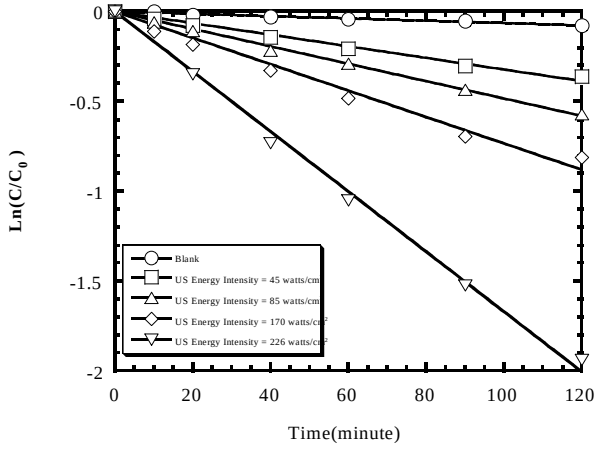

Figure 47. Effect of ultrasonic energy intensity on sonochemical decomposition of benzothiophene. Experimental conditions: total volume = 40 mL, C_0 = 0.12 mM, pH = 5, temperature = 25 °C, ionic strength = 0.05 M $NaClO_4$.

The rate constant, k, can be obtained as a function of ultrasonic energy input from the slopes of semi-log plots. From figure 48, a linear relationship is found between the energy intensity and the rate constant within the range studied here.

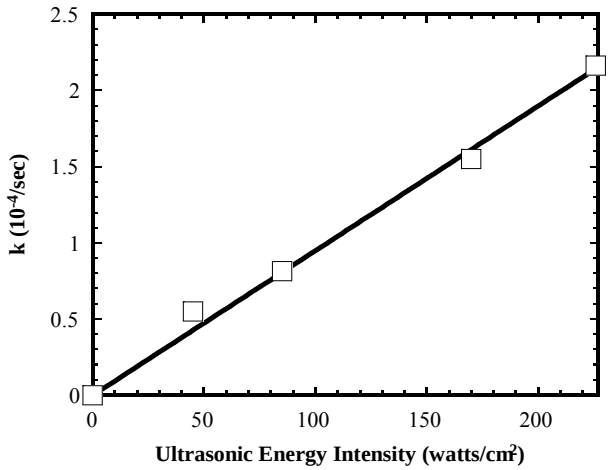

Figure 48. Ultrasonic energy intensity versus rate constant. Experimental conditions: total volume = 40 mL, C_0 = 0.12 mM, pH = 5, temperature = 25 °C, ionic strength = 0.05 M $NaClO_4$.

5.3.1.1 Effect of Temperature

Figure 49 shows the changes of BT concentration at various temperatures.

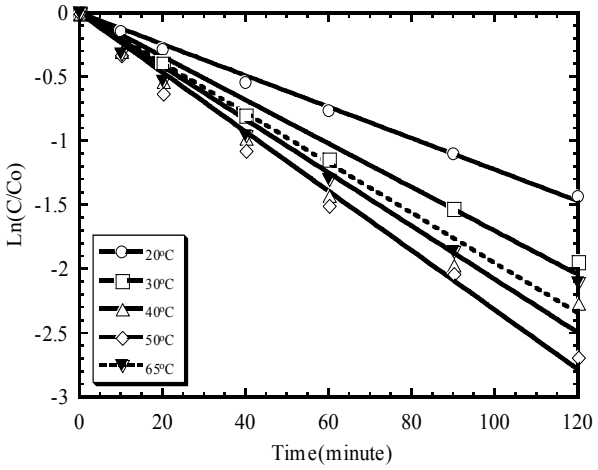

Figure 49. Effect of temperature on sonochemical decomposition of benzothiophene. Experimental conditions ultrasonic energy intensity = 226 W/cm^2, total volume = 40 mL, C_0 = 0.12 mM, pH = 5, ionic strength = 0.05 M $NaClO_4$.

Figure 50 shows that the reaction rate increases as the temperature increases from 20 to 50 °C, then decreases upon further increase in the temperature above 50 °C.

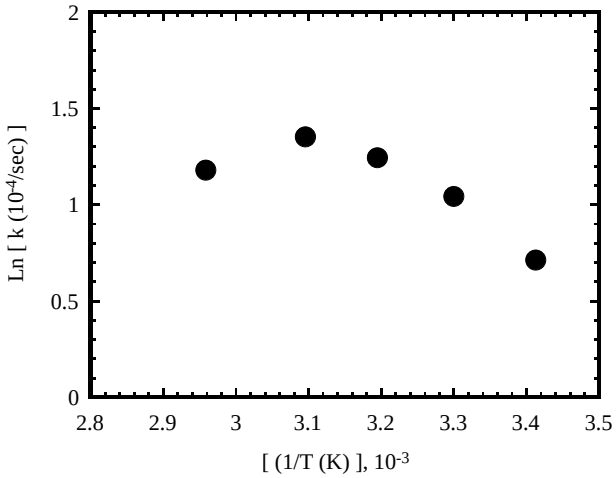

Figure 50. Temperature versus rate constant. Experimental conditions: ultrasonic energy intensity = 226 W/cm^2, total volume = 40 mL, C_0 = 0.12 mM, pH = 5, ionic strength = 0.05 M $NaClO_4$.

Various researchers have reported the effect of temperature on the sonochemical decomposition of organic compounds. Gondrexon et al. (1993) examined the effect of temperature on the decomposition of the chlorophenol in the range of 25 to 50 °C. Results show that the higher the temperature, the larger the reaction rate. Koszalka (1992) reported a high removal efficiency of 85% in the temperature range of 25 to 35°C for tetrachloromethane and a low removal efficiency of about 48% between 85 and 95 °C. It has been suggested to avoid somochemical reactions near the boiling point of the solvent. Since the negative pressure in the cavitation bubble decreases the boiling point, any cavitation bubbles formed will fill with water vapor almost instantaneously (Mason, 1990). This water vapor could reduce the extremes of temperature and pressure generated and, decrease the decomposition efficiency of the organic compounds. In the temperature range of 20 to 50 °C, the Arrhenius equation is shown as following:

$$k = 0.21 \exp\left(\frac{-0.002}{T}\right) \quad \left(r^2 = 0.98\right) \tag{4.11}$$

where, k = rate constant in S^{-1}, T = steady-state temperature in K.

The low apparent activation energy value, 16.7 kJ/mole indicates that the sonochemical reaction at least for BT is controlled by the diffusion step (Laidler, 1965).

5.3.2 Effect of the Solution pH

The solution pH is an important factor in determining the physical and chemical properties of the solution. Kotronarou et al. (1991) found that the reaction rate

decreased with increasing the initial pH of the solution, while Wu et al. (1992) showed that the reaction rate of carbon tetrachloride increased at high initial pH.

The pH of the solution should change as a result of sonochemical degradation of organic compounds. The pH decreased in all cases due to the formation of acids during sonochemical reactions. Figure 51 shows the changes of BT concentration as a function of initial pH.

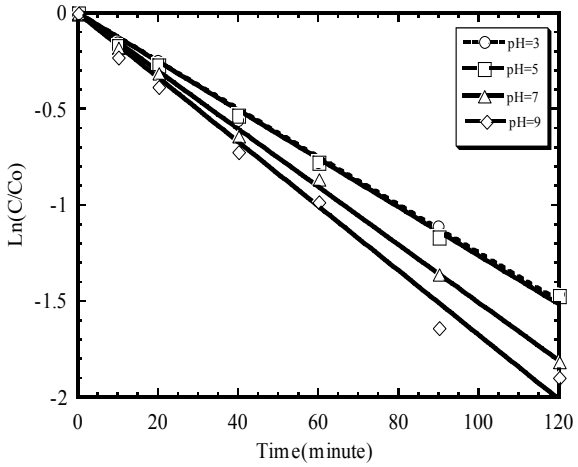

Figure 51. Effect of pH on sonochemical decomposition of benzothiophene. Experimental conditions: ultrasonic energy intensity = 226 W/cm^2, total volume = 40 mL, C_0 = 0.1 mM, temperature = 25 °C, ionic strength = 0.05 M $NaClO_4$.

The reaction rate remains constant in the pH range of 3 to 6 and slightly increases as pH becomes greater than 6 as shown in figure 52.

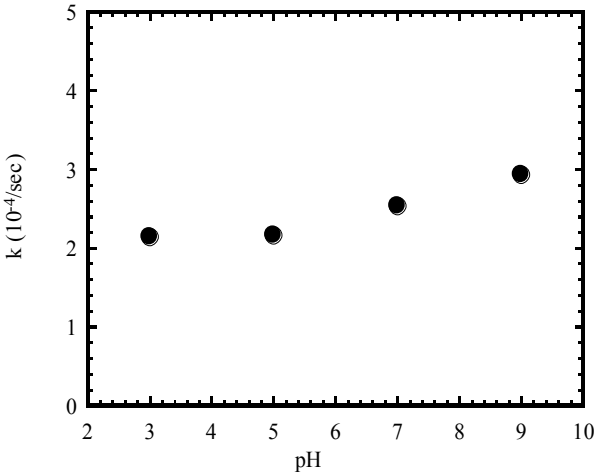

Figure 52. pH versus rate constant. Experimental conditions: ultrasonic energy intensity = 226 W/cm^2, total volume = 40 mL, C_0 = 0.1 mM, temperature = 25 °C, ionic strength = 0.05 M $NaClO_4$.

5.3.3 Effect of Initial Concentration

Though sonochemical reaction of BT appears to follow the first-order kinetics, the reaction rate was found to be dependent on the initial concentration of BT (figure 53).

While the residual concentration of BT decreases exponentially with time irrespective of the BT initial concentration, the first-order rate constant decreases from 8.2×10^{-4} sec^{-1} at $C_0 = 0.01$ mM to 2.3×10^{-4} sec^{-1} at $C_0 = 0.21$ mM. Figure 54 shows the plot of log k versus log C_0.

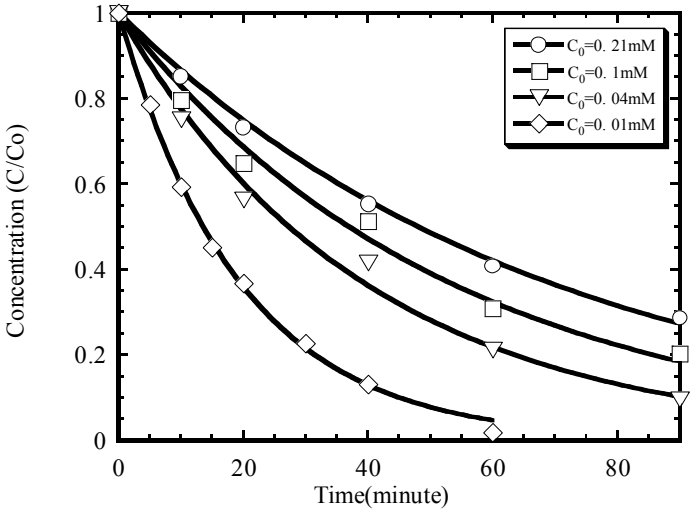

Figure 53. Effect of initial concentration on sonochemical decomposition of benzothiophene. Experimental conditions ultrasonic energy intensity = 226 W/cm^2, total volume = 40 mL, pH = 5, temperature = 25 °C, ionic strength = 0.05 M $NaClO_4$.

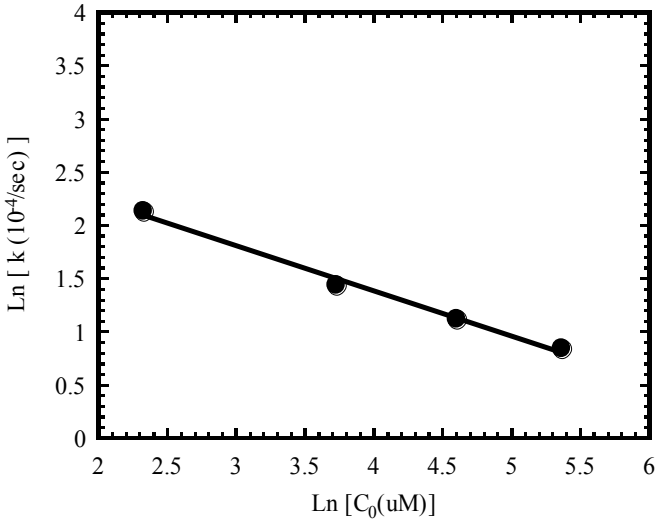

Figure 54. Ln(Co) versus Ln(k). Experimental conditions ultrasonic energy intensity = 226 W/cm^2, total volume = 40 mL, pH = 5, temperature = 25 °C, ionic strength = 0.05 M $NaClO_4$.

An emperical equation relating the rate constant to initial concentration was obtained:

$$k = 22.2\text{x}10^{-4}(C_0)^{-0.43} \qquad (4.12)$$

5.3.4 Effect of Ionic Strength (I)

The experiments were performed at various levels of ionic strength with sodium perchlorate (figure 55).

Figure 56 shows the relationship between the ionic strength and the decomposition rate of BT. The first-order rate constant increases from $2.97\text{x}10^{-4}$ sec^{-1} at I = 0.05 M $NaClO_4$ to $3.33\text{x}10^{-4}$ sec^{-1} at I = 2 M $NaClO_4$.

It is well known that the decomposition of organic compounds takes place in the bubble-bulk interface (Henglein, 1990). As described above, pollutants in the interfacial zone undergo decomposition due to exposure to free radicals and high temperature and pressure. We can assume that increasing concentration of pollutants in the interface enhances the overall decomposition rate. Salt may be used to push the pollutant molecules from the bulk aqueous phase toward the interfacial zone. Due to the hydrophobic repulsive interaction of nonpolar organic compounds with the aqueous phase, increasing the ionic strength in the aqueous phase enhances the hydrophilicity of the aqueous phase, which is not an favorable environment for the nonpolar organic compounds; hence, the organic compounds are driven to the interfacial zone of bubbles.

5.4 Decomposition of Dibenzothiophene

5.4.1 Effect of Steady-State Solution Temperature

It is observed that the amount of DBT present in solution decreases exponentially over reaction time. Little decomposition was observed in the control. Figure 57 shows the first-order plot of $\ln[C/C_0]$ versus time at various temperature values.

Figure 58 shows the changes of rate constant of DBT. It shows that the reaction rate increases as the temperature increases from 15 to 50 °C. In the temperature range of 15 to 50 °C, the value of activation energy for DBT is 12.6 kJ/mole, obtained from the Arrhenius expression. Therefore, the sonochemical reaction of DBT is limited by the diffusion step in the given experimental condition (Laidler, 1965).

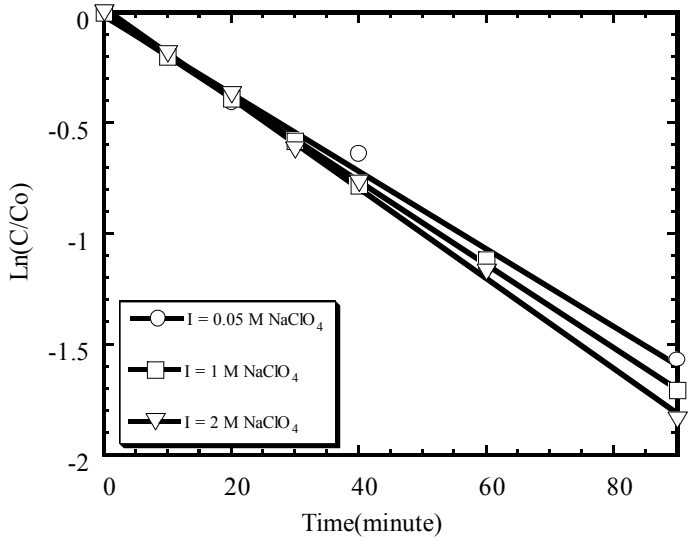

Figure 55. Effect of ionic strength on sonochemical decomposition of benzothiophene. Experimental conditions: ultrasonic energy intensity = 226 W/cm^2, total volume = 40 mL, pH = 5, C_0 = 0.1 mM, temperature = 25 °C.

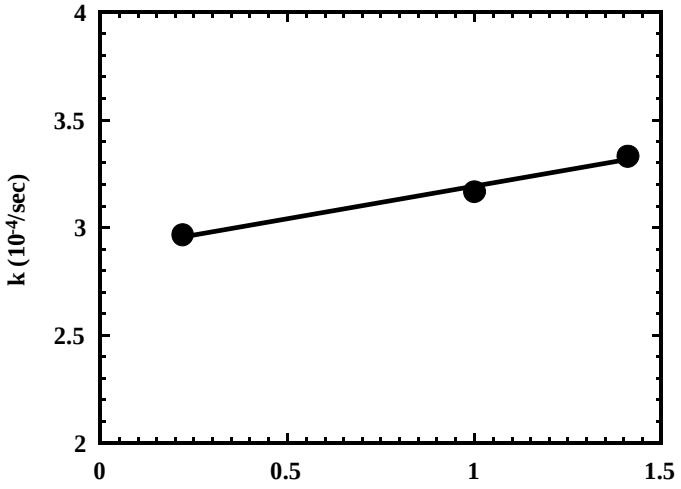

Figure 56. Ionic strength versus rate constant. Experimental conditions: ultrasonic energy intensity = 226 W/cm^2, total volume = 40 mL, pH = 5, C_0 = 0.1 mM, temperature = 25 °C.

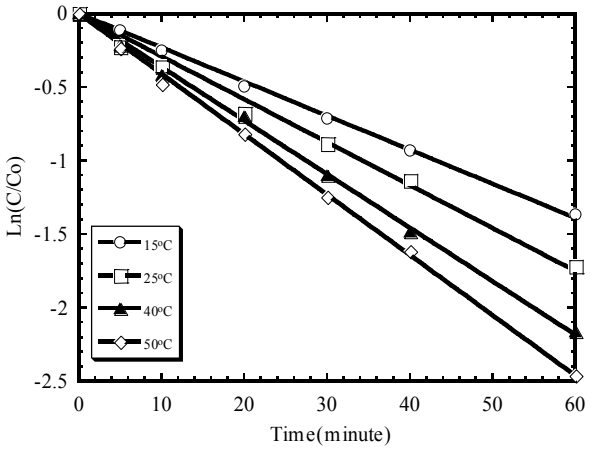

Figure 57. Effect of temperature on sonochemical decomposition of dibenzothiophene in aqueous solution. Experimental conditions: ultrasonic energy intensity = 226 W/cm^2, total volume = 40 mL, C_0 = 6.4 μM, pH = 5, temperature = 25 °C, ionic strength = 0.05 M $NaClO_4$.

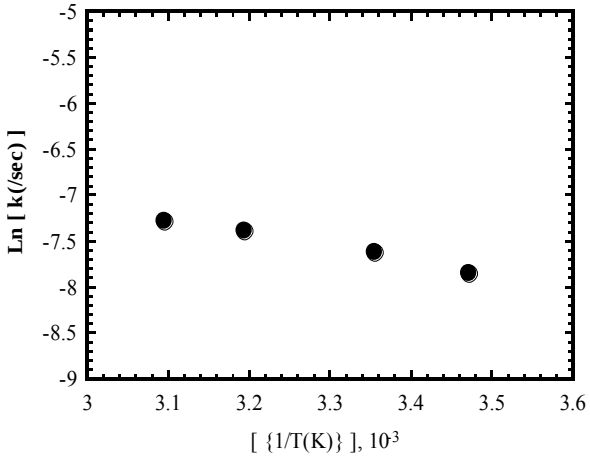

Figure 58. Temperature versus rate constant. Experimental conditions: ultrasonic energy intensity = 226 W/cm^2, total volume = 40 mL, C_0 = 6.4 μM, pH = 5, temperature = 25 °C, ionic strength = 0.05 M $NaClO_4$.

5.5 Decomposition of Trihalomethanes

Solutions with target organic compounds (THMs) were exposed to sonochemical irradiation at a pre-selected energy out-put. The amount of THMs remaining in solution decreases exponentially over reaction time (figure 59).

The decomposition of all THMs proceeded rapidly. Little decomposition was observed in the controls. The calculated rate constants are 19.2 x 10^{-4}sec^{-1} for chloroform, 14.9 x 10^{-4}sec^{-1} for dichlorobromomethane, 10.0 x 10^{-4}sec^{-1} for dibromochloromethane, and 5.2 x 10^{-4}sec^{-1} for bromoform. The decomposition rate decreases with increasing the number of bromine atoms in THM: chloroform > dichlorobromomethane > dibromochloromethane > bromoform.

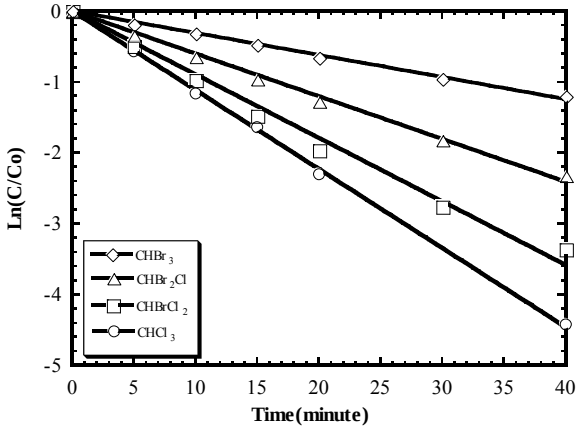

Figure 59. Sonochemical decomposition of trihalomethanes in aqueous phase. Experimental conditions: ultrasonic energy intensity = 226 W/cm^2, total volume = 40 mL, C_0 = 3.7 μM, pH = 7, temperature = 25 °C, ionic strength = 0.05M $NaClO_4$.

Figure 60 presents the evolution of chloride and bromide with reaction time. It is observed the amount of chlorine atoms in parent compounds (THMs) decreases rapidly, then little remains after a 40-minute reaction time. Since chlorine atoms are evolved faster than bromine atoms, 90% of chlorine and 85% of bromine are recovered in the solution as chloride and bromide ions after 120-minute reaction. This result agrees with the fact that the THM with a higher vapor pressure has a larger decomposition rate than that of the less-volatile THM in fixed experimental conditions.

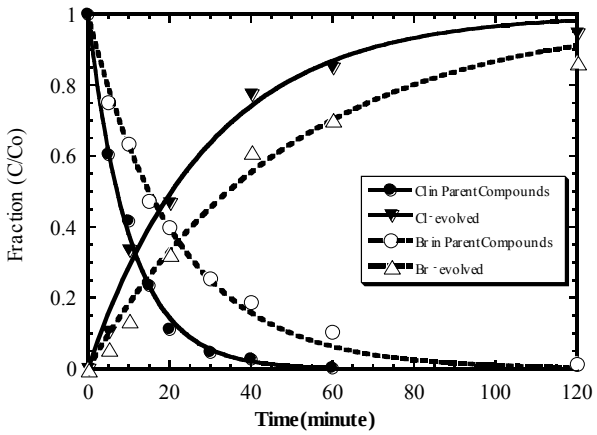

Figure 60. Chloride and bromine evolution over reaction time. Simultaneous treatment of four THMs. Experimental conditions: ultrasonic energy intensity = 226 W/cm^2, total volume = 40 mL, C_0 = 15 μM, pH = 7, temperature = 25 °C, ionic strength = 0.05 M $NaClO_4$.

5.5.1 Effect of Ultrasonic Energy Intensity

Increasing energy intensity will accelerate the decomposition rate of organic compounds. Huang (1994) reported that enhancing energy intensity increased the reactivity. Target organic compounds in aqueous solution were exposed to ultrasonic irradiation at different energy outputs from 40–400 watts. It is shown that the rate of decomposition increases with increasing energy intensity. That is, the rate of reaction depends on ultrasonic energy intensity, and higher energy intensity leads to faster reaction. The rate constant, k, can be obtained as a function of ultrasonic energy input from the slopes of semi-log plot. From figure 61, the rate constant is proportional to the energy intensity for all THMs. It is found that there is linear relationship between the energy intensity and the rate constant for all THMs within the range studied here.

5.5.2 Effect of Temperature

Figure 62 shows the changes of rate constants of four THMs at various temperature values. It shows that the reaction rates increase as the temperature increases from 18 to 35 °C, then decreases upon further increase in the temperature above 35 °C. In general, increasing the temperature will enhance the reaction rate.

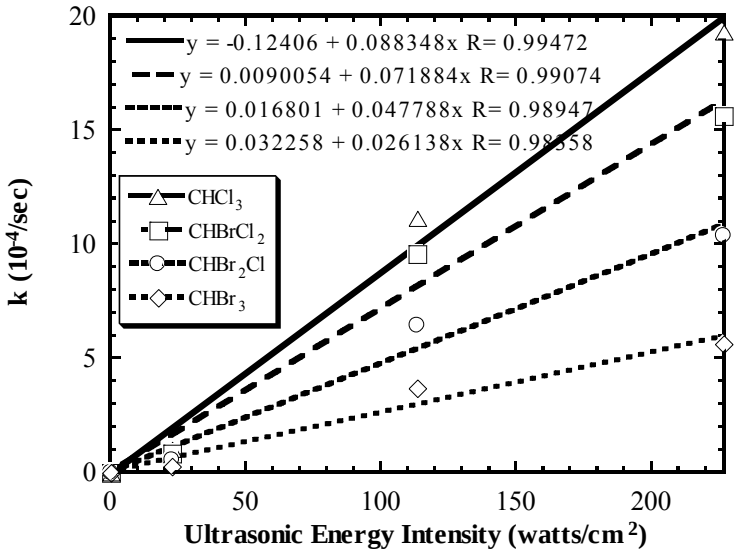

Figure 61. Effect of ultrasonic energy intensity on sonochemical decomposition rate of THMs. Experimental conditions: pH = 7, C_0 = 7.2 μM, temperature = 25 °C, ionic strength = 0.05 M $NaClO_4$.

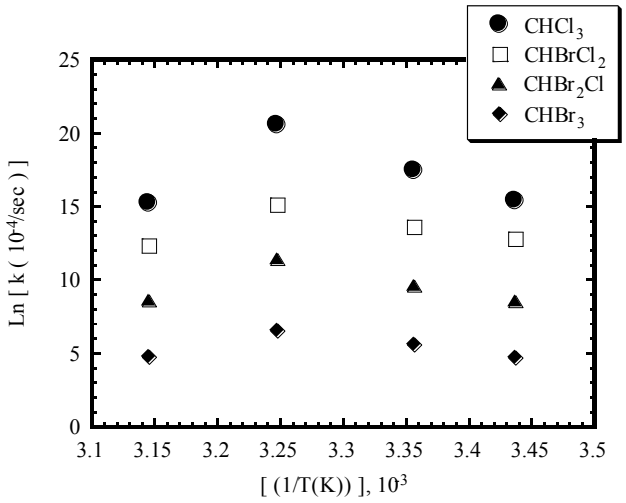

Figure 62. Effect of temperature on sonochemical decomposition rate of THMs. Experimental conditions: ultrasonic energy intensity = 226 W/cm^2, total volume = 40 mL, pH = 7, C_0 = 7.2 μM, ionic strength = 0.05M $NaClO_4$.

Various researchers have reported the effect of temperature on the sonochemical decomposition of organic compounds. Gondrexon et al. (1993) examined the effect of temperature on the decomposition of the chlorophenol in the range of 25–50 °C. Results showed that the higher the temperature, the larger the reaction rate. But Koszalka (1992) reported a high removal efficiency of 85% in the temperature range of 25–35 °C for tetrachloromethane and a low removal

efficiency of about 48% between 85–95 °C. It has been suggested to avoid sonochemical reactions near the boiling point of the solvent. Since the negative pressure in cavitation bubble causes the water and the volatile organic compound, such as methanol, in this work to decrease the boiling point, any cavitation bubbles formed will fill with water and volatile organic vapors almost instantaneously (Mason, 1990). These vapors can cause the cushion effect on collapse of bubbles, reduce the extremes of temperature and pressure generated, and, thus, decrease the decomposition efficiency of the organic compounds.

In the temperature range of 18–35 °C (figure 63), the values of activation energy for THMs are in table 5, obtained from the Arrhenius expression.

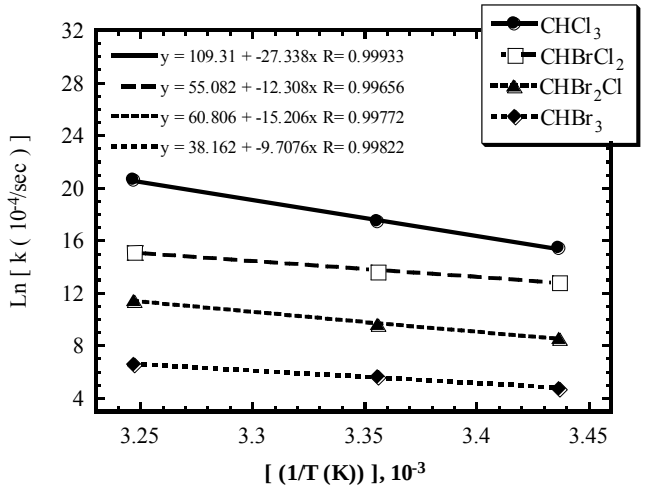

Figure 63. Effect of temperature on sonochemical decomposition rate of THMs. Experimental conditions: ultrasonic energy intensity = 226 W/cm^2, total volume = 40 mL, pH = 7, C_0 = 7.2 μM, ionic strength = 0.05M $NaClO_4$.

Table 5. Activation Energy Values of THMs in Sonochemical Reaction

THM	Activation Energy (kJ/mole)
Chloroform	12.7
Dichlorobromomethane	7.3
Dibromochloromethane	12.6
Bromoform	14.6

5.5.3 Effect of Initial Concentration

Though sonochemical reaction of THMs follows the first-order kinetics, the reaction rate is found to be dependent on the initial concentration of THMs (figure 64).

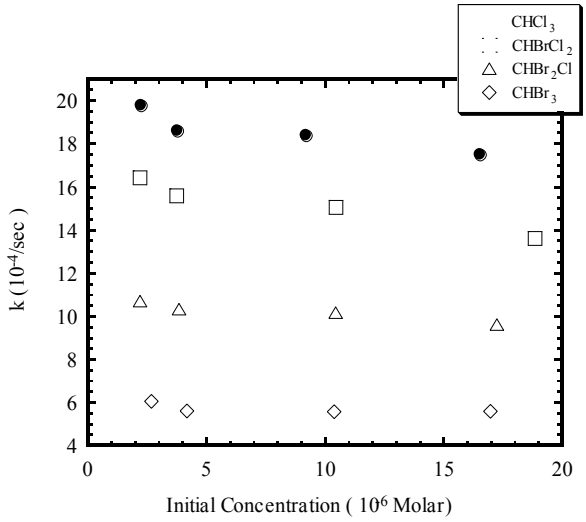

Figure 64. Effect of initial conce ntration on sonochemical decomposition rate of THMs. Experimental conditions: ultrasonic energy intensity = 226 W/cm^2, total volume = 40 mL, pH = 7, temperature = 25 °C, ionic strength = 0.05 M $NaClO_4$.

While the residual concentration of THMs decreases exponentially with time irrespective of the initial concentration of THMs, the first-order rate constant decreases as the initial concentration of THMs increases. Figure 65 shows the plots of log k versus log C_0 have the linear relationships for four THMs.

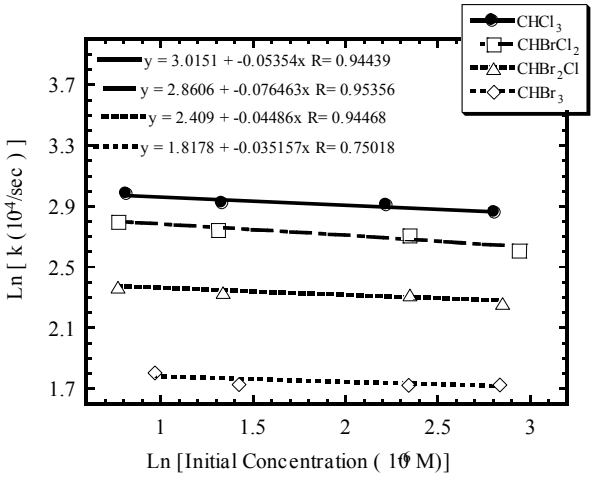

Figure 65. Effect of Initial concentration on sonochemical decomposition rate of THMs. Experimental conditions: ultrasonic energy intensity = 226 W/cm^2, total volume = 40 mL, pH = 7, temperature = 25 °C, ionic strength = 0.05 M $NaClO_4$.

5.5.4 Effect of Ionic Strength (I)

The experiments were performed at various levels of ionic strength with sodium perchlorate (figure 66).

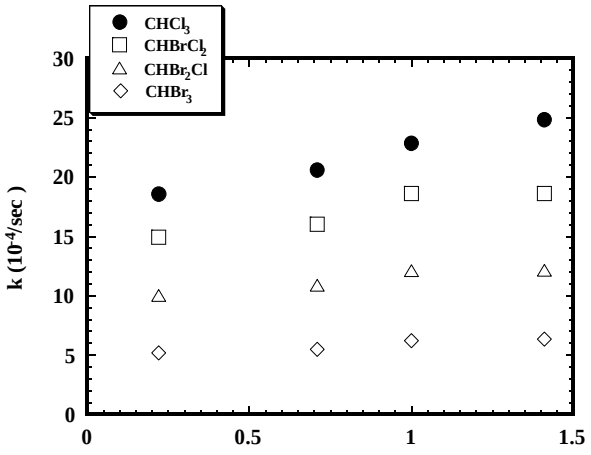

Figure 66. Effect of ionic strength on sonochemical decomposition rate of THMs. Experimental conditions: ultrasonic energy intensity = 226 W/cm^2, total volume = 40 mL, C_0 = 7.2, pH = 7, temperature = 25 °C.

Figure 67 shows the relationship between the decomposition rates of THMs and the ionic strength in the range from 0.05 to 2 M $NaClO_4$.

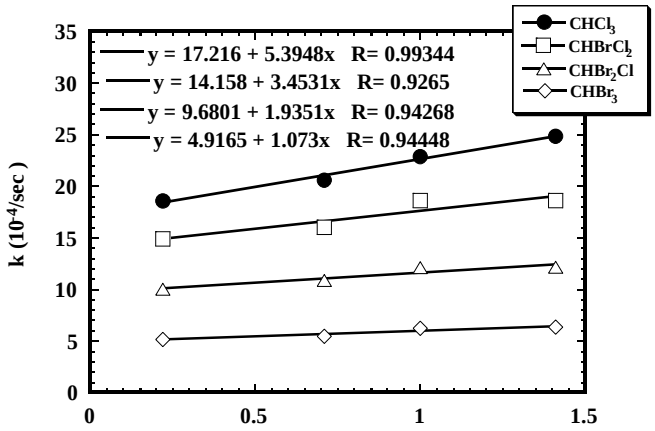

Figure 67. Effect of ionic strength on sonochemical decomposition rate of THMs. Experimental conditions: ultrasonic energy intensity = 226 W/cm^2, total volume = 40 mL, C_0 = 7.2, pH = 7, temperature = 25 °C.

The first-order rate constant increases as the ionic strength increases. It is well known that the decomposition of volatile organic compounds takes place inside bubbles and at the bubble-bulk interface (Henglein, 1990). Since organic compounds in the bubbles and the interfacial zone undergo decomposition due to exposure to free radicals and high temperature and pressure, we can assume that increasing concentration of organic compounds in the bubbles and interface

enhances the overall decomposition rate. It is proposed that salt pushes the pollutant molecules from the bulk aqueous phase toward the bubbles. Due to the hydrophobic repulsive interaction of less-polar organic compounds with the aqueous phase, increasing the ionic strength in the aqueous phase enhances the hydrophilicity of the aqueous phase, which is not a favorable environment for the less-polar organic compounds; hence, the organic compounds are driven to the bubbles.

6. Nearfield™ Acoustical Processor

To demonstrate the feasibility of the sonochemical process, results reported in section 5 were repeated using a probe type sonochemical reactor (figure 68). Obviously, this is an energy intensive reactor. A great deal of the acoustical energy is lost through the glass reactor. Also, there are many —dead" zones within the reactor because the acoustical waves are directional (figure 68). To eliminate these problems, a stainless steel commercial reactor was utilized.

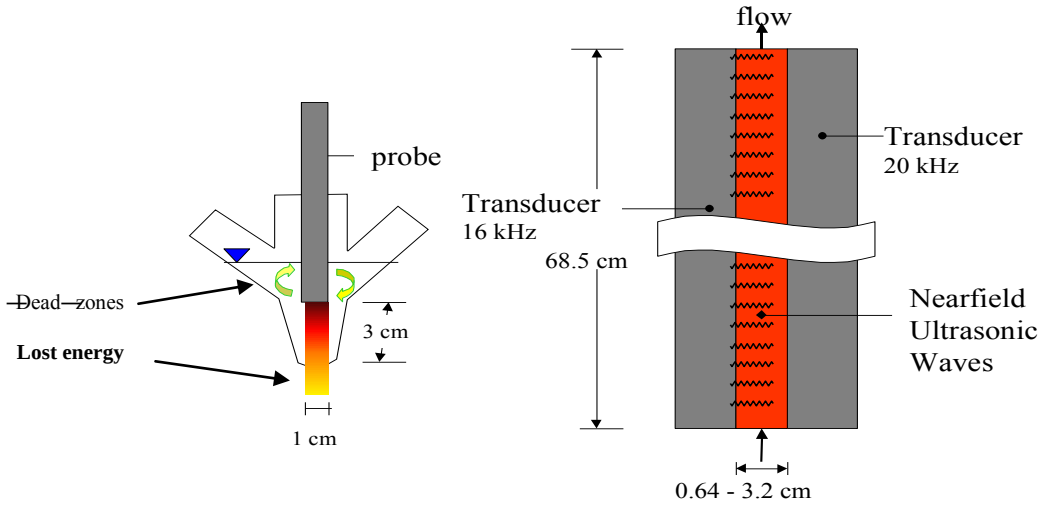

Figure 68. The probe reactor versus the Nearfield™ reactor.

6.1 Nearfield™ Acoustical Reactor

A Nearfield™ NAP-3606-HP-TC acoustical processor was purchased from Advanced Sonic Processing Systems, Oxford, Connecticut, (figure 69) to demonstrate both the technical and financial feasibility of the ultrasonic process in pilot and treatment plant scales. This reactor is equipped with 2,000-W, 16-kHz and 2,000-W, 20-kHz transducers and is capable of treating a maximum flow rate of 15 gal/minute.

Figure 70 shows the cross-sectional details of the reactor layout. In addition to the benefits realized by its increased power and physical layout that ensure there are no —dead" areas within the reactor, the interaction between the two different frequencies doubles the relative pressure amplitude produced by either the 16-kHz or 20-kHz waves individually. The large pressure differential between the high and low pressure zones create intense implosive forces within the processing chamber.

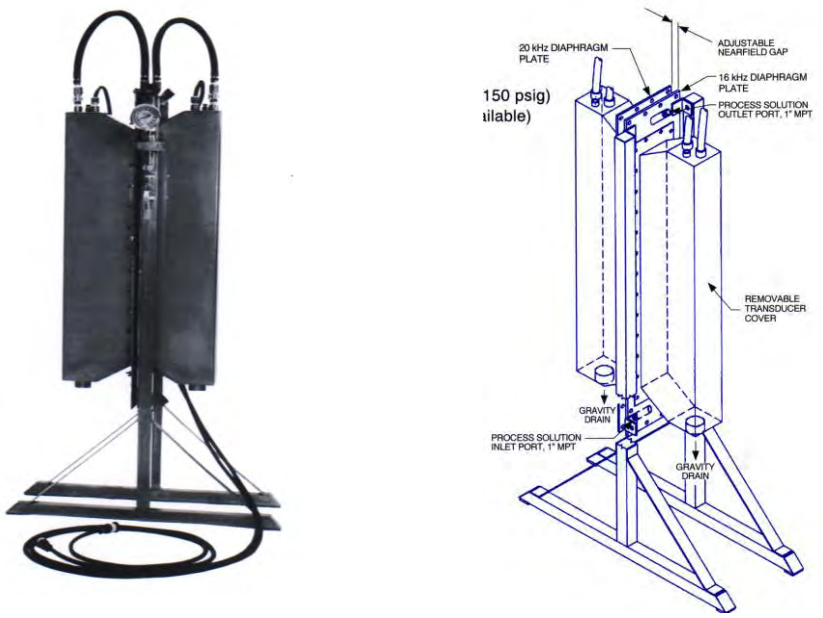

Figure 69. The Nearfield™ NAP-3606-HP-TC acoustical processor.

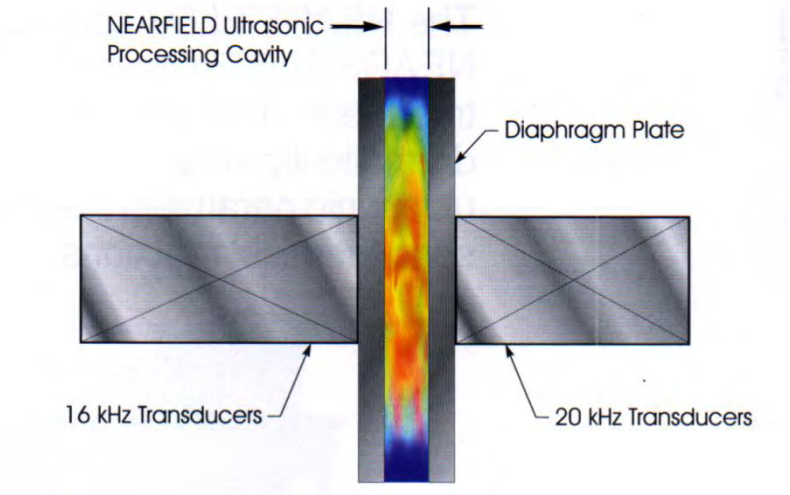

Figure 70. The Nearfield™ reaction chamber.

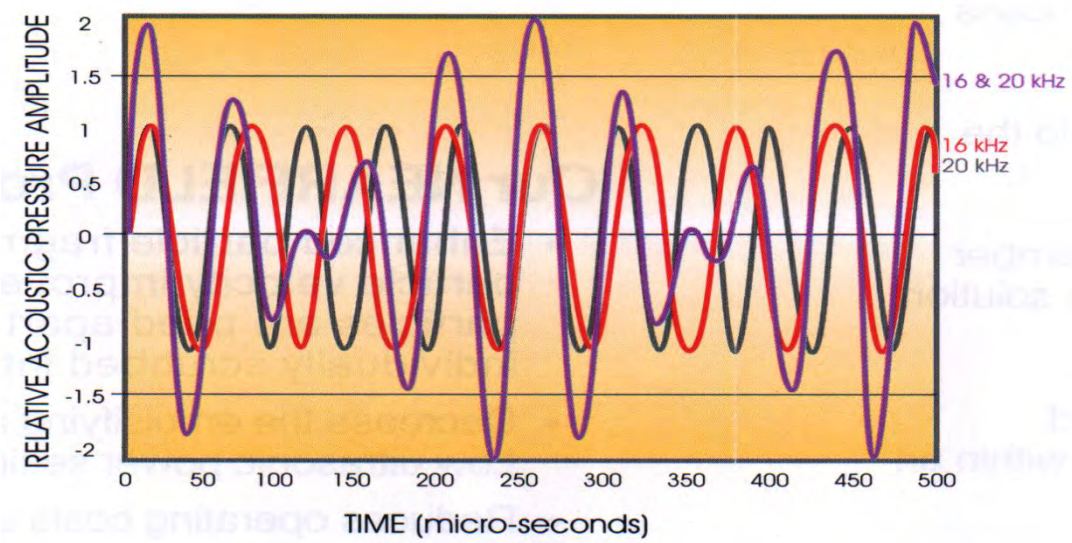

Figure 71. Acoustic pressure wave amplification, the superposition of 16- and 20-kHz frequencies.

The Nearfield™ reactor set up is shown in figure 72. A spiked sample was loaded into the sample container and was kept homogeneous with a magnetic stirrer. The sample then was pumped (12-volt [V], 2.5-gal/min marine pump) up into the reaction chamber and subjected to the ultrasonic waves. After treatment, the sample could either be drawn out of the sample port for analysis, discarded via the waste stream into the sink, or recycled back into the sample container for further treatment. The temperature of the reactor was controlled using cold water flowing down through the transducers and into the cooling water bucket. It was important not to allow any back pressure to build up in the transducers so that energy would not be absorbed by the cooling water. To facilitate this, a float switch and pump (12-V, marine switch and bilge pump) were installed to drain the cooling water bucket into the sink before it could fill up over the cooling water inlet. The reactor was equipped with drain valves to flush the system, and the generators were plugged into separate 20-ampere (amp) circuits.

6.2 Preliminary Nearfield™ Results

The preliminary results obtained using the Nearfield™ reactor show a dramatic improvement over the probe reactor. The time required to destroy *Cryptosporidium* was reduced from minutes to seconds (figure 73), and the time required to reduce the THMFP was reduced from hours to minutes (figure 74) with no effect on the turbidity of the water.

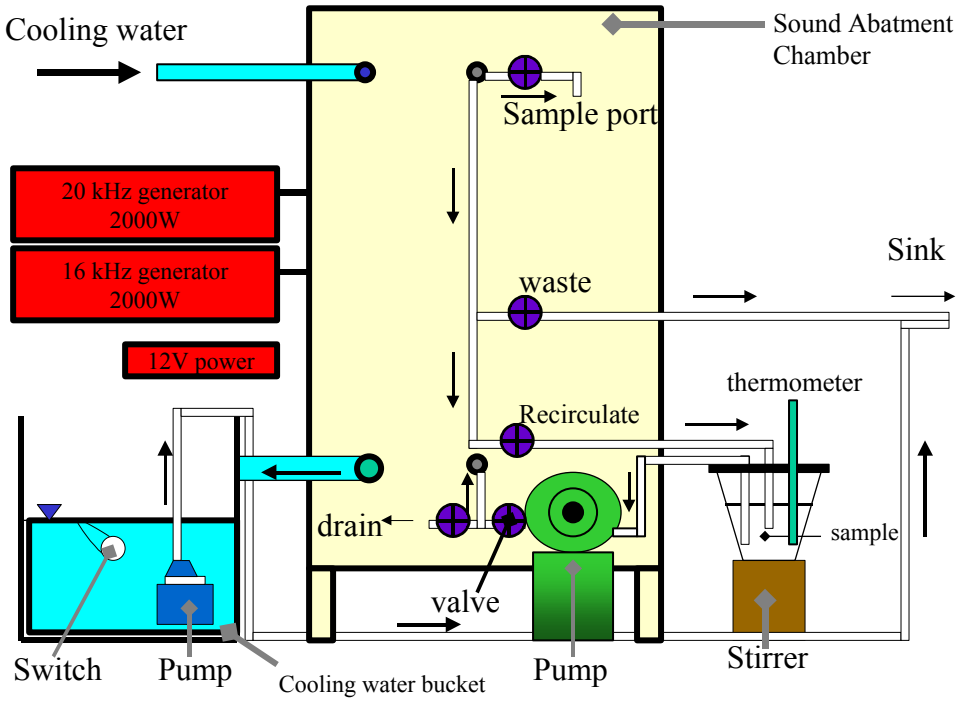

Figure 72. Schematic diagram of the Nearfield™ reactor.

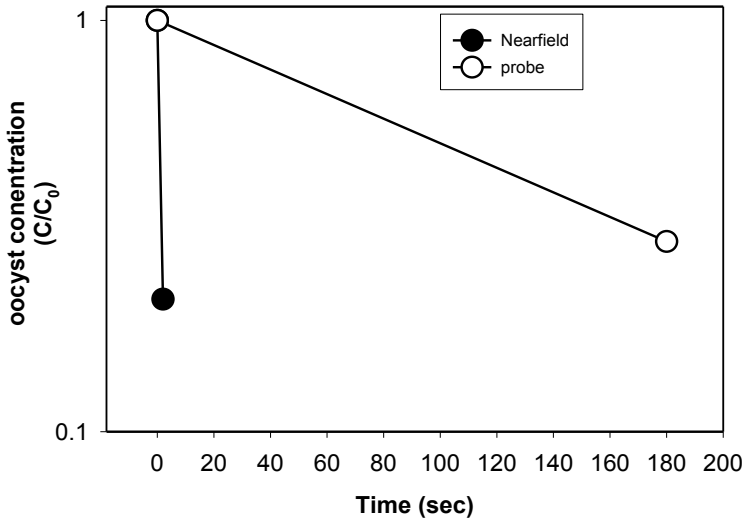

Figure 73. *Cryptosporidium* destruction: Probe versus Nearfield™ reactor.

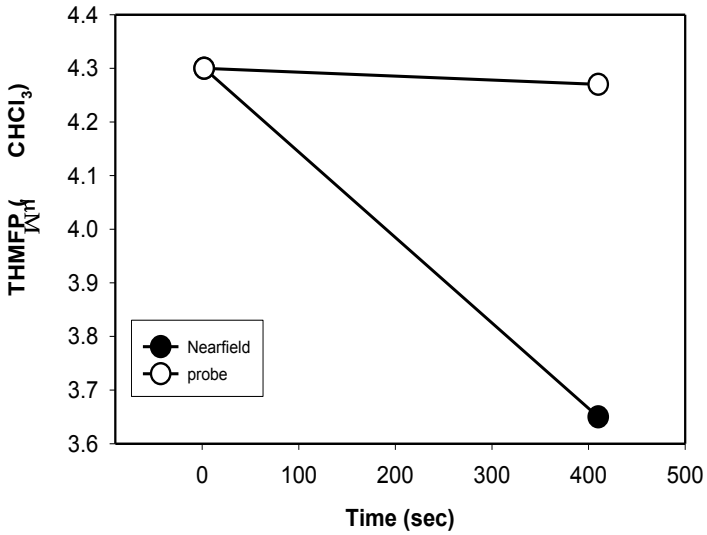

6.3 Treatment Costs

Along with the increase in efficiency comes a decrease in cost. Figure 75 illustrates the cost of the treatment process using the Nearfield™ reactor. The energy cost to achieve log *Cryptosporidium* removal for 1,000 gallons drops from approximately $179.00 with the probe reactor to $0.20–0.33 with the Nearfield™ reactor.

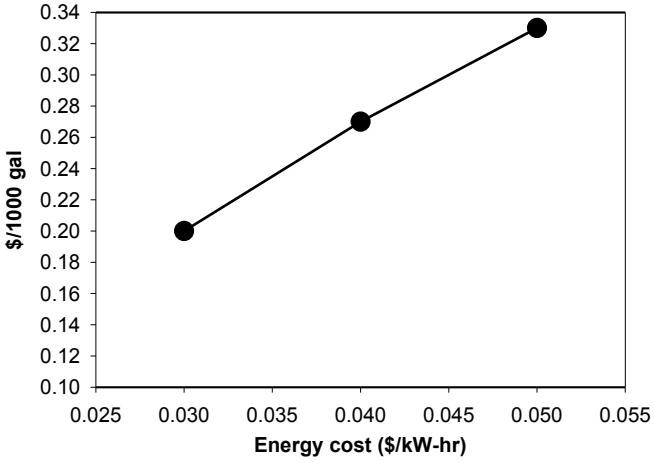

The flow rate to achieve log *Cryptosporidium* removal is calculated to be 14,400 gallons per day (gal/day). This flow rate corresponds to a retention time within the reaction chamber of 3 seconds. Table 6 illustrates the monthly payment to purchase a Nearfield reactor ($26,000). Figure 76 illustrates the combined equipment and energy cost to run the Nearfield™.

Table 6. Monthly Payment for the Nearfield™ Reactor

Interest rate (%)	20 years	25 years
5	171.59	151.99
6	186.27	167.52
7	201.58	183.76
8	217.47	200.67
9	233.93	218.19
10	250.91	236.26

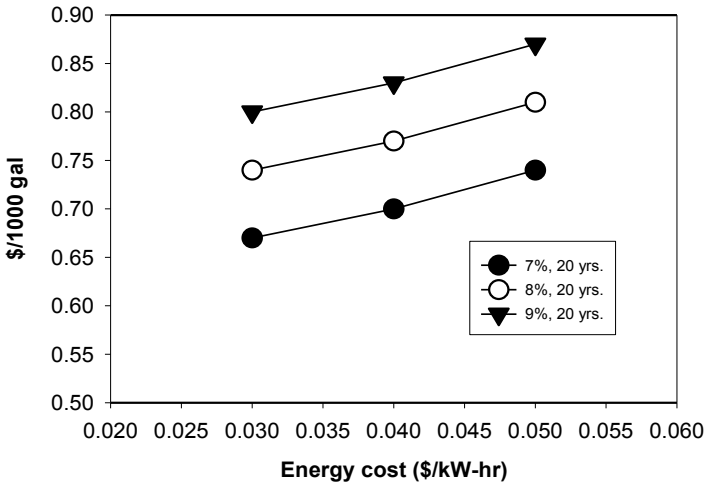

Figure 76. Combined equipment and energy costs for the Nearfield™ reactor.

6.4 Alternative Technology Cost Comparison

Figure 77 compares the treatment cost of the ultrasonic process versus five generally accepted treatment options for the removal of *Cryptosporidium* from water. These cost estimates come from the High Quality Water Conference in Sydney, Australia (MacCormick, T., and R. Wale, 1999). Other alternative treatment methods include direct (coagulation + filtration) and conventional (coagulation + gravity settling + filtration) filtration. The capital and operating

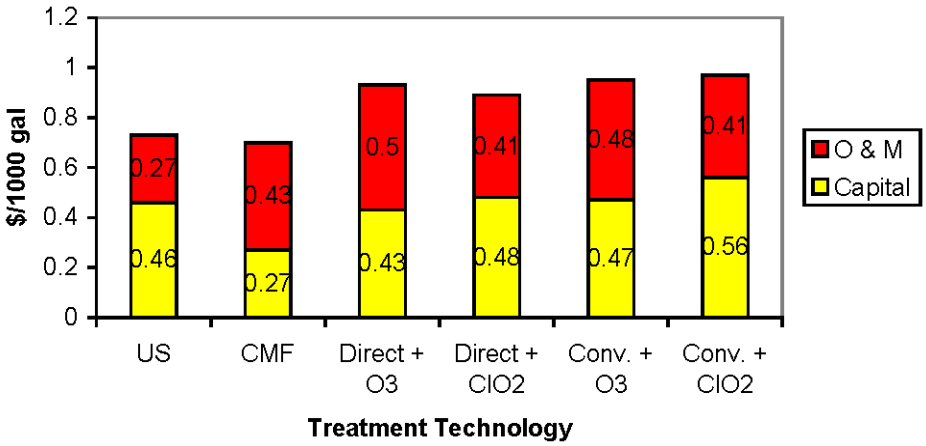

Figure 77. Cost comparison for alternate technologies.

costs are based on a 2.6-million-gallon-per-day facility with an average temperature of 22 °C. Costs are for the process equipment and exclude site civils, head works, pumping, and storage. The ultrasonic cost estimates are based on the preliminary data, an energy cost of $0.04 per kilowatthour and an equipment purchase financed at 8% over 25 years with no down payment. This cost estimate reflects individual unit pricing. Certainly, a substantial discount could be obtained when purchasing multiple units, significantly lowering capital costs. With further experimentation, the efficiency of the ultrasonic process can be maximized, further reducing the operating costs.

Where: US is ultrasound (1 log removal),

CMF is conventional microfiltration (6 log removal),

Direct + O_3 is direct multimedia filtration + O_3 (5 log removal),

Direct + ClO_2 is direct multimedia filtration + ClO_2 (5 log removal),

Conventional + O_3 is conventional multimedia filtration + O_3 (5 log removal),

Conventional + ClO_2 is conventional multimedia filtration + ClO_2 (5 log removal).

One of the big advantages the ultrasonic process has over filtration processes not reflected in the cost estimates is the elimination of backwash water. Filtration processes generate a high volume of backwash water (3–5% of finished water) that has significantly higher oocyst concentrations and turbidity than the raw water. Currently, the primary criterion in the United States for *Cryptosporidium* monitoring is that, in 95% of combined filter samples, turbidity is > 0.3 nephelometric turbidity units (NTU), with no sample > 1 NTU. The backwash water requires additional and expensive treatment to meet these

standards. The filtration methods were developed with water treatment in mind, not wastewater reclamation. The initial turbidity of wastewater (~34 NTU) is higher than most conventional water intakes, making filtration methods less attractive.

When comparing ultrasonic methods to the methods that contain O_3 or ClO_3^-,[1] one must consider the formation of DBPs. The ultrasonic method does not produce any THMs, haloacetic acids (HAAs), etc. It should also be noted that, if the ultrasonic process replaces the current disinfection procedures, the costs associated with those procedures are eliminated.

The ultrasonic process seems to be a financially feasible and technically viable technology that can provide an excellent disinfection alternative. It doesn't produce the harmful DBPs, backwash water, or sludge that the other treatment strategies do, and it can mineralize some of the contaminants in the water. Further experimentation with the Nearfield™ acoustical processor is warranted to develop the ultrasonic disinfection process even further.

[1] O_3 = ozone; ClO_3^- = chlorate anion.

7.0 References

Abel, M., W. Giger, and M. Koch. "Behavior of Alkyiphenol Polyethoxylate Surfactants in the Aquatic Environment. 1. Occurrence and Transformation in Rivers," in *Water Res.* (G.B.), 1994, **28**(51), 1143–1149.

Ahel, M., W. Giger, and M. Koch. "Behavior of Alkyiphenol Polyethoxylate Surfactants in the Aquatic Environment. 2. Occurrence and Transformation in Sewage Treatment," in *Water* Res. (G.B.), 1994, **28**(5), 1131–1137.

Alder, A.C., H. Siegrist, and W. Gujer. "Behaviour of NTA and EDTA in biological wastewater treatment," in *Wat. Res.* (G.B.), 1990, **24**(6), 733–738.

Amy G.L., C.W. Bryant, and M. Belyani. "Molecular Weight Distributions of Soluble Organic Matter in Various Secondary and Tertiary Effluents," in *Wat. Sci. Tech.*, 1987, **19,** 529–538.

Anderson, J.T. and S. Bobinger. "Polycyclic Aromatic Sulfur Heterocycles. II. Photochemical Oxidation of Benzothiophene in Aqueous Solution," in *Chemosphere,* 1992, **24**, 383–392.

Ball, H.A. and M. Reinhare. "Discharge of Halogenated Octyiphenol Polyethoxylate Residues in a Chlorinated Secondary Effluent," in *Water Chlorination. Chemistry, Environmental Impact, and Health Effects.* R.L. Jolley, R.J. Bull, W.P. Davis, S. Katz, M.H. Roberts, and V.A. Jacobs, eds., Chelsea, Michigan, Lewis Publishers, Inc., 1984.

Becher G., G.E. Carlberg, E.T. Gjessing, J.K. Hongslo, and S. Monarca. "High-performance Size Exclusion Chromatography of Chlorinated Natural Humic Water and Mutagenicity Studies Using the Microscale Fluctuation Assay," in *Environ. Sci. Technol.,* 1985, **19,** 422–426.

Berthou, F., Y. Gourmelun, Y. Dreano, and M.P. Friocourt. *J. Chromatogr.,* 1981, **203**, 279–292.

Bobinger, S. and J.T. Andersson. "Degradation of the Petroleum Components Monomethylbenzothiophenes on Exposure to Light,"in *Chemosphere,* 1998, **36**(12), 2569–2579.

Boehm, P.D., J.E. Barak, D.L. Fiest, and A.A. Elskus. *Mar. Environ. Res.,* 1982, **6**, 157–188.

Boehm, P.D., D.L. Fiest, and A. Elskus. "In Amoco Cadiz: Fates and effects of the oil spill," in *Proceedings, International Symposium Centre Oceanologique de Bretagne*, Brest; le Centre National pour VExploration des Oceans: Paris, 1981, 159–173.

Bose, P. and D.A. Reckhow. "Modeling pH and Ionic Strength Effects on Proton and Calcium Complexation of Fulvic Acid: a Tool for Drinking Water-NOM Studies," in *Environ. Sci. and Technol.,* 1997, **31**(3), 765–770.

Buxton, G.V., L. Ashton, and C.R. Stuart. "Temperature-Dependence of the Rate of Reaction of Hydroxyl Radical with Some Aromatic-Compounds in Aqueous-Solution-Evidence for the Formation of a Pi-Complex Intermediate," in *J. Chem. Soc. Paraday,* 1995, **91**(11), 1631–1633.

Cheung, H.M., A. Bhatnagar, and G. Jansen. "Sonochemical Destruction of Chlorinated Hydrocarbons in Dilute Aqueous Solutions," in *Env. Sci. Technol.*, 1991, **26**, 1460–1462.

Chow, D. and M. David. "Compounds Resistant to Carbon Adsorption Municipal Wastewater Treatment," in *J. AWWA,* 1997, **69,** 555–561.

Clark, R.M., J.Q. Adams, and B.W. Lynkins. "DBP Control in Drinking Water: Cost and Performance," in *J. Env. Eng.,* 1994, **120**(4), 759–782.

Collins M.R., G.L. Amy, and C. Steelink. "Molecular Weight Distribution, Carboxylic Acidity, and Humic Substances Content of Aquatic Organic Matter: Implications for Removal during Water Treatment," in *Environ. Sci. Technol.,* 1986, **20**(10), 1028.

Cooper, W.J., E. Cadavid, M.G. Nickelsen, K. Lin, C.N. Kurucz, and T.D. Waite. "Removing THMs from Drinking Water Using High-Energy Electron-Beam Irradiation," in *J. Am. Water Works Assoc.*, 1993, **85**(9), 106–112.

Deng, M.Q., D.O. Cliver, and T.W. Mariam. "Immunomagnetic Capture PCR to Detect Viable *Cryptosporidium* Parvum Oocysts from Environmental Samples," in *Appl. Environ. Microbiol,* 1997, **60**(8), 3134–3138.

DeWalle, F. and E. Chian. "Removal of Organic Matter by Activated Carbon Columns," in *J. Environmental Engineering Division, ASCE,* EE5 100, 1089–1104.

Dillon, T.M., J.M. Neff, and J.S. Warner. "Toxicity and Sublethal Effects of NO-2 Fuel Oil on Supralittoral Isopod Lygia-Exotica," in *Environ. Contam. Tox.,* 1978, **20**(3), 320–327.

Eastmond, D.A., G.M. Booth, and M.L. Lee. "Arch," in *Environ. Contam. Toxicol.,* 1974, **13,** 105–112.

Eaton, R.W. and J.D. Nitterauer. "Biotransformation of Benzothiophene by Isopropylbenzene-Degrading Bacteria" in *J. Bacteriolgy,* 1994, **176**(13), 3992–4002.

Eganhouse, R.P. and I.R. Kaplan. "Extractable Organic Matter in Municipal Wastewater. 1. Petroleum Hydrocarbons: Temporal Variations and Mass Emission Rates to the Ocean," in *Environ. Sci. Technol.*, 1982, **16,** 180–186.

Eisenhauer, H. "The Oxidation of Phenolic Wastes," in *J. Water Pollut. Control. Fed.,* 1964, **36**(9), 1116–1128.

Eisenhauer, H. "The Oxidation of Phenolic Wastes," in *J. Water Pollut. Control. Fed.,* 1968, **40**(11), 1887–1899.

El-Dib, M. and R. Ali. "THMs Formation During Chlorination of Raw Nile River Water," in *Wat. Res.,* 1995, **29**(1), 375–378.

Fedorak, P.M. and D. Grbic-Galic. "Aerobic Microbial Cometabolism of Benzothiophene and 3-Methylbenzothiophene," in *Appl. Environ. Microbiol.*, 1991, **57**, 932–940.

Fedorak, P.M. and D. Westlake. "Degradation of Sulfur Heterocycles in Prudhoe Bay Crude-Oil by Soil Enrichments," in *Wat. Air. Soil Pollut.,* 1984, **21**(1–4), 225–230.

Fedorak, P.M. and D. Westlake. "Microbial-Degradaton of Alkylcarbazoles in Norman Wells Crude-Oil," in *Appl. Environ. Microbiol.,* 1984, **47**(4), 858–862.

Flint, E.B. and K.S. Suslick. "The Temperature of Cavitation," in *Science,* 1991, **253***,* 1397–1399.

Fort, C.L., M.K. Koczwara, E.J. Kirsch, and C.P. Leslie Grady. "Evaluation of the Quality of Wastewater Treatment Effluent Following Chlorination or Ozonation," in *Water Chlorination,* Chapter 91, 1981.

Gardiner, J. "Complexation of Trace Metals by Ethylenediaminetetraacetic Acid (EDTA) in Natural Waters," in *Wat. Res.*, 1976, **10,** 507–514.

Garric, J., B. Bollat, D.K. Mguyen, M. Bray, B. Migeon, and A. Kosmala. "Ecotoxicological and Chemical Characterization of Municipal Wastewater Treatment Plant Effluents," in *Wat. Sci. Tech.,* 1996, **33**(6), 83–91.

Glaze, W.H. and J.W. Kang. "Advanced Oxidation Processes for Treating Groundwater Contaminated with TEC and PCE: Laboratory Studies," in *J. Am. Water Works. Assoc.*, 1988, **5**, 57–63.

Glaze, W.H., J.E. Henderson, J.E. Bell, and V.A. Wheeler. "Analysis of Organic Materials in Wastewater Effluents After Chlorination," in *J. Chromagraphic Sci.*, 1973, **11,** 580–584.

Glaze, W.H., P. Bose, and D.S. Maddox, "Degradation of RDX by Various Advanced Oxidation Processes: I. Reaction Rates," in *Wat. Res.,* 1998, **32**(4), 997–1004.

Gondrexon, N., V. Renaudin, A. Bernis, Y. Gonthier, and P. Boldo. "Ultrasonic Degradation Kinetic Study of Chlorophenol Aqueous Solution," in *Environmental Technology,* 1993, **14,** 587–593.

Gracia, R., J.L. Aragues, and J.L. Ovelleiro. "Study of the Catalytic Ozonation of Humic Substances in Water and Their Ozonation Byproducts," in *Ozone Sci. Eng.,* 1996, **18**, 195–208.

Henglein, A. "Sonochemistry: Historical Development and Modem Aspects, in *Ultrasound,* 1987, **25**, 6–16.

Henglein, A. *Advances in Sonochemistry,* T.J. Mason, Ed.; JAT Press, Greenwich, Connecticut, 1990.

Ho, P.C. "Photooxidation of 2,4-Dinitrotoluene in Aqueous Solution in the Presence of Hydrogen Peroxide," in *Environ. Sci. and Technol.,* 1986, **20**, 260–267.

Huang, C.K. and O.J. Hao. "Degradation of Monochiorophenols by Sonochemical Process," in *Proceedings, 25th Mid-Atlantic Industrial Waste Conference,* 1994, Sup. Vol. 61–69.

Huang, C.P., D. Dong, and W.T. Tang. "Advanced Chemical Oxidation: Its Present Role and Future Potential in Hazardous Waste Treatment," in *Waste Management,* 1993, **13,** 36 1–177.

James, H.E., P. Catharina, N. Maria, and A. Bert, "Potentiometric Titrations of Humic Substances," *Environ. Sci. and Technol.,* 1995, **29**(3), 622–628.

Jardim, W.F., C. Pasquini, J.R. Guimaraes, and L.C. DeFaria. "Short-Term Toxicity Test Using Echerichia coli: Monitoring CO_2 Production by Flow Injection Analysis," in *Water Res.,* 1990, **24**(3), 351–354.

Jayasundera, S. and A. Torrents. "Natural Organic Matter Sortion by Kaolinite: Modified Langmuir Isotherm," in *J. Environ. Eng-ASCE,* 1997, **123**(11), 1162–1165.

Johnson, M.G., C.K. Minns, and J. Kelso. "Large-Scale Risk Assessment of Acid-Rain Impacts on Fisheries-Models and Lessons," in *Can. J. Fish. Aquat. Sci.,* 1986, **43**(4), 900–921.

Jolley, R.L., R.J. Bull, W.P. Davis, S. Katz, M.H. Roberts, Jr., and V.A. Jacobs. *Water Clorination Chemistry, Environmental Impact and Health Effects.* CRC Press, Boca Raton, Florida, 1985.

Jolley, R.L., R.B. Cumming, N.E. Lee, L.R. Lewis, and J.E. Thompson, "Nonvolatile Organics in Disinfected Wastewater Effluents: Chemical Characterization," in *Water Chlorination,* Chapter 35, 1981.

Karcher, W., A. Nelen, R. Depans, J. Van Eijk, P. Glande, and J. Jacob. *Polynuclear Hydrocarbons: Chemical Analysis and Biological Fate.* Columbus, Ohio, 1981, 317–332.

Koszalka, D.P., J.F. Soodsma, and R.A. Bever. Ultrasonic Decomposition of Groundwater. Paper presented at the AIChE 1992 Summer National Meeting, Minneapolis, Minnesota.

Kotronarou, A., G. Mills, M. Hoffmann. "Decomposition of Parathion in Aqueous Solutions," *Env. Sci. and Technl.*, 1992, **26**(6), 15–21.

Kotronatou, A., G. Mills, and H.R. Hoffmann. "Ultrasonic Irradiation of p-Nitrophenol in Aqueous Solution," in *J. Phys. Chem.,* 1991, **95**, 3630–3638.

Kropp, K.G., J.T. Andersson, and P.M. Fedorak. "Biotransformations of Three Dimethyldibenzothiophenes by Pure and Mixed Bacterial Cultures," in *Environ. Sci. Technol.,* 1997, **31,** 1547–1554.

Kruithol, J.C. *Chlorination Byproducts: Production and Control – a Report from the Committee on the Side Effects of Chlorination*, KIWA Communication No. 74, American Water Works Association, Research Foundation, 1998.

Laidler, K.J. *Chemical Kinetics,* McGraw-Hill, New York, 1965.

LaGrega et al. *Hazardous Waste Management,* 1994.

Laseter, J.L., G.C. Lawler, E.B. Overton, J.R. Patel, J.P. Holmes, M.I. Shields, and M. Maberry. "In Amoco Cadiz: Fates and Effects of the Oil Spill," in

Proceedings, International Symposium Centre Oceanologique de Bretagne. Brest; le Centre National pour l'Expioration des Oceans, Paris, 1981, 633–644.

LeChevallier, M.W. and W.D. Norton. "Occurrence of *Giardia* and *Cryptosporidium* in Raw and Finished Drinking Water, in *J. Am. Water Works Assoc.,* 1996, **87**(9), 54–68.

Leenheer J.A. "Comprehensive Approach to Preparative Isolation and Fractionation of Dissolved Organic Carbon from Natural Waters and Wastewaters," in *Environ. Sci. Technol.*, 1982, **15**, 578–587.

Linstedt et al. *Potable Reuse of Municipal Wastewater,* EPA-600/9-75-007, 1975.

Ma, H. Thermodynamics and Kinetics of Complexation of Copper with Natural Humic Substances and Suspended Particulate Solids. Doctoral Thesis, University of Delaware, Newark, Delaware, 1999.

MacKenzie, M. J. and J.V. Hunter. "Sources and Fates of Aromatic Compounds in Urban Stormwater Runoff," in *Environ. Sci. Technol.,* 1979, **13**(2), 179–183.

MacKenzie, W.R., N.J. Hoxie, M.E. Proctor, M.S. Gradus, K.A. Blair, D.E. Peterson, J.J. Kazzmierczak, D.G. Addiss, K.R. Fox, J.B. Rose, and J.P. Davis. "A Massive Outbreak in Milwaukee of *Cryptosporidium* Infection Transmitted through the Public Water Supply," in *N. Engl. J. Med.* 1994, **331**, 161–167.

Mak, F.T., W.J. Cooper, C.N. Kurucz, M.G. Nickelsen, and T.D. Waite. "Removal of Chloroform from Drinking Water Using High-Energy Electron-Beam Irradiation," in *Disinfection Byproducts in Water Treatment: The Chemistry of Their Formation and Control*, R.A. Minear and G.L. Amy, eds., CRC Press, Boca Raton, Florida, 1996.

Makino, K., M. Mossoba, and P. Riesz. "Chemical Effects of Ultrasound on Aqueous Solutions. Evidence for OH and H by Spin Trapping," in *J. Am. Chem. Soc.,* 1982, **104**, 3537–3539.

Makino, K., M. Mossoba, and P. Riesz. "Chemical Effects of Ultrasound on Aqueous Solutions. Formation of Hydroxyl Radicals and Hydrogen Atoms," in *J. Phys. Chem.,* 1983, **87**, 1369–1377.

Manka, J., M. Rebhun, A. Mandelbaum, and A. Bortinger. "Characterization of Organics in Secondary Effluents," in *Envron. Sci. Technol.*, 1974, **8**(12), 1017–1022.

Maron, D.M. and B. Ames. "Revised Methods for the *Salmonella* Mutagenicity Test," in *Mutation Res.,* 1983, **113,** 173–179.

Mason, T.J. and J.P. Lomier. *Sonochemistry,* Ellis Horwood Ltd., New York, New York, 1988, 252.

Mason, T.J. *Chemistry with Ultrasound,* Elsevier Appl'd. Sci., New York, New York, 1990, 195.

Mason, T.J. *Practical Sonochemistry,* Ellis Horwood Pubi., New York, New York, 1991, 186.

McCarty P.L., and M. Reinhard. "Trace Organics Removal by Advanced Wastewater Treatment," in *Res. J. WPCF,* 1980, **52**(7), 1907–1911.

McFall, T., G.M. Booth, M.L. Lee, Y. Tominaga, R. Pratap, M. Tedjamulia, and R.N. Castle, Mutagenic activity of methyl-substituted tri-and tetracyclic aromatic sulfur heterocycles. *Mutation Research/Genetic Toxicology*, 1984, **135**(2), 97–103.

Minear, R A., R.G. Song, and G. Amy. "Comparison of Bromide-Ozone Reactions with NOM Separated by XAD-8 Resin and UF RO Membrane Methods," *Abstr. Pap. Am. Chem.,* 1993, 206: 60-ENVR Part 1.

Mirenda, R.J. and W.S. Hall. "The Application of Effluent Characterization Procedures in Toxicity Identification Evaluations," in *Wat. Sci. Tech.*, 1992, **25**(3), 39–44.

Namour, P. and M.C. Muller. "Fractionation of Organic Matter from Wastewater Treatment Plants Before and After a 21-Day Biodegradability Test: A Physical-Chemical Method for Measurement of the Refractory Part of Effluents," in *Wat. Res.,* 1998, **32**(7), 2224–2231.

Nishioka, M., M.L. Lee, and R.N. Castle. "Surphur Heterocycles in Coal-Derived Products," in *Fuel,* 1986, **65**(3), 390–396.

Ogata, M., and K. Fujisawa. *Water Res.,* 1985, **19,** 107–118.

Okouchi, S., O. Nojima, and T. Arai. "Cavitation-Induced Degradation of Phenol by Ultrasound," in *Wat. Sci. Technol.,* 1992, **26**(9–11), 2053–2056.

Orshansky, F. and N. Narkis. "Characteristics of Organic Removal by PACT Simultaneous Absorption and Biodegradation," in *Wat. Res.,* 1997, **31**(3), 391–398.

Orzechowaska, G.E., E.J. Poziomek, V.F. Hodge, and W. H. Engelmann. "Use of Sonochemistiy in Monitoring Chlorinated Hydrocarbons in Water," in *Environ. Sci. and Technol.*, 1995, **29**(5), 1373–1379.

Ozawa, H. and T. Tsukioka. "Gas Chromatographic Separation and Determination of Chloroacetic Acids in Water by a Difluoroanilide Derivatization Method," in *Analyst,* 1990, **115**(10), 1343–1347.

Paciolla, M.D., G. Davies, and S.A. Jansen. "Generation of Hydroxyl Radicals from Metal-Loaded Humic Acids,"in *Environ. Sci, and Technol.,* 1999, **33**(11), 1814–1818.

Paxeus, N. "Organic Plilutants in the Effluents of Large Wastewater Treatment Plants in Sweden," in *Wat. Res.,* 1996, **30**(5), 1115–1122.

Pelroy, R.A., D.L. Stewart, Y. Tominaga, M. Iwao, R.N. Castle, and M.L. Lee, *Mutation Res.,* 1983, **117**, 31.

Peschel G. and T. Wildt. "Humic Substances of Natural and Anthropogeneous Origin," in *Wat. Res*. (G.B.), 1988, **22**(1), 105.

Petrasek, A.C., I.J. Kugelman, B.M. Austern, A.P. Thomas, L.A. Winslow, and R.H. Wise. "Fate of Toxic Organic Compounds in Wastewater Treatment Plants," in *J. WPCF,* 1983, **55**(10), 1286.

Petrier, C., Y. Jiang, and M. Lamy. "Ultrasound and Environment: Sonochemical Destruction of Chloroaromatic Derivatives," in *Environ. Sci. Technol.,* 1998, **32**(9), 1316–1318.

Price, G. "The Use of Ultrasound for the Controlled Degradation of Polymer Solutions," in *Advances in Sonochemistry*, T.J. Mason, ed., 1: JAI Press, 1990.

Rappaport, S.M., M.G. Richard, M.C. Holistein, and R.E. Talcott. "Mutagenic Activity in Organic Wastewater Concentrates," in *Environ. Sci. Technol.*, 1979, **13**(8), 957–961.

Rebhun, M. and J. Manka. "Classification of Organics in Secondary Effluents," in *Environ. Sci. Technol.*, 1971, **5**(7), 606–9.

Reinhard, M., W.H. Ding, and Y. Fujita. *Organic Carbon Characterization of Advanced Treated Wastewater at Water Factory 21, Orange County,* Department of Civil Engineering, Stanford University, 1994.

Riesz, P., T. Kondo, and C.M. Krisna. *Ultrasonics,* 1990, **28**, 295–299.

Rook J.J. "Haloforms in drinking water," in *J. Am. Water Works Assoc.,* 1976, **68**, 168–172.

Sachdev, D., J. Ferris, and N. Clesceri. "Apparent Molecular Weight of Organics in Secondary Effluents," *J. WPCF,* 1976, **48,** 570–579.

Scheier, A. and D. Gominger. "A Preliminary Study of the Toxic Effects of Irradiated Versus Non-Irradiated Water Soluble Fractions of #2 Fuel Oil," in *Bull. Environ. Contam. Toxicol.,* 1976, **16**, 595.

Schnitzer, M., and E.H. Hansen. "Organic-Metallic Interactions in Soils: An Evaluation of Methods for the Determination of Stability Constants of Metal-Fulvic Acid Complexes," in *Soil Sci.,* 1970, **109**, 333–340.

Schnitzer, M. and S.U. Khan. *Humic Substances in the Environment.* Dekker, New York, 1972.

Schumb, W C., C.N. Satterfield, and R.L. Wentworth. *Hydrogen Peroxide,* New York, Reinhold Publishing Company, 1955.

Scott, J.P. and D.F. Ollis. "Integration of Chemical and Biological Oxidation Processes for Water Treatment: Review and Recommendations," in *Environmental Progress,* 1995, **14**(2), 88–103.

Seo, G.T., Y. Suzuki, and S. Ohgaki. "Biological Powdered Activated Carbon (BPAC) Microfiltration for Wastewater Reclamation and Reuse," in *Desalination,* 1996, **106**(1-3), 39–45.

Seymour, J.D. and R.B. Gupta. "Oxidation of Aqueous Pollutants Using Ultrasound: Salt-Induced Enhancement," in *Ind. Eng. Chem. Res.*, 1997, **36,** 3453–3457.

Singer, P.C. "Control of Disinfection Byproducts in Drinking Water," in *J. Env. Eng.,* 1994, **120**(4), 727–744.

Singer, P.C. and S.D. Chang. "Correlations Between Trihalomethanes and Total Organic Halides Formed During Water Treatment," *J. Am. Water Works Assoc.*, 1989, **81**(8), 61–67.

Solomons, T.W.G. *Organic Chemistry*, 4th edition, Wiley, New York, New York, 1988, 137–138.

Spark, D.L. *Environmental Soil Chemistry*, Academic Press, San Diego, California, 1995.

Speight, J.G., and S.E. Moschopedis. "Production of Low-Sulfur Liquids and Coke from Athabasca Bitumen," in *Fuel Process Technol.,* 1979, **2**(4), 295–302.

Stowell, J.P., J.N. Jensen, and A.S. Weber. "Sequential Chemical/Biological Oxidation of 2-Chlorophenol," in *Wat. Sci. Technol.,* 1992, **26**, 9–11.

Summers, R. and P. Roberts. "Size Effects in Adsorption of Macromolecular Organic Matter," Proceeding of the 1984 ASCE National Conference on Environmental Engineering, 1984, 400.

Suslick, K.S. *Ultrasound, Its Chemical, Physical and Biological Effects,* VCR Publ., New York, New York, 1986, 138–150.

Suslick, K.S. *Ultrasound: Its Chemical, Physical, and Biological Effects,* VCR Publ., New York, New York, 1998.

Symons, J.M., et al. "Treatment Techniques for Controlling Trihalomethanes in Drinking Water," in *J. AWWA,* Denver, Colorado, 1982.

Tang, W.Z. and S. Tassos. *Oxidation Kinetics and Mechanisms of Trihalomethanes by Fenton's Reagent*, 1997, **31**(5), 1117–1125.

Tchobanoglous et al. *Wastewater Engineering,* 3rd edition, 1992.

Teal, J.M., K. Bums, and J. Fangton. *Can. J. Fish. Res.,* 1978, **35***,* 510–520.

Terranova, N. and C.P. Huang. "Reduction of THMF Potential by Fenton's Reagent,"in *Proceedings, 26th Mid-Atlantic Industrial Waste Conference,* 1994, 205–211.

Thurman, E.M. *Organic Geochemistry of Natural Wastes.* Academic Press, London, 1983.

Tilak, B.D. *Tetrahedron.,* 1960, **9**, 76–82.

Van Steenderen, R. and A. Maiherbe. "The Molecular Mass Distribution of Organic Compounds in Activated Sludge Plant Effluent Determined by Means of Gel Permeation Chromatography," in *Wat. Res.,* 1982, **16,** 745–748.

Vassilaros, D.L., P.W. Stoker, G.M. Booth, and M.L. Lee. "Capillary Gas-Chromatograpic Determination of Polycyclic Aromatic-Compound in Vertebrate Fish Tissue," in *Anal. Chem.,*1982, **54**(1), 106–112.

Verschueren, V. *Handbook of Environmental Data on Organic Chemicals,* 2nd edition, Van Nostrend Reinhold Co., New York, New York, 1982.

Victoria-Rueda, C.H. "Nonpolar Orgamcs Toxicity in a Municipal Effluent. National Conference on Enviromnental Engineering Saving a Threatened Resourcein Search of Solutions," in *1992 National Conference on Env. Engr. Water Forum*, August 2–6 1992, Baltimore, Maryland, 549–554.

Von Gunten, U. and J. Hoigne. "Bromate Formation During Ozonation of Bromide-containing Waters: Interaction of Ozone and Hydroxy Radical Reaction," in *Environ. Sci. Technol.,* 1994, **28**, 1234–1242.

Watt B.E., R.L. Malcolm, M.H.B. Hayes, N.W.E. Clark, and J.K. Chipman. "Chemistry and potential mutagenicity of humic substances in waters from different watersheds in Britain and Ireland," in *Wat. Res.* 1996, **30**, 1502–1516.

Weast, R.C., D.R. Lide, M.J. Astle, and W.H. Beyer (eds). *Handbook of Chemistry and Physics*, 70th edition, CRC Press, Boca Raton, Florida, 1992.

Wu, J.M., H.H. Huang, and C.D. Linergood. "Ultrasound Destruction of Chlorinated Compounds in Aqueous Solutions," in *Environ. Progress*, 1992, **11,** 195–201.

Yang, R. and S. Zhou. "Study on the Low Pressure Wet Oxidation Treatment of High Concentration and Refractory Organic Wastewater," in *Environmental Science,* 1997, **18**(5), 71–74.

Yochiko Fujita, W.H. Ding, and M. Reinhard. "Identification of Wastewater Dissolved Organic Carbon Characteristics in Reclaimed Wastewater and Recharged Groundwater," in *Wat. Environ. Res.*, 1996, **68**(5), 867–876.

Zelazny, L.W. and V.W. Carlisle. "Physical, Chemical, Elemental, and Oxygen-containing Functional Group Analysis of Selected Florida Histosols," in *SSSA Spec. Publ.*, 1974, **6**, 63–78.

Zuckerman, M. and A. Molof. "High Quality Reuse Water by Chemical-Physical Wastewater Treatment," in *J. WPCE,* 1970, **42**, 437–456.

Appendix A

Principles of Ultrasound

The human ear can detect sound waves from 16 hertz (Hz) to 16 kilohertz (kHz). Ultrasound is the name given to the range of the frequencies of the sound waves from 16 kHz (16,000 cycles per second) to 10 megahertz (MHz) (107 cycles per second) (Mason, 1988; Suslick, 1988). Ultrasound has been widely applied in industry, medicine, engineering, and chemistry. A number of these applications are summarized in table A-1; most of them can be dated back to the 1950s or earlier. Some have fallen into disuse in recent years, but many are being given a new lease of life with recent advances in ultrasonic engineering. A large proportion of ultrasonic equipment currently in industry is involved in welding of plastic moldings for the consumer.

Table A-1. Industrial Uses of Ultrasound (Mason, 1988; Mason, 1990b)

Field	Application
Biology, biochemistry	Homogenization and cell disruption: Power ultrasound is used to rupture cell walls to release contents for further studies.
Engineering	Ultrasound has been used to assist drilling, grinding, and cutting. It is particularly useful for processing hard, brittle materials such as glass and ceramics. Other uses of ultrasound are welding (both plastics and metals) and metal tube drawing. High-frequency (millihertz [mHz]) ultrasound is used in nondestructive material and flaw detection.
Dentistry	For both cleaning and drilling of teeth.
Geography, geology	Pulse/echo techniques are used in the location of mineral and oil deposits and in depth gauges for seas and oceans. Echo ranging at sea has been used for many years.
Industrial	Pigments and solids can be easily dispersed in paint, inks, and resins. Engineering tools often are cleaned and depressed by immersion in ultrasonic baths. Two less widely used applications are acoustic filtration and ultrasound drying.
Medicine	Ultrasound imaging (2–10 MHz) is used, particularly in obstetrics, for observing the fetus and for guiding subcutaneous surgical implements. In physiotherapy, lower frequencies (20–50 kHz) are used in the treatment of muscle strains.
Plastics, polymers	The welding of thermoplastics is effectively achieved using power ultrasound. Polymerization initiation and polymer degradation are also affected. Cure rates of resins and their composition can be measured with high frequency ultrasound.

A.1 The Physics of Ultrasound

Ultrasound, sound wave, is transmitted through any substance—solid, liquid or gas—that possesses elastic properties. The movement of the vibrating body (i.e., sound source) is communicated to the molecules of the medium, each of which transmits the motion to an adjoining molecule before returning to its approximately original position. For a liquid or gas, particle oscillation takes place in the direction of the wave and produces longitudinal waves.

The physical aspect of this motion is best understood by examining the action of a tuning fork vibrating in air (figure A-1). The prong is considered to be the transducer; while it moves forward, it compresses the layer of air next to it (figure A-1a). The fork then returns to its original position (figure A-1b). Then, the movement of prong R to the left (figure A-1c) causes displacement of the air to the left (figure A-1d), and the wave will proceed with a series of compression and rarefaction portions.

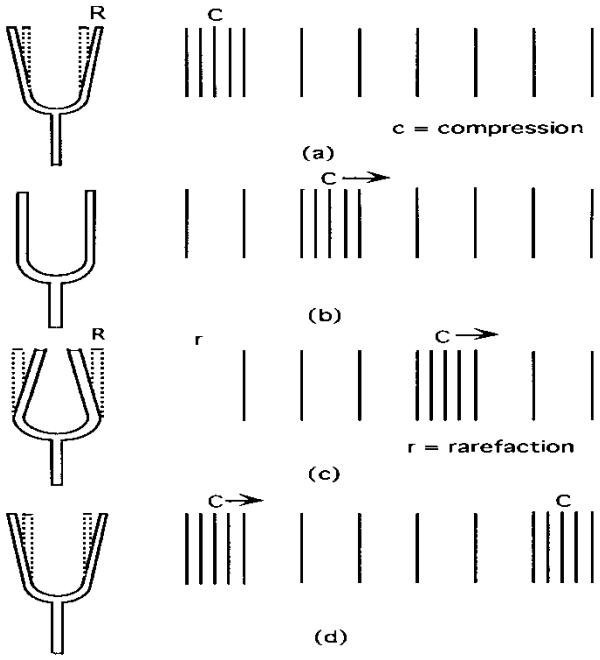

Figure A-1. Longitudinal waves in air: (a) first outstroke of prongs; (b) prongs in normal position; (c) first instroke of prongs; (d) second outstroke of prongs.

As shown in figure A-2, from a displacement and pressure distribution as well as the movement of prong, at any time (t), the displacement (x) of an individual air molecule from its mean rest position is given by:

$$x = x_o \sin 2\pi ft \tag{1}$$

where x_0 is the displacement amplitude, or maximum displacement of the particle, and f is the frequency of the sound wave.

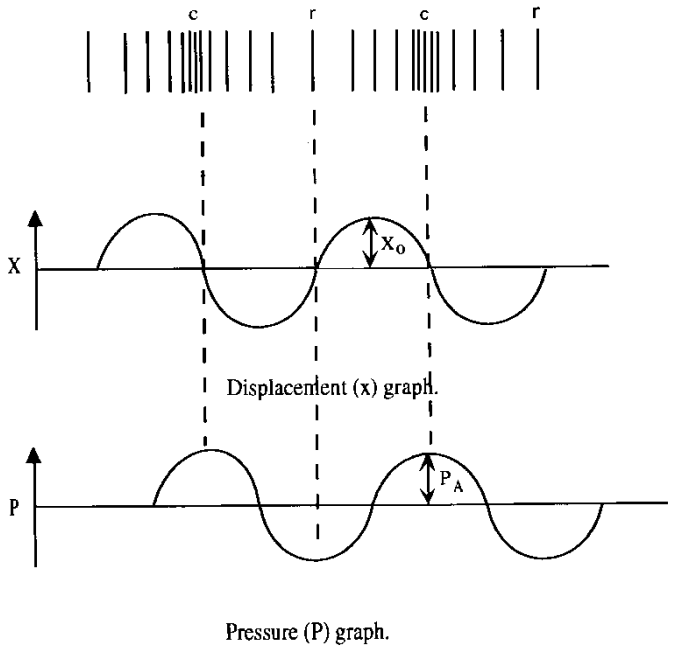

Figure A-2. Displacement and pressure graph.

Besides the variation in the molecules position when the sound wave travels through together (i.e., where the molecules are compressed), the pressure is higher than normal at that instant; whereas, at the region where the layers are furthest apart (i.e., the rarefaction region), the pressure is lower than normal. The acoustic pressure at any time t is given by:

$$P(t) = P_a \sin 2\pi ft \tag{2}$$

where P_a is the maximum pressure amplitude and f is the frequency of the sound wave.

Because the particles are in motion, they will possess kinetic energy—this energy being derived from the wave itself. However, it is not usual to refer to the energy of a wave, whether it is an optical or a sound wave; it is more usual to refer to the intensity of the wave. Intensity is, in fact, energy flowing per unit area per unit

time; and using the ideas of physics, it can be shown that it is related to the maximum acoustic pressure, P_a, by:

$$I = \frac{P_a^2}{2\rho c} \tag{3}$$

where p is the density of the medium and c is the velocity of sound in the medium.

For sonochemical applications, the usual unit of intensity is watts per square centimetre (W/cm^2); and, obviously, the larger the intensity, the greater the value of P_a and the greater the displacement of the molecules. The intensity, 1, at a distance, 1, from the source is given by (Mason, 1988):

$$I = I_o e^{-2\alpha l} \tag{4}$$

where I_0 is the intensity at the source and α is an overall attenuation coefficient that includes frictional losses, thermal conduction losses, and other energy losses represented by the bulk viscosity.

A.2 Acoustic Cavitation

When an ultrasonic wave passes through a liquid or a gas, the molecules of the medium vibrate longitudinally in the direction that the waves travel. Meanwhile, the variation of the strength holding molecules causes two different sound waves: compression and rarefaction cycles. During the compression cycle, the average distance between molecules decreases, while during the rarefaction, the distance increases. A large negative acoustic pressure (expansion cycle) is formed to exceed the molecular distance necessary to keep the liquid intact; and as a result, the liquid will break down, and the voids or cavities will be created—i.e., the cavitation bubbles will be generated (Mason, 1988).

These bubbles can be filled with gas or vapor and form in a wide variety of liquids. Cavitation can occur in many fluids such as water, organic solvents, biological fluids, liquid helium, and molten metals. The origins of cavitation can be hydrodynamic, thermal, or acoustic (Suslick, 1988).

In general, two models have been proposed to explain how gas bubbles can be stabilized in a liquid (Crum, 1982). One of the earliest of these was the crevice model. Figure A-3 shows the nucleation sites.

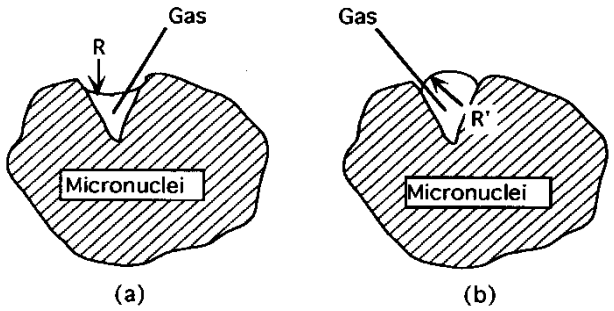

Figure A-3. Crevice model for stabilizing cavitation micronuclei: (a) for external positive pressure, (b) for external negative pressure.

When an external pressure is applied, such as from a time-varying acoustic wave, the contact angle increases until it reaches its maximum value. If the pressure is increased further, the interface moves toward the apex and may completely disappear if the pressure is sufficiently high. When the pressure is decreased, the interface becomes convex, as shown in figure A-3b, and will eventually reach the receding contact angle. A further decrease in pressure causes the interface to move away from the apex; and if the pressure becomes sufficiently low, a free gas bubble will be liberated. This process is called nucleation.

Another model to explain the stabilization of cavitation micronuclei suggests that a film of surface-active substances exist on the water gas interface. In this model, an organic skin is composed of molecular chains—each containing both a polar and a nonpolar end. The polar end bonds to the water surface while the nonpolar end extends into the gas.

Acoustic cavitation involves at least three discrete stages: nucleation, bubble growth, and, under proper conditions, implosive collapse. Nucleation and bubble growth are due to stable cavitation. The dynamics of cavity growth and collapse are strikingly dependent on local environment, and cavitation in a homogeneous liquid should be considered separately from cavitation near an interface.

Traditionally, cavitation has been classified into two types—stable and transient. Stable cavitation has bubbles oscillating rapidly at some equilibrium size and often will persist for many acoustic cycles. Transient cavitation, on the other hand, usually involves large-scale variations in the bubble size for only one or two acoustic cycles, expanding to at least two or three times original size before violently collapsing during a single compression half-cycle. Stable cavitation may become unstable, leading to transient cavitation, and the collapse of transient cavitation can produce smaller bubbles that undergo stable cavitation. During this short period of time when the bubbles collapse, a temperature approaching 5,000 Kelvin (K) had been measured (Mason, 1988; Suslick, 1988), and a pressure reaching to several hundred atmospheres had been calculated.(Shutilov,

1988). Under adiabatic conditions, the maximum pressure, P_{max}, and the maximum temperature, T_{max}, can be calculated by the following equations (Mason, 1988):

$$T_{max} = T\left(\frac{P_m(\gamma-1)}{P}\right) \quad (5)$$

$$P_{max} = P\left(\frac{P_m(\gamma-1)}{P}\right)^{\gamma/(\gamma-1)} \quad (6)$$

where: T_0 = ambient temperature
γ = ratio of specific heats of the gas
P = pressure in bubble at its maximum size
P_m = pressure in the liquid at the moment of transient collapse
P_{max} = maximum pressure in the liquid at the moment of transient collapse

It is recognized that T_{max} and P_{max} are highest for gases which possess a large value of (γ - 1). This explains why monatomic and diatomic gases are most effective. Calculations using these equations suggest that for water at 25 °C , the average temperatures of 5,000 K and pressure similar to 1,000 atmospheres are generated by the collapse of cavitation bubbles due to power ultrasound (Flint, 1991; Suslick, 1986).

However, high temperatures and pressures also are produced in stable cavitation bubbles which are in resonance with the exciting ultrasonic field. Equation 7 has been derived as an expression for the ratio T_0/T_{max}:

$$\frac{T_o}{T_{max}} = 1 - Q\left[\left(\frac{P}{P_{max}}\right)^{1/3} - 1 - 1\right]^{-3(\gamma-1)} \quad (7)$$

where Q is the ratio of the resonance amplitude to the static amplitude of vibration of the bubble.

Calculations of the local pressures due to these resonance vibrations have resulted in values that exceed the hydrostatic pressure by a factor of 150,000. There is no doubt that the intense local strains in the vicinity of the resonating bubbles are the cause of the many disruptive mechanical effects of sound.

A.3 Sonochemistry of Aqueous Solutions

In sonochemistry, high temperatures and pressures within the collapsing cavitation bubbles are generated. Under these extremely and transient conditions,

the water molecule undergoes thermal dissociation to form hydroxyl radical ($OH^{\bullet}$), hydrogen atom ($H^{\bullet}$), and hydroperoxyl ($HOO^{\bullet}$). Evidence for the formation of three radicals by ultrasound in aqueous solution has been demonstrated by Mankino et al. (1982, 1983). Usually, transient cavitation is regarded to be the principal contributor to sonochemistry effects, but stable cavitation also may be important (Henglein, 1987).

Sonochemical reactions can be divided into pyrolysis reactions (i.e., combustion) and free-radical reactions. Pyrolysis reactions involve thermal decomposition of solvent, solute, or gases inside the cavitation bubbles where the temperature and pressure are so high that the solute molecule breaks down. Free radicals produced from the decomposition of water can react within the collapsing bubble, at the liquid gas interface of the bubbles, and in the bulk aqueous phase. The reactions occurring in the gas phase and interfacial region of the bubbles are similar to combustion (Henglein, 1987).

Figure A-4 represents the regions of sonochemical reactions. The estimated temperatures of the cavitation within the bubble or the bulk liquid phase had been reported for sonication of metal carbonyls in mixtures of hydrocarbons (Hart, 1990). Because of the lower vapor pressure and the higher thermal conductivity of water, it is reasonable that the average estimated temperature in the interfacial region is around 800 K during sonication in water at 20 kHz. Figure A-4 is only an idealization, since the cavitation will lose its spherical shape due to the violently collapsing cavitation bubbles.

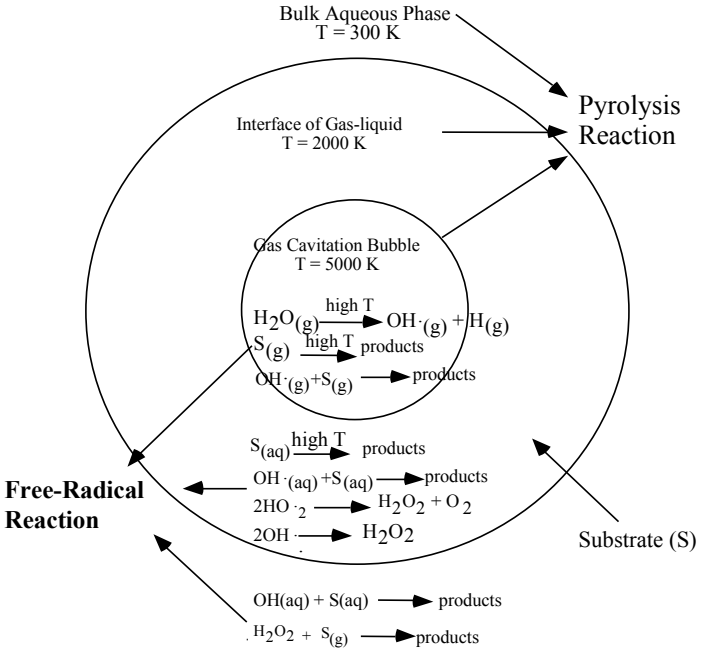

Figure A-4. Schematic of sonochemical processes insides of a micro-bubble (Price, 1990).

Appendix B

Decomposition Mechanisms for Humic Substances by Sonochemical Process

B.1 Humic Substances

Humic substances (HS) are ubiquitous, heterogeneous polymers that are isolated from many types of terrestrial and aqueous environments. They are amorphous, organic materials that possess a variety of physical and chemical properties that make them unique to other types of environmental substances.

The functional groups of HS are amine, carboxylic, carbonyl, phenol, catechol, and quinone. These groups are on the HS surface or are chemically combined to cross link the molecular backbone. So far, the structure for HS is unknown; only proposed building blocks exist in Scheme 1(figure B-1) (Schnitzer et al., 1972; Paciolla et al., 1999).

Cleavage of a covalent bond can occur in two ways: homolytically, resulting in one elctron from the bond going to each fragment to produce radical species, or heterolytically, with both electrons going to one fragment, leading to formation of an ion pair. Both of these possibilities have been observed during polymer degradation (Scheme 2) (figure B-2). The production of macromolecular radicals is perhaps the most common breakdown mechanism and has been observed for many carbon skeleton polymers (Henglein, 1954; Henglein, 1955). The radical species and ion pairs of HS undergo further chain scission, reaction with other radicals, and stabilization by water molecules. The heterolytic bond cleavage of polymers and the stabilization mechanism of ion pairs by water molecules were studied (Thomas and de Vries, 1959). Consequently, the monomers can be formed as intermediates of HS, shown in Scheme 2.

The radical reaction is conducted by the radicals produced from the decomposition of hydrogen peroxide and water molecules by sonochemical irradiation. The mechanism of radical reaction is rapid oxidation. The radicals are so reactive that most of them are consumed by HS. The hydroxide (OH) radicals can act on organic solutes by hydroxy addition, hydrogen abstraction, and electron transfer. In other words, the radical reaction can open aromatic rings and form carbonyl compounds and organic acids (Ho, 1986; Hashimoto et al., 1984). The depolymerization and radical reaction of HS appears to occur simultaneously. The final step(s) of the reaction is the conversion of organic acids to carbon dioxide.

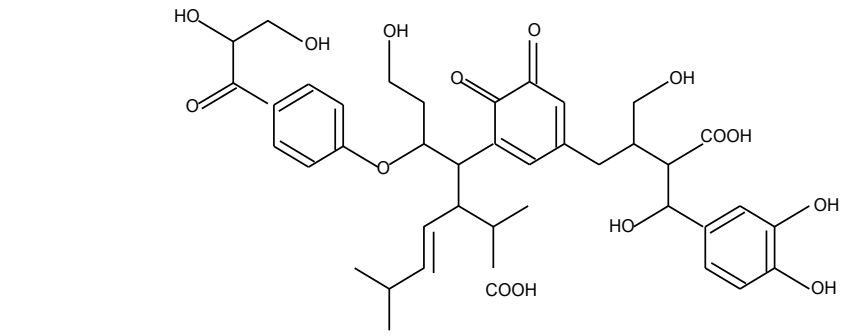

(A)

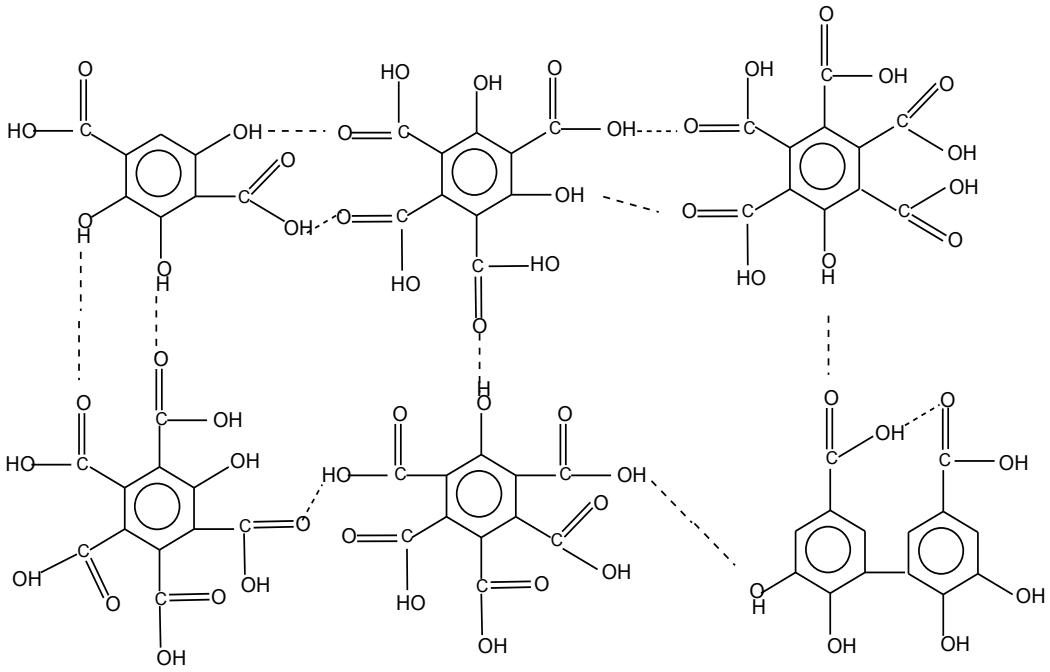

(B)

Figure B-1. Scheme 1, proposed building blocks of humic substances (Schnitzer et al., 1972; Paciollar et al., 1999).

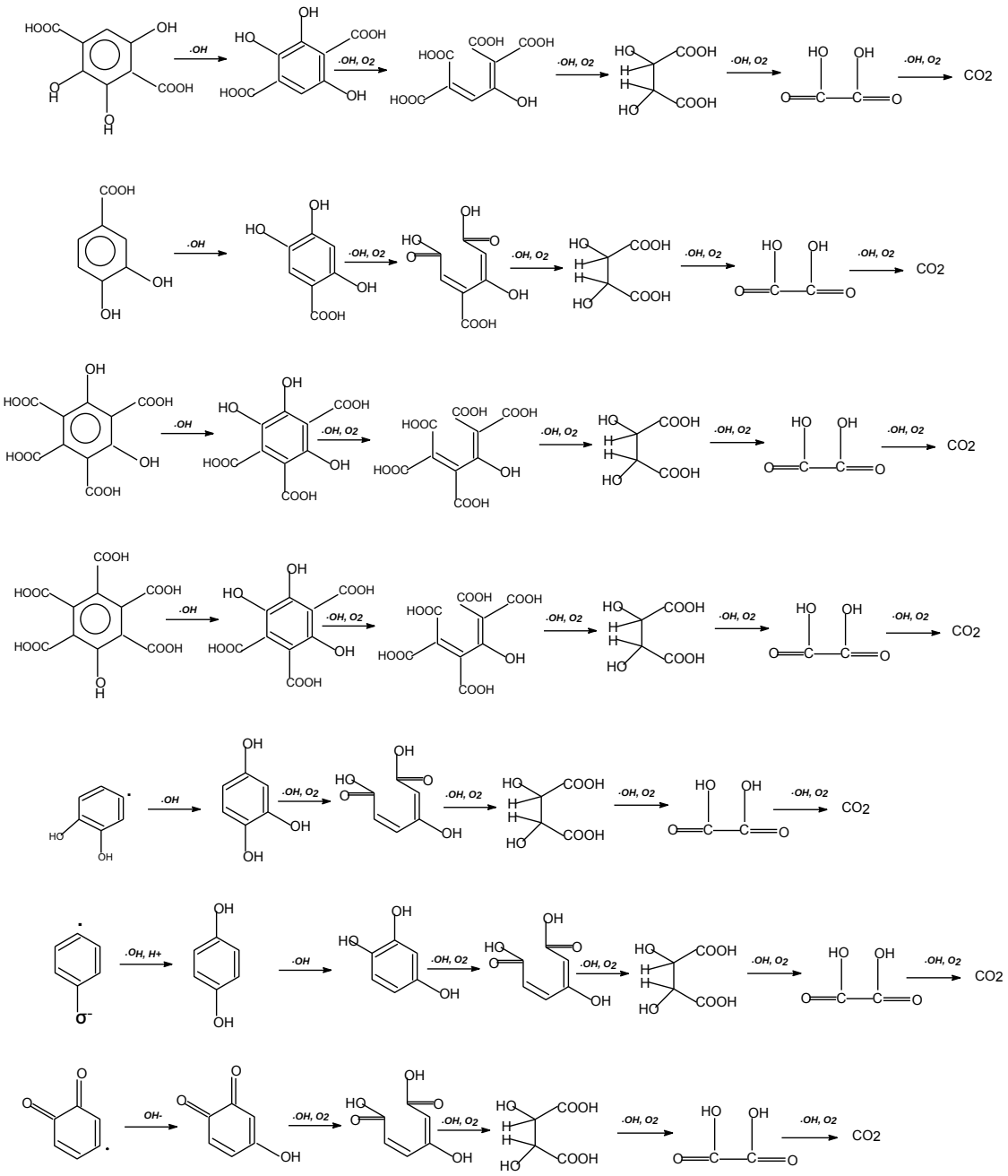

Figure B-2. Scheme 2, proposed decomposition pathways of HS monomers.

B.2 Benzothiopene

B.2.1 Identification of Benzothiophene Intermediates

The sonochemical reaction in aqueous phase gives rise to water (H_2O) sonolysis with production of radical species such as hydrogen (H), OH, and hydrated electrons e^-_{aq}. These radicals can either combine to form hydrogen (H_2) and hydrogen peroxide (H_2O_2) or attack solute molecules. π electrons of the aromatic ring are excellent targets for hydroxyl radicals. The chromatogram and the mass spectra of the parent compound and its intermediates are shown in figures B-3a, b, c, d, e, f, g, and h.

The peaks were examined with the computer database of the National Institute of Science and Technology (NIST) mass spectral library and the published mass spectra of benzothiophene (BT) intermediates. Figure B-3a and b show the chromatogram of BT intermediate and the spectrum of BT, respectively.

The peak emerging from the GC at 11.04 minutes has major ions at m/z (percentage of intensity, proposed composition of ions) 166(36, [M]+), 137(100, [M-COH]+), 109(59, [M-COH-CO]+), 76(15, [M-COH-COH-S]+) and 50(19) in figure B-3h. Its spectrum appears that of 2,3-dihydroxylbenzothiophene .

The peak emerging from the GC at 9.94 minutes has major ions at m/z 164(5, [M]+), 136(100, [M-CO]+), 108(45, [M-CO-CO]+), 92(5), 82(11), 76(6) and 69(23) shown in figure B-3c. This mass spectrum is identical to that obtained from an authentic standard, benzothiophene-2,3-dione (Fedorak et al., 1991).

The peaks emerging from the GC at 10.00, 10.07, 10.20, and 10.25 minutes have major ions at m/z 150 (94, [M]+), 122 (74, [M-CHO]+), 121 (100, [M-CHO]+), 78 (37) and 69 (15) in figures B-3d, e, f, and g. These mass spectra are identical to that obtained from an authentic standard, 3-hydroxybenzothiophene (Eaton et al., 1994). The mass spectra are the expected isomers: 2-hydroxybenzothiophene, 4-hydroxybenzothiophene, 5-hydroxybenzothiophene, 6-hydroxybenzothiophene, and 7-hydroxy-benzothiophene. Among them, the peaks at 10.07 and 10.25 minutes appear to be 2-hydroxybenzothiophene and 3-hydroxybenzothiophene. The major reaction products retaining the intact benzene ring such as sulfobenzoic acid were obtained from all cases of radical reactions for benzothiophene and methylbenzothiophenes (Andersson et al., 1992; Bobinger et al., 1998).

Figure B-4 presents the concentration change of benzothiophene and evolution of carbon dioxide and inoganic sulfur species. Carbon dioxide evolves faster than sulfite. The concentrations of other sulfur species stay at low values during the reaction.

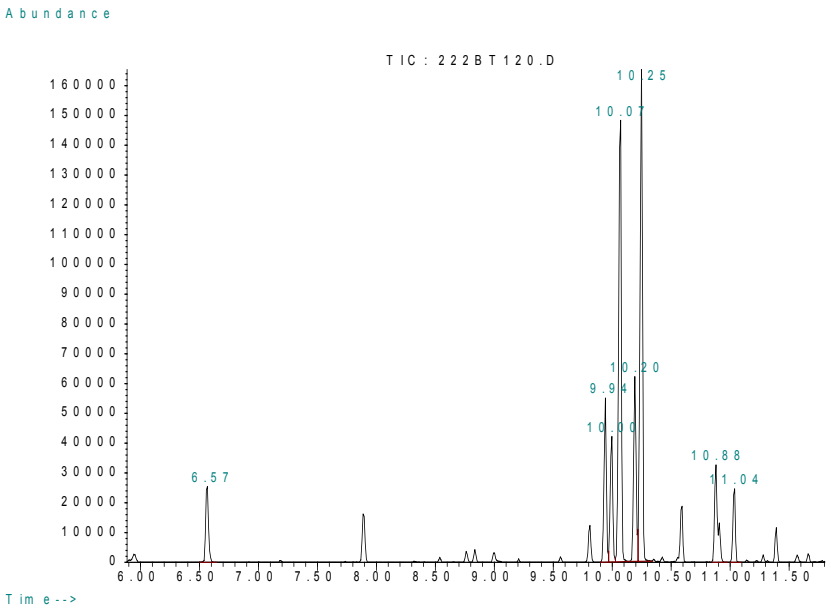

Figure B-3a. The total ion chromatogram of benzothiophene (BT) decomposition from sonochemical reaction.

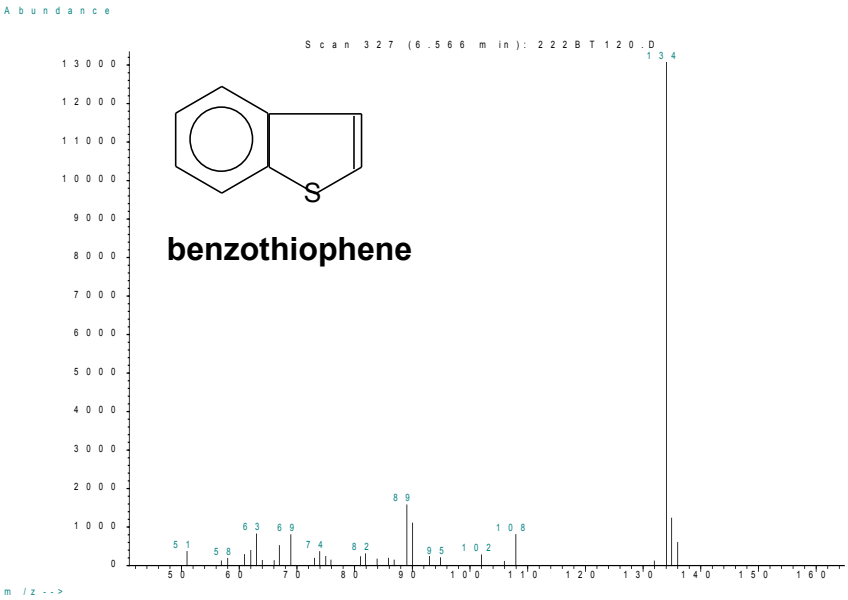

Figure B-3b. The mass spectrum of benzothiophene from sonochemical reaction.

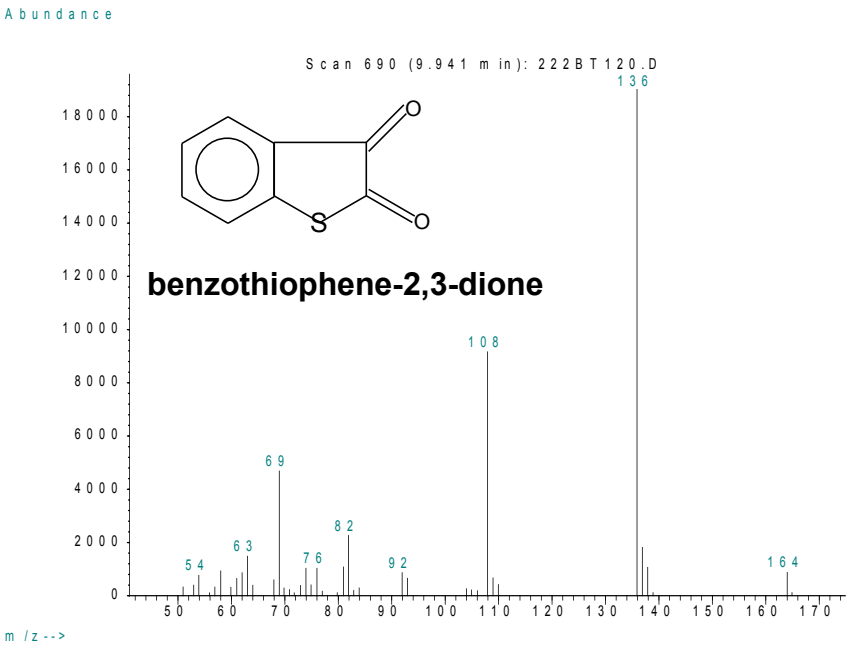

Figure B-3c. The mass spectrum of benzothiophene-2,3-dione from sonochemical reaction.

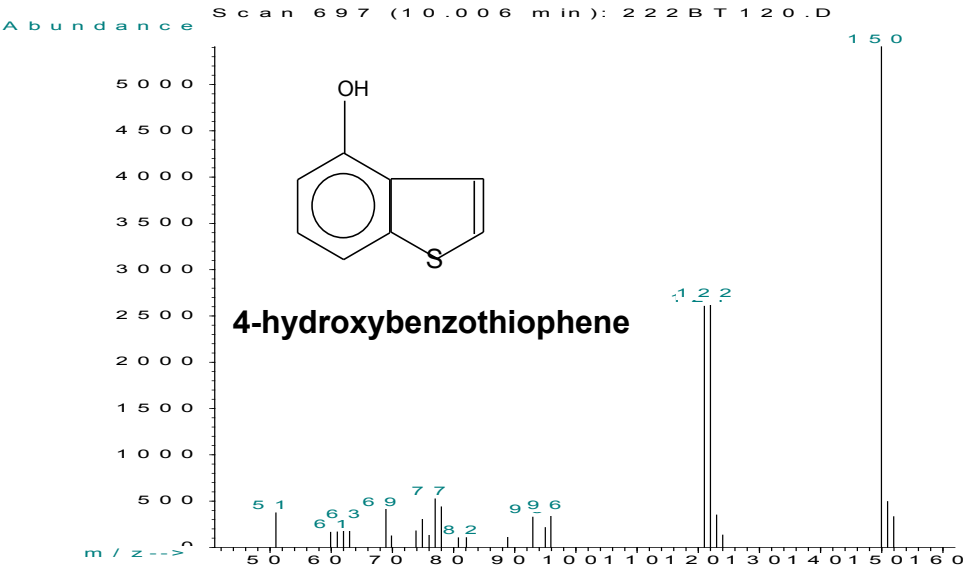

Figure B-3d. The mass spectrum of 3-hydroxylbenzothiophene isomer from sonochemical reaction.

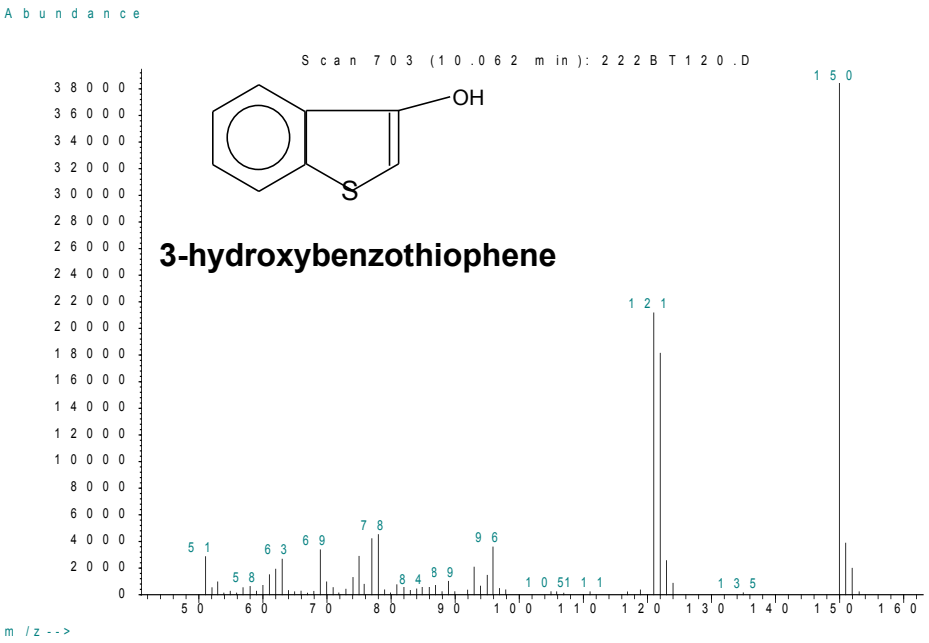

Figure B-3e. The mass spectrum of 3-hydroxylbenzothiophene from sonochemical reaction.

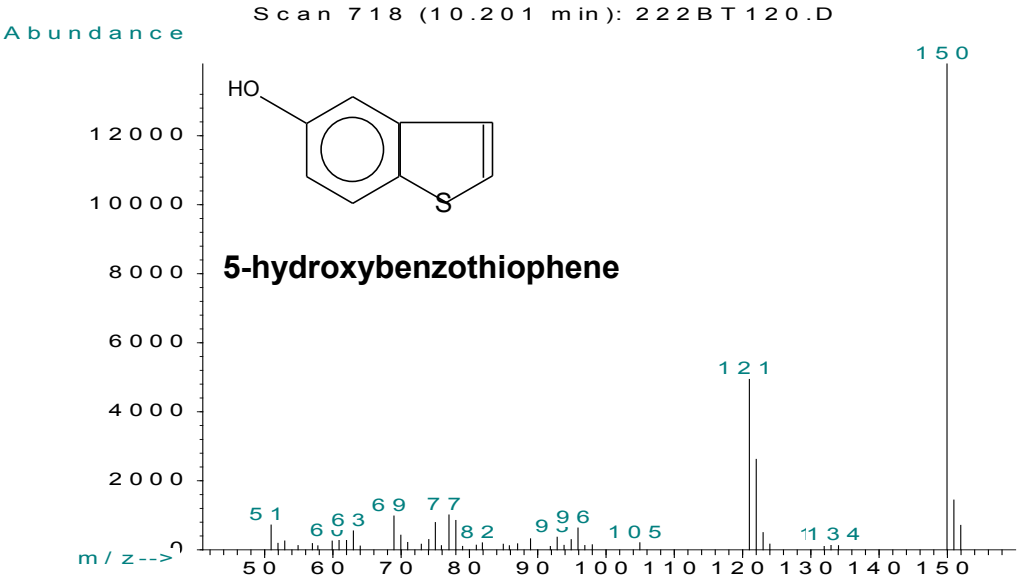

Figure B-3f. The mass spectrum of 3-hydroxylbenzothiophene isomer from sonochemical reaction.

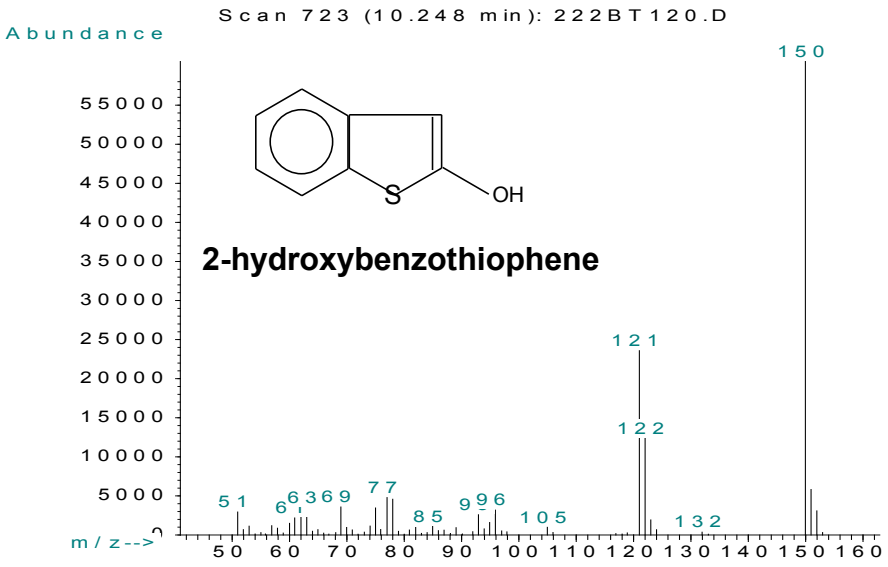

Figure B-3g. The mass spectrum of 3-hydroxylbenzothiophene isomer from sonochemical reaction.

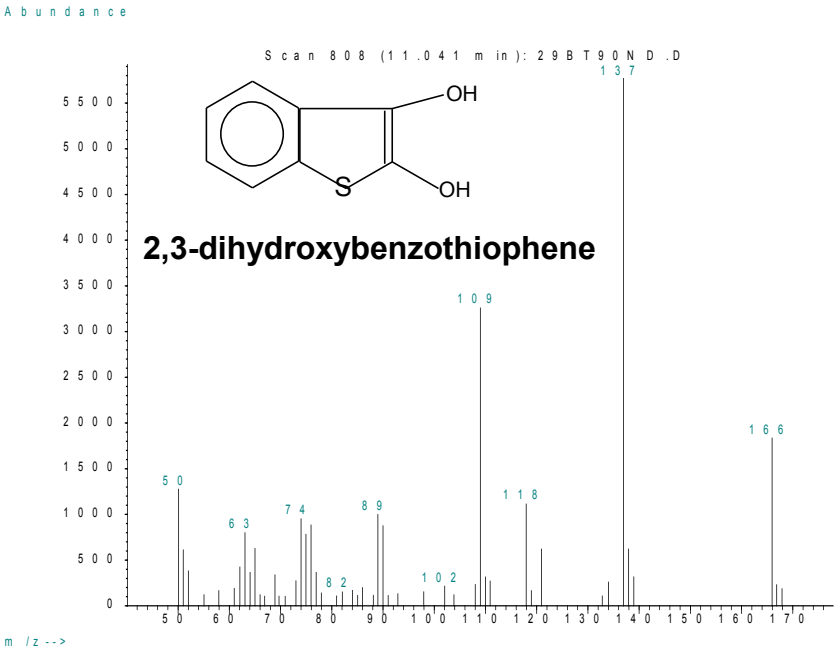

Figure B-3h. The mass spectrum of 2,3-dihydroxylbenzothiophene from sonochemical reaction.

The toxicity of sonochemically treated solutions was checked by *E. coli*. A severe inhibition in bacterial respiration was obtained from the untreated BT sample, while little inhibition was showed from the 120-minute treated BT sample. Consequently, the sonochemical reaction reduced the toxicity of the treated organic compounds.

Our analysis of intermediates and reactions leads to the proposed reaction pathways describing the sonochemical decomposition of BT in aqueous solution. The sonochemical reaction is brought about by OH radicals, which are formed mainly from sonolytic water decomposition in the cavitation bubbles. The radicals can either directly react with the organic species at the bubble-water interface or diffuse to the solution and then react with the organic species in the solution phase. Both reactions lead to formation of hydroxylated products such as 3-hydroxybenzothiophene (Scheme 3) (figure B-5). Eventually, the reaction will mineralize these intermediates to end products such as carbon dioxide and inorganic sulfur species. Scheme I shows one of the possible reaction pathways involving ·OH radicals. Only nonradical species were detected in this reaction pathway.

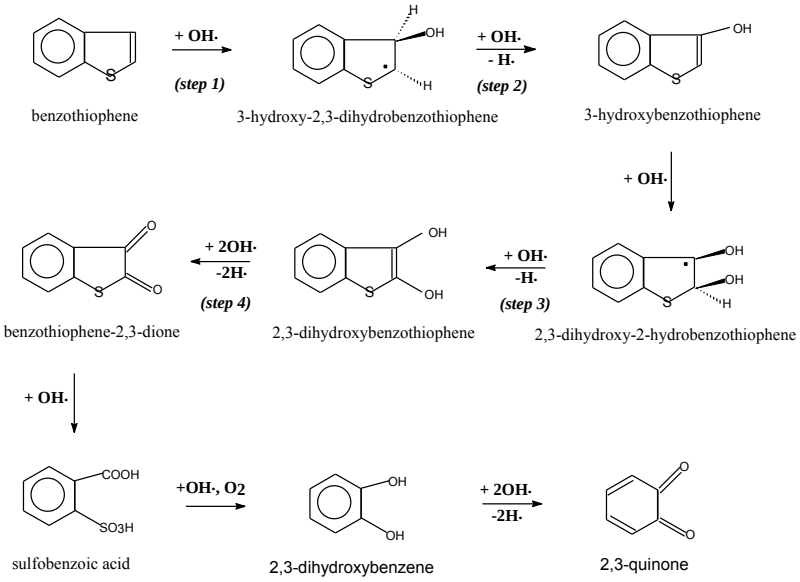

Figure B-5. Scheme 3, proposed sonochemical decomposition pathway for BT.

The first step of the reaction is the ·OH radical addition which yields the 3-hydroxy-2,3-dihydrobenzothiophene (step 1). The thiophene ring is more attractive to the hydroxyl radicals than the benzene ring (Andersson et al., 1992; Bobinger et al., 1998). After the addition of first ·OH radical, 3-hydroxy-2,3-dihydrobenzothiophene can be changed to 3-hydroxybenzothiophene by the elimination of a proton to recover the aromatic resonance stability at the thiophene ring (step 2). The electron-releasing property of OH functional group increases the opportunity of attack by the electrophilic OH radical at the thiophene ring. Then, further reaction with OH radical will generate 2,3-dihydroxybenzothiophene as a main intermediate product (step 3). The 2,3-dihydroxybenzothiophene undergoes hydrogen abstraction, which is the usual reaction with unsaturated organic compounds, then generates the benzothiophene-2,3-dione (step 4). Further decomposition would generate sulfobenzoic acid and 2,3-quinone (Bobinger et al., 1998; Eisenhauer, 1964).

The subsequent cleavage of the 2,3-quinone would result in the formation of muconic acid. The reactions that follow are oxidation of the unsaturated bonds in muconic acid, which later changes into maleic acid (Eisenhauer, 1968). Theoxidation proceeds further to break down the C = C bond and decarboxylate to form acrylic acid. The hydroxyl radicals will further attack the double bond in acrylic acid to yield 3-hydroxyl propionic acid that would further oxidize into malonic acid.

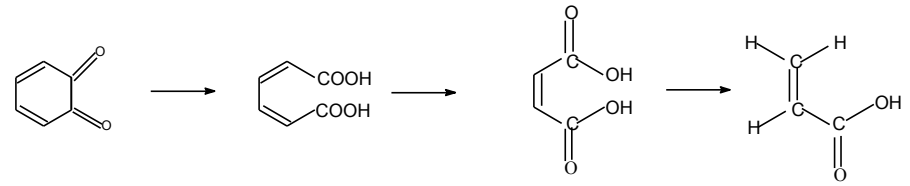

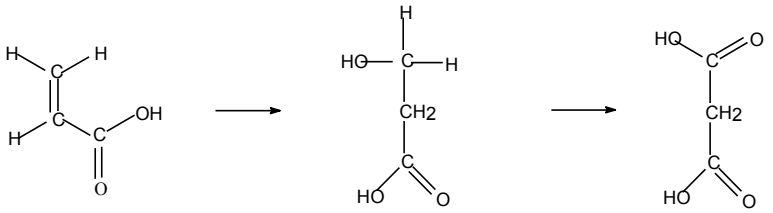

The malonic acid then will be converted to acetic acid and carbon dioxide as the end products. The other pathway is the rearrangement of the acrylic acid to oxalic acid and glyoxylic acid generating the formic acid as depicted in the following scheme:

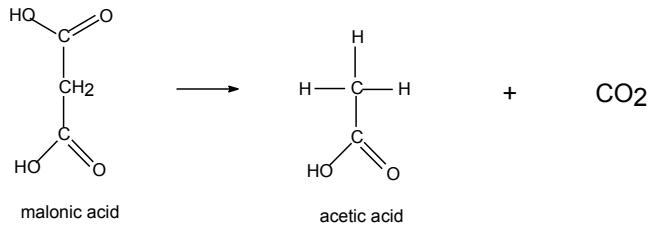

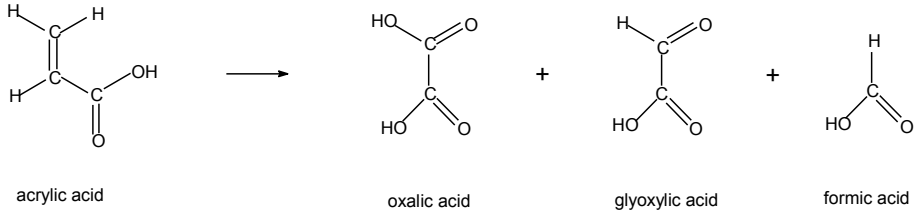

Another decomposition pathway of benzothiophene is proposed in Scheme 4 (figure B-6). The benzothiophene would generate monohydroxybenzothiophene and dihydroxybenzothiophene subsequently through the addition of hydroxyl radicals to benzene ring. Then further decomposition of intermediates to end products, carbon dioxide, and sulfite is proposed.

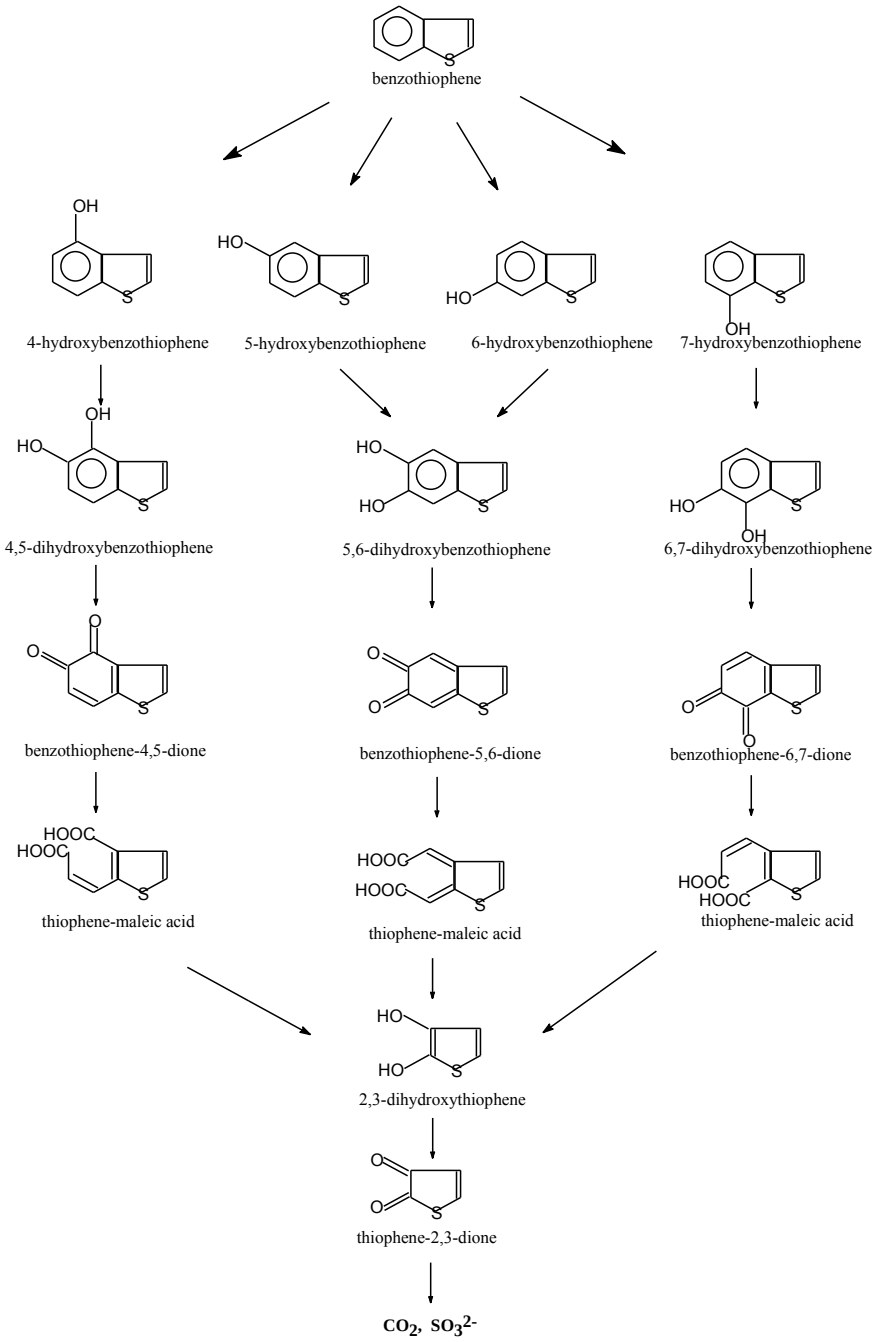

Figure B-6. Scheme 4, proposed sonochemical decomposition pathway for BT.

B.2.2 Kinetic Modeling of Reaction Pathways

With the experimental observations of the reaction products from the decomposition of benzothiophene, it is possible to develop a reaction network that describes the decomposition of benzothiophene leading to the formation of hydroxylated aromatic compounds. Scheme 5 (figure B-7) shows the reaction network of benzothiophene decomposition in sonochemical reaction:

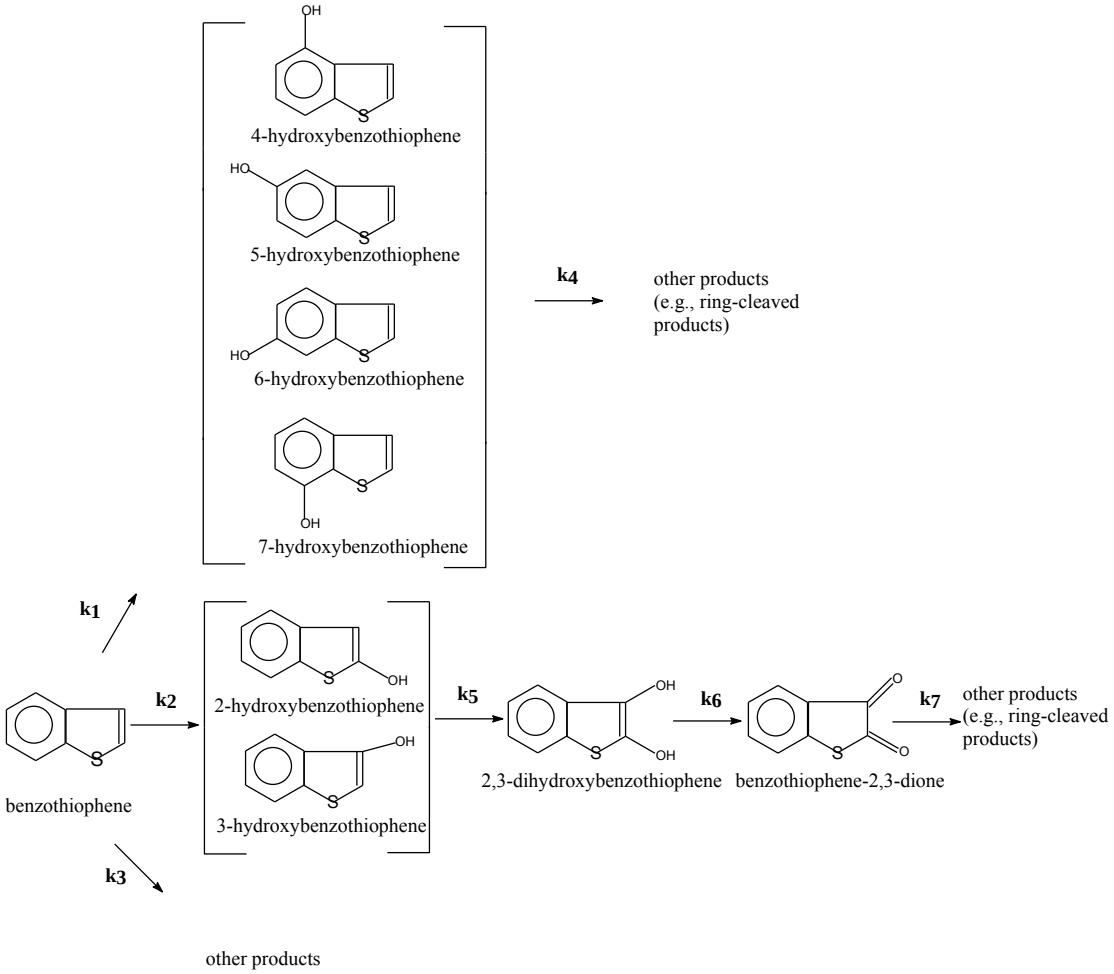

Figure B-7. Scheme 5, pathways of benzothiophene decomposition in sonochemical reaction.

The following notation is used in this analysis:

C_{BT} : Concentration of benzothiophene (M)
C_{23HXBT} : Total concentration of 2-, and 3-hydroxybenzothiophenes (M)
C_{23OH} : Concentration of 2,3-dihydroxybenzothiophenes (M)
C_{BT23DN} : Concentration of benzothiophene-2,3-dione (M)
$C_{4567HXBT}$: Total concentration of 4-, 5-, 6-, and 7-hydroxybenzothiophenes (M)

For benzothiophene, the rate of decomposition is described as:

$$\frac{dC_{BT}}{dt} = -k_1 C_{BT} - k_2 C_{BT} - k_3 C_{BT} \tag{1}$$

All steps of the rate of decomposition of benzothiophene have been taken to be first order in benzothiophene. The first order effect was used in this modeling because the rate law describing benzothiophene decomposition was determined to be first order in benzothiophene with the reaction conditions used. This first order effect was assumed for all compounds in the reaction network.

The following definition can be made:

$$k_A = k_1 + k_2 + k_3 \tag{2}$$

With the definition of k_A (or k_{obs}), the rate of reaction is written as:

$$\frac{dC_{BT}}{dt} = -k_A C_{BT} \tag{3}$$

For 4-, 5-, 6-, and 7-hydroxybenzothiophenes, the rate equation is:

$$\frac{dC_{4567HXBT}}{dt} = k_1 C_{BT} - k_4 C_{4567HXBT} \tag{4}$$

For 2-, and 3-hydroxybenzothiophenes:

$$\frac{dC_{23HXBT}}{dt} = k_2 C_{BT} - k_5 C_{23HXBT} \tag{5}$$

For 2,3-dihydroxybenzothiophene:

$$\frac{dC_{23OH}}{dt} = k_5 C_{23HXBT} - k_6 C_{23OH} \tag{6}$$

For benzothiophene-2,3-dione:

$$\frac{dC_{BT23DN}}{dt} = k_6 C_{23OH} - k_7 C_{BT23OH} \tag{7}$$

Each differential equation can be solved analytically and the solution substituted in the following equations. The exact solution of each equation follows:

For benzothiophene :

$$C_{BT} = C_{BT,0} \exp(-k_A t) \tag{8}$$

with $C_{BT,0}$ equal to the initial benzothiophene concentration (M).

For 4-, 5-, 6-, and 7-hydroxybenzothiophenes:

$$C_{4567HXBT} = \frac{k_1 C_{BT,0}}{(k_4 - k_A)} [\exp(-k_A t) - \exp(-k_4 t)] \tag{9}$$

For 2-, and 3-hydroxybenzothiophenes:

$$C_{23HXBT} = \frac{k_2 C_{BT,0}}{(k_5 - k_A)} [\exp(-k_A t) - \exp(-k_5 t)] \tag{10}$$

For 2,3-dihydroxybenzothiophene:

$$C_{23OH} = C_{BT,0}\left[\frac{k_2 k_5 \exp(-k_A t)}{(k_6 - k_A)(k_5 - k_A)} - \frac{k_2 k_5 \exp(-k_A t)}{(k_6 - k_A)(k_5 - k_A)} - \frac{k_2 k_5 \exp(-k_6 t)}{(k_6 - k_A)(k_5 - k_A)}\right] \tag{11}$$

For benzothiophene-2,3-dione

$$\begin{aligned}\frac{C_{BT23DN}}{C_{BT,0}} = {} & \frac{k_6 k_5 \exp(-k_2 t)}{(k_5 - k_2)(k_6 - k_2)(k_7 - k_2)} - \frac{k_6 k_5 \exp(-k_5 t)}{(k_5 - k_2)(k_6 - k_5)(k_7 - k_5)} \\ & + \frac{k_5 (k_5 - k_2) \exp(-k_6 t)}{(k_5 - k_2)(k_6 - k_2)(k_6 - k_5)(k_7 - k_6)} - \frac{k_6 k_5 \exp(-k_7 t)}{(k_5 - k_2)(k_6 - k_2)(k_6 - k_5)(k_7 - k_2)} \\ & + \frac{k_6 k_5 \exp(-k_7 t)}{(k_5 - k_2)(k_6 - k_2)(k_6 - k_5)(k_7 - k_5)} - \frac{k_5 (k_5 - k_2) \exp(-k_7 t)}{(k_5 - k_2)(k_6 - k_2)(k_6 - k_5)(k_7 - k_6)}\end{aligned} \tag{12}$$

With these analytical solutions of equations, it is possible to determine the reaction rate constants. In this case, for the set of conditions:

1.2 x 10^{-4} M $C_{BT,0}$, pH 7, 40-milliliter (mL) reaction volume, and 0.05 molar (M) sodium perchlorate ($NaClO_4$) ionic strength:

$$k_A = 3.5 \text{ x } 10^{-4} \text{ sec}^{-1} \tag{13}$$

As a result, both the actual benzothiophene molarity and the predicted benzothiophene concentration can be plotted as a function of reaction time with a $R^2 = 0.99$.

Nonlinear curve-fitting techniques have been used to determine other reaction rate constants. A computer program has been written on the *Matlab* software, which allows one to minimize the sum of the squares for the given experimental data of organic concentration versus time. For example, for the formation of 4-, 5-, 6-, and 7-hydroxybenzothiophene, the rate constants of k_1 and k_4 are unknown. The minimization function can be expressed as:

$$0 = C_{4567\,HXBT} - \frac{k_1 C_{BT,0}}{(k_4 - k_A)}\left[\exp(-k_A t) - \exp(-k_4 t)\right] \tag{14}$$

The solutions obtained were:

$$k_1 = 8 \times 10^{-5}\ \text{sec}^{-1} \tag{15}$$

and

$$k_4 = 1.7 \times 10^{-4}\ \text{sec}^{-1} \tag{16}$$

The actual and the predicted concentration of 4-, 5-, 6-, and 7-hydroxybenzothiophene can be plotted as a function of reaction time with a $R^2 = 0.93$.

Applying the same technique, the reaction rate constants associated with 2-, and 3-hydroxybenzothiophenes, 2,3-dihydroxybenzothiophene, and benzothiophene-2, 3-dione can be determined. For this analysis, the minimization function can be expressed as:

For 2-, and 3-hydroxybenzothiophenes:

$$0 = C_{23HXBT} - \frac{k_2 C_{BT,0}}{(k_5 - k_A)}\left[\exp(-k_A t) - \exp(-k_5 t)\right] \tag{17}$$

For 2,3-dihydroxybenzothiophene:

$$0 = C_{23OH} - C_{BT,0}\left[\frac{k_2 k_5 \exp(-k_A t)}{(k_6 - k_A)(k_5 - k_A)} - \frac{k_2 k_5 \exp(-k_5 t)}{(k_6 - k_A)(k_5 - k_A)} - \frac{k_2 k_5 \exp(-k_6 t)}{(k_6 - k_A)(k_5 - k_A)}\right] \tag{18}$$

For benzothiophene-2,3-dione

$$\begin{aligned} 0 = &-\frac{C_{BT\,23DN}}{C_{BT,0}} + \frac{k_6 k_5 \exp(-k_2 t)}{(k_5 - k_2)(k_6 - k_2)(k_7 - k_2)} - \frac{k_6 k_5 \exp(-k_5 t)}{(k_5 - k_2)(k_6 - k_5)(k_7 - k_5)} \\ &+ \frac{k_5 (k_5 - k_2)\exp(-k_6 t)}{(k_5 - k_2)(k_6 - k_2)(k_6 - k_5)(k_7 - k_6)} - \frac{k_6 k_5 \exp(-k_7 t)}{(k_5 - k_2)(k_6 - k_2)(k_6 - k_5)(k_7 - k_2)} \\ &+ \frac{k_6 k_5 \exp(-k_7 t)}{(k_5 - k_2)(k_6 - k_2)(k_6 - k_5)(k_7 - k_5)} - \frac{k_5 (k_5 - k_2)\exp(-k_7 t)}{(k_5 - k_2)(k_6 - k_2)(k_6 - k_5)(k_7 - k_6)} \end{aligned} \tag{19}$$

From the minimization of both 2- and 3-hydroxybenzothiophenes, 2,3-dihydroxy-benzothiophene, and benzothiophene-2, 3-dione functions using the multiple nonlinear regression, the reaction rate constants, k_2, k_5, k_6, and k_7, can be calculated as:

$$k_2 = 1.9 \times 10^{-4} \text{ sec}^{-1} \quad (20)$$

$$k_5 = 2.0 \times 10^{-4} \text{ sec}^{-1} \quad (21)$$

$$k_6 = 1.82 \times 10^{-4} \text{ sec}^{-1} \quad (22)$$

$$k_7 = 1.6 \times 10^{-4} \text{ sec}^{-1} \quad (23)$$

The actual and the predicted concentrations of 2- and 3-hydroxybenzothiophenes and benzothiophene-2,3-dione can be plotted as a function of reaction time with a $R^2 = 0.98$ and 0.93, respectively.

The only reaction rate constant remaining to be determined is k_3, which can be solved using equation 24 since k_1 and k_2 are known:

$$k_3 = 0.08 \times 10^{-3} \text{ sec}^{-1} \quad (24)$$

The above calculated rate constants, k_A, k_1, and k_2, allow us to predict the percent of benzothiophene that reacts to form the sum of 4-, 5-, 6-, and 7-hydroxyben-zothiophenes and the sum of 2-, and 3-hydroxybenzothiophenes as the reaction products. The percentage is provided by the ratio $(k_1 + k_2)/ k_A$. From this ratio, 77.1 % of the benzothiophene goes to form monohydroxybenzothiophenes as the reaction products at the initial step. The remaining 22.9 % of reacted benzothiophene would form other reaction products.

B.3 Dibenzothiophene (DBT)

The sonochemical reaction in aqueous phase gives rise to H_2O sonolysis with production of radical species such as $H^{\cdot}$, OH, and hydrated electrons e^{-}_{aq}. These radicals either can combine to form H_2 and H_2O_2 or attack solute molecules. π electrons of the aromatic ring are excellent targets for hydroxyl radicals. The chromatogram and the mass spectra of the parent compound, DBT, and its intermediate are shown in figures B-8a, b, c, d, e, f, and g. The peak at 24.05 minutes (figure B-8c) was identified as an intermediate, monohydroxydibenzothiophene. The spectrum of the monohydroxydiben-zothiophene derivative is shown in figure B-8e. The intermediates in figures B-8d, f, and g were not identified.

Each peak was examined with the computer database of the National Institute of Science and Technology mass spectral library.

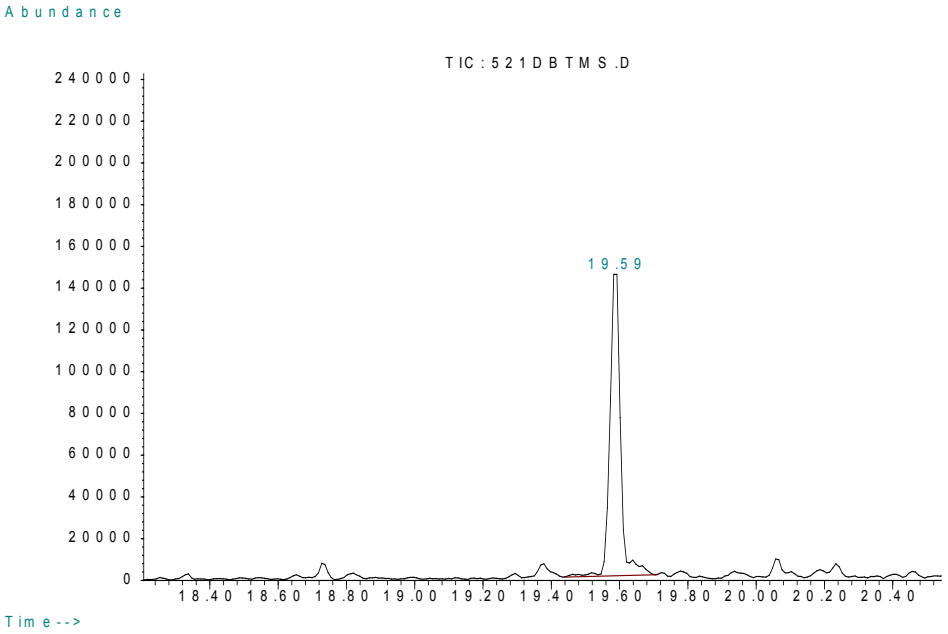

Figure B-8a. The chromatogram of dibenzothiophene.

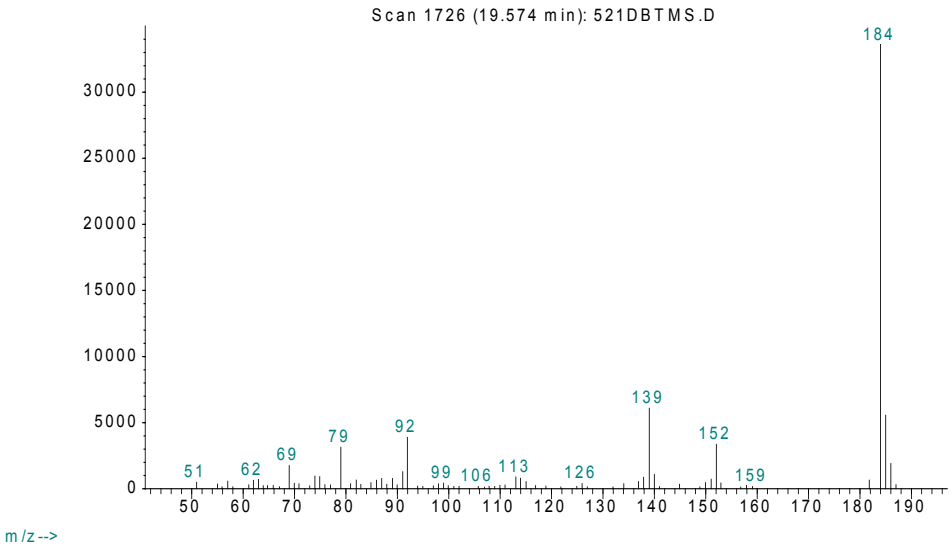

Figure B-8b. The mass spectrum of dibenzothiophene from sonochemical reaction.

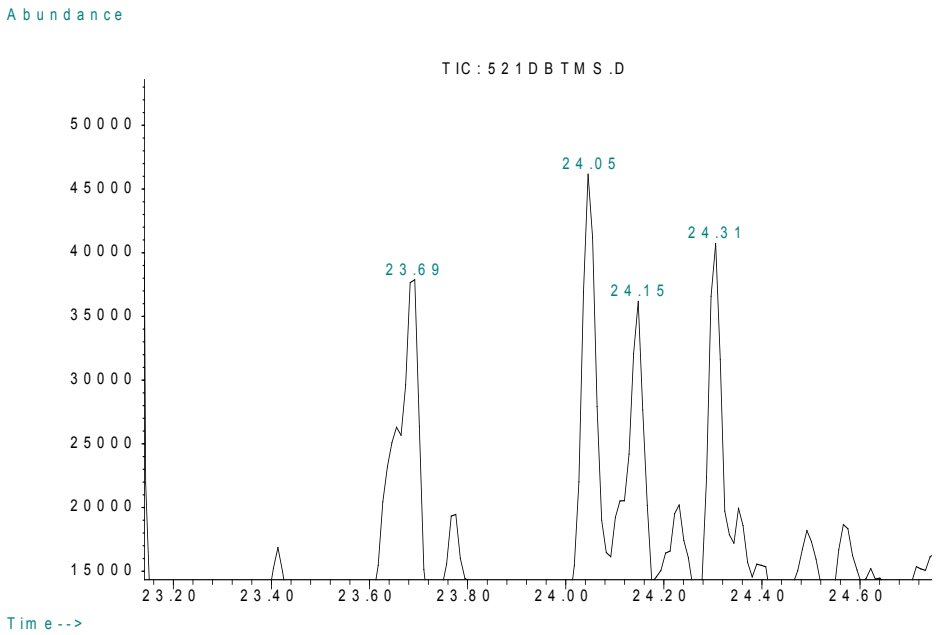

Figure B-8c. The chromatogram of dibenzothiophene decomposition from sonochemical reaction.

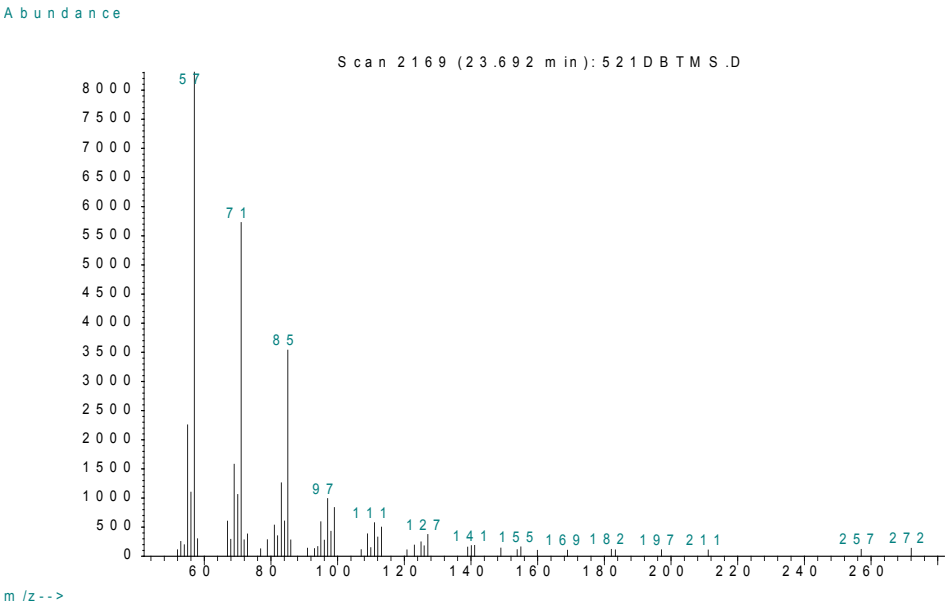

Figure B-8d. The mass spectrum of a dibenzothiophene intermediate derivative from sonochemical reaction.

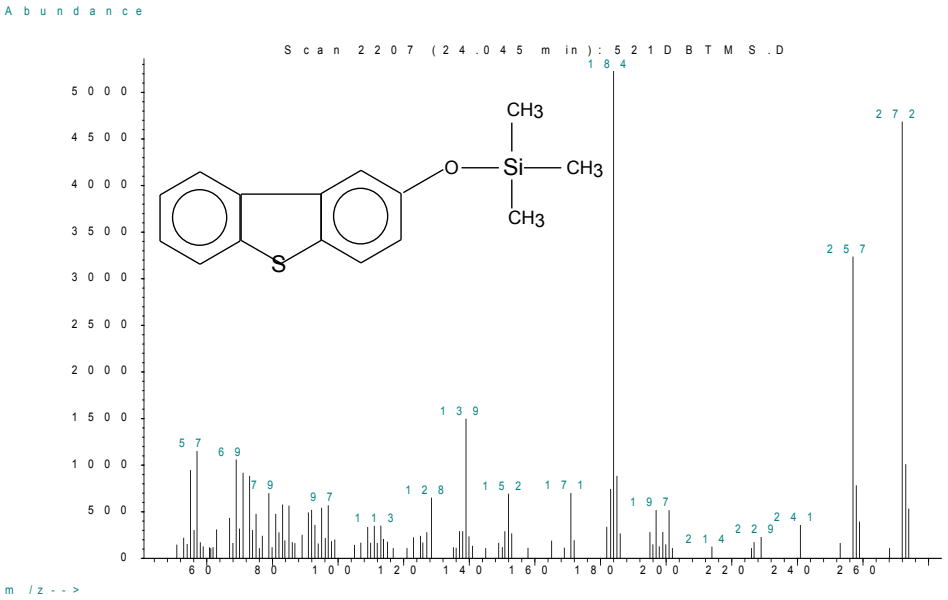

Figure B-8e. The mass spectrum of monohydroxydibenzothiophene TMS derivative from sonochemical reaction.

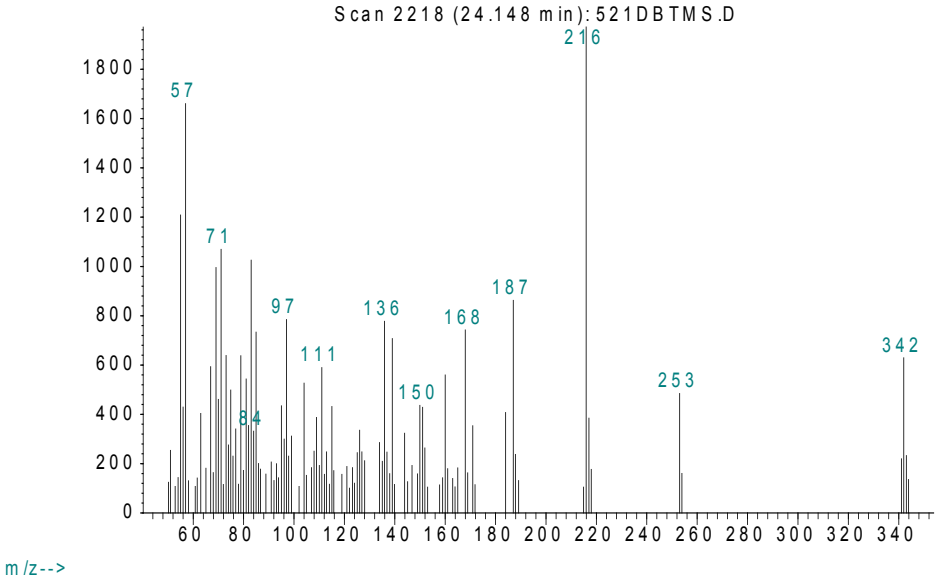

Figure B-8f. The mass spectrum of a dibenzothiophene intermediate derivative from sonochemical reaction.

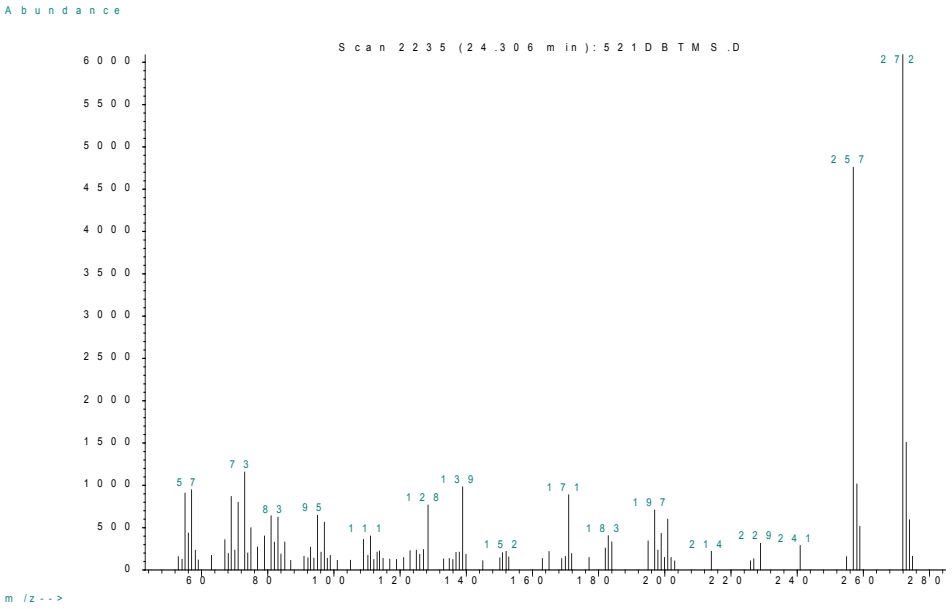

Figure B-8g. The mass spectrum of a dibenzothiophene intermediate derivative from sonochemical reaction.

Our analysis of intermediates of dibenzothiophene decomposition together with the reaction mechanism developed for benzothiophene leads to the proposed reaction pathway describing the sonochemical decomposition of dibenzothiophene in aqueous solution. The sonochemical reaction is brought about by ·OH radicals, which are formed mainly from sonolytic water decomposition in the cavitation bubbles. The radicals can react either directly with the organic species in the bubbles-water interface or diffuse to the solution and then react with the organic species in the solution phase. Both reactions lead to formation of hydroxylated products such as monohydroxybenzothiophene (figure B-8d). Eventually, the reaction will mineralize these intermediates to end products such as carbon dioxide and inorganic sulfur species. Scheme 6 (figure B-9) shows one of the possible reaction pathways involving ·OH radicals.

The first step of the reaction is the ·OH radical addition that yields the monohydroxydibenzothiophene (step 1). The benzene ring is attractive to the attack of hydroxyl radicals. After the addition of first ·OH radical, monohydroxydibenzothiophene can be changed to dihydroxydibenzothiophene by the addition of another OH radical (step 2). The electron-releasing property of OH functional group increases the opportunity of attack by the electrophilic OH radical at the benzene ring. The dihydroxydibenzothiophene undergoes hydrogen abstraction, which is the usual reaction with unsaturated organic compounds, then generates the dibenzothiophene-2,3-dione (step 3). Further decomposition would generate 2,3-dihydroxybenzothiophene and benzothiophene-2,3-dione.

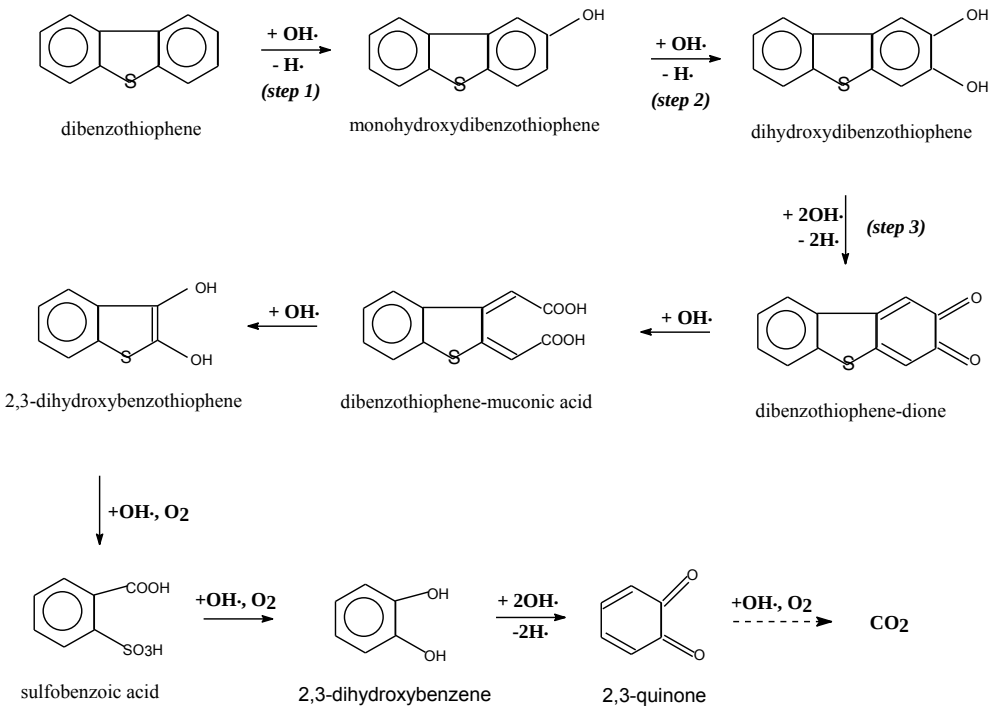

Figure B-9. Scheme 6, proposed sonochemical decomposition pathway for DBT.

The subsequent cleavage of the 2,3-quinone would result in the formation of muconic acid. The reactions that follow are oxidation of the unsaturated bonds in muconic acid, which later changes into maleic acid (Eisenhauer, 1968). Theoxidation proceeds further to break down the C = C bond and decarboxylate to form acrylic acid. The hydroxyl radicals will further attack the double bond in acrylic acid to yield 3-hydroxyl propionic acid, which would further oxidize into malonic acid.

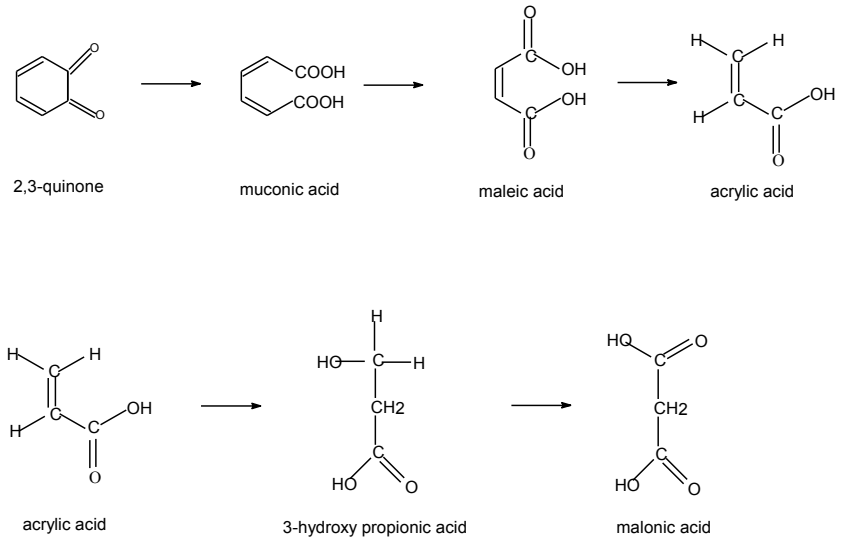

The malonic acid then will be converted to acetic acid and carbon dioxide as the end products. The other pathway is the rearrangement of the acrylic acid to oxalic acid and glyoxylic acid generating the formic acid as depicted in the following scheme:

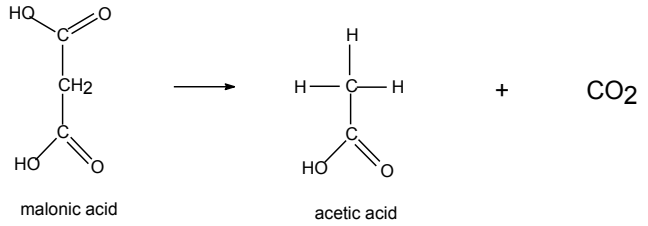

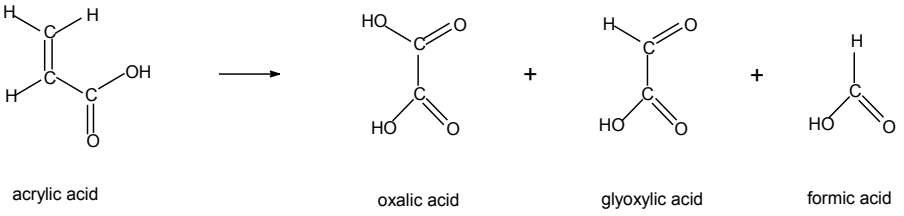

B.4 Trihalomethanes (THMs)

The decomposition rate decreases with increasing the number of bromine atoms in THM: chloroform is greater than (>) dichlorobromomethane > dibromochloromethane > bromoform. Figure B-10 shows the relationship of the Henry's law constant and the sonochemical reaction rate constant of THMs.

To better explain the order of the decomposition rate of THMs, a schematic two-phase reaction diagram was proposed in this study for the sonochemical reaction of THMs, as shown in figure B-10. At first, the decomposition of THMs may be supposed to take place in the gaseous (bubble), interfacial zone and bulk solution by either pyrolysis or free radical attack. The pyrolysis is highly dependent on the reaction temperature, according to the previous literature (Suslick et al., 1986). The temperature in the gaseous zone (up to 5,000 degrees Kelvin [°K]) is much higher than that in the interface (about 1,000 °K); thus, the pyrolysis of THMs was more likely to happen in the gaseous region. Free radical attack of THMs appears to be minimal in the bulk solution because the free radicals generated in the cavitation bubbles are poorly transferred the room-temperature bulk solution through the much higher-temperature interface. Therefore, the decomposition of THMs in the bulk solution by either pyrolysis or free radical attack can be supposed to be negligible. Also, it was clearly shown that the presence of a compound with a higher vapor pressure hinders the decomposition of a less

volatile compound (Petrier, 1998); but this inhibition must not to be considered as an inhibition of cavitation. In the bubble, the decomposition of a more volatile compound takes the place of the OH radical formation. Thus, the overall decomposition of the more volatile compound (chloroform) is attributed to the pyrolysis and free radical attack that occurred in both the gaseous and interfacial zones. Conversely, transfer of the less-volatile compound into the gaseous zone is hindered by chloroform, leaving the decomposition of dichlorobromomethane to mainly occur in the interface and, thereby, decreasing the decomposition rate. This relationship between vapor pressure and decomposition rate is depicted by the sonochemical hot spot study (Suslick, 1986).

B.4.1 Activation Energy of THMs

The values in figure B-10 indicate that chloroform and dibromochloromethane have almost the same value, and bromoform has the largest activation energy. It is notable that dichlorobromomethane has the lowest activation energy value (7.3 kilojoule per mole [kJ/mole]) in the sonochemical reaction, though dichlorobromomethane has a lower decomposition rate than that of chloroform. Normally, it is expected that the compound with a lower activation energy decomposes more rapidly. These results can be explained by two properties of THMs—vapor pressure and bonding force. As described above, since chloroform boils at low temperature, 62 degrees Celsius (°C), high-temperature reaction mechanism (pyrolysis) of chloroform vapor inside the cavitating bubbles can be the preferable reaction mechanism due to its high vapor pressure (160 millimeters of mercury [mm Hg at 20 °C]). It was shown that a THM with a higher vapor pressure had a larger rate of decomposition than that of a less-volatile THM under fixed experimental conditions. Also, the methanol spiked with THMs into the solution acts as a radical scavenger to reduce the radical reactions inside bubbles and in the interface and bulk of solution. Moreover, the low apparent activation energy values of four THMs in figure B-10 indicate that the sonochemical reaction for THMs is controlled by the diffusion step.

An explanation for the lower activation energy of dichlorobromomethane in sonochemical reaction is based on the reasoning described below. Bromine substituents are better leaving groups than chlorine substituents; it is easier for bromine substituents to leave the parent molecule than for chlorine substituents (Solomons, 1988). Values of bonding energy for carbon-chlorine and carbon-bromine bonds are 95 and 67 kilocalorys per mole (kcal/mole), respectively, as reported by Weast et al. (1992). The ease of dehalogenation of an organic compound is directly proportional to the bond energy between carbon and halogen atoms. This can explain why the activation energy of dichlorobromomethane is lower than that of chloroform in sonochemical reaction, even though the sonochemical rate of dichlorobrommethane is lower than that of chloroform.

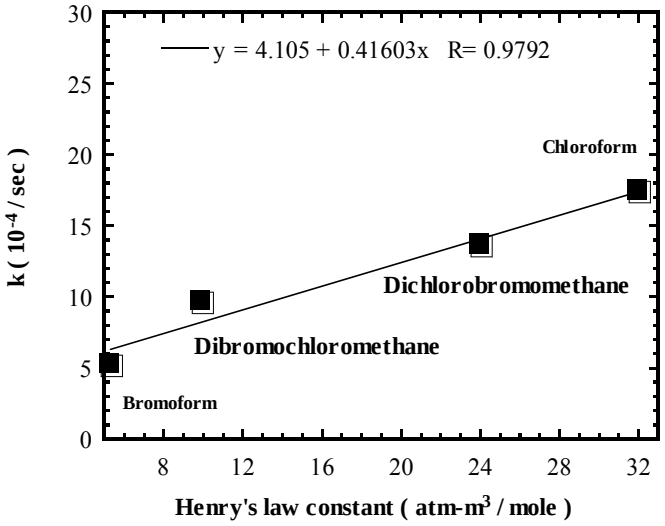

Figure B-10. Relationship between the Henry's law constant and the sonochemical rate constant of trihalomethanes in aqueous phase. Experimental conditions: ultrasonic energy intensity = 226 watts per square centimeter, total volume = 40 milliliters, C_0 = 3.7 micromolars, pH = 7, temperature = 25 °C, ionic strength = 0.05 molar $NaClO_4$.